Understanding the Role of SNRPB in Embryonic Development by Modeling Cerebrocostomandibular Syndrome (CCMS) in Mice

Sabrina Shameen Alam

Department of Human Genetics, Faculty of Medicine and Health Sciences,

McGill University, Montreal, Canada

DECEMBER 2022

A thesis submitted to the McGill University in partial fulfillment of the requirements of the degree of Doctor of Philosophy

DEDICATION

"We never know the love of a parent till we become parents ourselves"

- Henry Ward Beecher

To my beloved parents- Dr. M. Shafiqul Alam and Ms. Rawshan Ara Haque,

My beautiful children- Nibras, Nora, Nuraisha and Yusuf

&

My strongest motivation in life- Dr. Abu Shadat Mohammod Noman.

Abstract

SNRPB is a major splicing factor and a core component of all the small nuclear ribonucleoproteins (SnRNPs). Patients with Cerebrocostomandibular syndrome (CCMS) carry heterozygous mutations in a highly conserved alternative exon 2 of *SNRPB,* which plays a crucial role in regulating *SNRPB* levels. CCMS patients mainly have craniofacial and rib defects with variable penetrance and expressivity. However, it is not clear why mutations in *SNRPB* result in the range of tissue specific abnormalities seen in CCMS. Here, we generated a mutation in *Snrpb*, to elucidate its role in embryonic development and shed light on CCMS. Our first mouse model which harbored a 61-base pair intronic deletion near the regulatory alternative exon 2 in *Snrpb,* shows CCMS craniofacial, rib and limb abnormalities at the embryonic and postnatal stages at a very low penetrance. This model suggests that the intron 2 region that we deleted is important for *SNRPB* regulation. We showed heterozygous constitutive knockout of *Snrpb* (*Snrpb*$^{+/-}$) is embryonic lethal as early as embryonic day (E)7.5, restricting embryonic development before morphogenesis. To know the requirement of *Snrpb* in mesodermal cell lineage, we then used *Mesp1-Cre* mice to remove *Snrpb* from the mesodermal cell lineages. We found the *Snrpb* heterozygous mutants in the mesodermal cells (*Snrpb*$^{mes+/-}$) are not born. These mutants display craniofacial and cardiac abnormalities with variable expressivity from E9.5 and onward. By E14.5, all *Snrpb*$^{mes+/-}$ mutants are abnormal with dorsal edema, and smaller head and lower jaw. We also found a reduction in cartilage development of the head and sternum, and abnormal development of the ribs. Intriguingly, neural crest cell derived Meckel's cartilage was abnormal in *Snrpb*$^{mes+/-}$ mutants, suggesting a disruption in the crosstalk between the two cell lineages. To gain insights of the role of *SNRPB* in neural crest cells, we mated *Wnt1-Cre* line with our *Snrpb* conditional mice to remove *SNRPB* from these cells. Here, the mutants (*Snrpb*$^{ncc+/-}$) showed abnormal craniofacial development that mimics CCMS patients and die between E17.5 and shortly after birth. We

also saw perturbed skeletal development in the craniofacial region of the mutants. An increased cell death was found in the mutant heads along with elevated nuclear P53. RNAseq of the E9.0 mutant heads revealed an elevated p53 pathway and significant changes in gene splicing, primarily increased exon skipping and intron retention. We found higher exon skipping in two p53 master regulators, *Mdm2* and *Mdm4.* RNAseq analyses also uncovered aberrant splicing of 13 genes required for craniofacial development in which we validated transcription factors such as *Smad2, Pou2f1* and *Rere*. Moreover, *in situ* hybridization exhibited aberrant expression of key craniofacial developmental genes such as *Fgf8, Shh* and *Msx2* in the *Snrpb*$^{ncc+/-}$mutants. Our findings suggest that the splicing changes occurring in the key developmental genes along with the increased P53 mediated cell death causes abnormal craniofacial development in *Snrpb*$^{ncc+/-}$ mutants and presumably in CCMS patients. Taken together, we proved that normal level of *SNRPB* is critical for proper embryonic development and our *Snrpb* mutant mouse models can be used for understanding CCMS disease mechanism with possible therapeutic targets in the future.

Résumé

SNRPB est un facteur d'épissage majeur et un composant essentiel de toutes les petites ribonucléoprotéines nucléaires (SnRNP). Les patients atteints du syndrome cérébrocostomandibulaire (CCMS) sont porteurs de mutations hétérozygotes, toutes situées dans l'exon 2 alternatif hautement conservé (AE2) de *SNRPB*, qui joue un rôle crucial dans la régulation des niveaux d'expression de *SNRPB*. Les patients atteints de CCMS ont principalement des malformations au niveau craniofacial et des côtes, avec une pénétrance et une expressivité variable. Cependant, les raisons pour lesquelles les mutations de *SNRPB* provoquent ces malformations de manière spécifique demeurent incomprises. Dans ce projet, nous avons tenté de comprendre comment *SNRPB* contribue au développement embryonnaire, en générant une mutation dans *Snrpb* dans un modèle murin. Notre premier modèle murin généré comporte une délétion intronique de 61 paires de bases près de l'exon alternatif régulateur 2 (AE2) dans *Snrpb*. Les souris mutantes présentent des anomalies embryonnaires au niveau du crâne, du visage, des côtes et des membres, avec une très faible pénétrance. Ceci suggère que la région de l'intron 2 que nous avons supprimée est importante pour la régulation de *SNRPB*. Dans un deuxième modèle murin, nous avons montré qu'une délétion constitutive hétérozygote de *Snrpb* (*Snrpb*$^{+/-}$) est létale dès le 7e jour embryonnaire (E)7.5, empêchant le développement embryonnaire avant la morphogenèse. Par la suite, nous avons tenté de comprendre le rôle de *Snrpb* dans le feuillet intermédiaire de l'embryon, le mésoderme, en utilisant des souris transgéniques *Mesp1-Cre* . Les mutants *Snrpb*$^{mes+/}$ ne naissent pas et ont des anomalies du développement craniofacial et cardiaque, avec une expressivité variable à partir de E9,5. À E14.5, tous les mutants *Snrpb*$^{mes+/-}$ sont anormaux au niveau de la tête et des côtes. De manière intrigante, le cartilage de Meckel, dérivé des cellules de la crête neurale, est plus court chez les mutants *Snrpb*$^{mes+/-}$, ce qui suggère une mauvaise communication cellulaire entre le mésoderme et la crête neurale. Finalement, nous avons utilisé

la lignée murine transgénique *Wnt1-Cre* pour éliminer *SNRPB* des cellules de la crête neurale. Les mutants *Snrpb*$^{ncc+/-}$ ont aussi un développement craniofacial anormal avec une expressivité variable, et meurent entre E17.5 et peu après la naissance. De plus, nous avons démontré une augmentation de la mort cellulaire dans les têtes des mutants à E9.5, ainsi qu'une augmentation de l'expression de P53 nucléaire comparativement aux souris de type sauvage. L'analyse RNAseq de l'ARN isolé des têtes des embryos mutants à E9.0 a révélé une augmentation de la voie P53 et des changements significatifs dans l'épissage des gènes. Plus spécifiquement, nous avons trouvé une augmentation du saut d'exon dans deux régulateurs majeurs de P53, *Mdm2* et *Mdm4*. 13 gènes importants au cours du développement craniofacial ayant un épissage aberrant ont été identifiés et validés par RT-PCR, parmi lesquels les facteurs de transcription *Smad2*, *Pou2f1* et *Rere*. De plus, nous avons démontré une expression aberrante de gènes clés du développement craniofacial tels que *Fgf8*, *Shh* et *Msx2* chez les mutants *Snrpb*$^{ncc+/-}$ par hybridation *in situ*. Nos résultats suggèrent que les changements d'épissage dans les gènes clés du développement ainsi que l'augmentation de la mort cellulaire médiée par P53 provoquent un développement craniofacial anormal chez les mutants *Snrpb*$^{ncc+/-}$ et probablement chez les patients atteints de CCMS. Dans l'ensemble, nous avons prouvé qu'un niveau d'expression normal de *SNRPB* est essentiel au bon développement embryonnaire et nous pensons que nos modèles de souris mutantes *Snrpb* peuvent être utilisés pour comprendre le mécanisme de la maladie CCMS et potentiellement identifier des cibles thérapeutiques à l'avenir.

Detailed table of contents

CHAPTER II

List of abbreviations

A3E	Alternative 3′ss exons
A5E	Alternative 5′ss exons
AE2	Alternative exon 2
AS	Alternative splicing
ASD	Aorticopulmonary septal defect
BABB	benzyl alcohol: 2 benzyl benzoate
BP	Branch point
CBC	Complete blood count
CCMS	Cerebrocostomandibular syndrome
cDNA	Complementary DNA
CFTR	Cystic fibrosis transmembrane conductance regulator
CNCC	Cranial neural crest cell
COG1	Component of Oligomeric Golgi Complex 1
CT scan	Computed tomography scan
CWC27	CWC27 Spliceosome Associated Cyclophilin
DAB	3,3′-Diaminobenzidine
DAPI	4′,6-diamidino-2-phenylindole
ddH2O	Double distilled water
DEA	Differential expression analysis
DEAD box	asp-glu-ala-asp helicase
DGE	Differential gene expression
DLX5	Distal-less homeobox 5
DMD	Duchenne muscular dystrophy
DNA	Deoxyribonucleic acid

DSBs	Double strand breaks
DSE	Differentially spliced exon
E	Embryonic day
EFTUD2	Elongation factor Tu GTP binding domain containing 2
EMT	Epithelial mesenchymal transition
ESE	Exonic splicing enhancer
ESS	Exonic splicing silencer
EXIT	Ex-utero intrapartum treatment
FDR	False discovery rate
FEZ	Frontonasal ectodermal zone
FGF8	Fibroblast growth factor 8
FNP	Frontonasal prominence
GCPS	Greig cephalopolysyndactyly syndrome
GFP	Green fluorescence protein
gRNA	Guide RNA
hnRNPs	Heterogeneous ribonucleoprotein particles
HPE	Holoprosencephaly
HRP	Horse redox peroxidase
IF	Immunofluorescence
IR	Intron retention
ISE	Intronic splicing enhancer
ISH	in situ hybridization
ISS	Intronic splicing silencer
IUGR	Intra uterine growth retardation
KEGG	Kyoto Encyclopedia of Genes and Genomics

KOH	Potassium hydroxide
lncRNA	Long non-coding RNA
$MgCl_2$	Magnesium chloride
MDM2	Double minute 2 protein
MDM4	Double minute 2 protein
mRNA	Messanger RNA
MX	Maxilla
MXE	Mutually exclusive exon
NCC	Neural crest cell
NMD	Non-sense mediated decay
OH	Hydroxyl group
P53	Tumor protein 53
PAGE	Polyacrylamide gel electrophoresis
PBS	Phosphate buffer saline
PBS	Protein binding site
PCR	Polymerase chain reaction
PFA	Paraformaldehyde
PHH3	Phosphorylated histone 3
PMX	Premaxilla
PRS	Pierre Robin sequence
PTA	Phosphotungstinic acid
PTC	Pre termination codon
PUF60	Poly(U) binding splicing factor 60
RBC	Red blood cell
RBPs	RNA binding proteins

RIPA	Radioimmunoprecipitation assay buffer
RNA	Ribonucleic acid
RNP	Ribonucleoprotein
RNU4ATAC	RNA, U4atac small nuclear (U12-dependent splicing)
RT-PCR	Reverse transcription-Polymerase chain reaction
RT-qPCR	Reverse transcription quantitative real-time PCR
SE	Skipped exon
SEM	Standard error of mean
SF1	Splicing factor 1
SF3B4	splicing factor 3b subunit 4
SHH	Sonic Hedgehog
SnRNA	Small nuclear RNA
SnRNP	Small nuclear ribonucleoprotein
SNRPB	Small nuclear ribonucleoprotein polypeptides B and B2
SOX10	SRY-Box Transcription Factor 10
SR protein	Serine-arginine protein
SS	Splice site
STAR	Spliced Transcripts Alignment to a Reference
TCS	Treacher Collin Syndrome
TE	Transposable element
TGF	Transforming growth factor
TUNEL	Terminal deoxynucleotidyl transferase dUTP nick end labeling
TXNL4A	Thioredoxin Like 4A
UTR	Untranslated region
WBC	White blood cell

WMISH	Wholemount *in situ* hybridization
WT	Wildtype
Δ-46	Deletion 46
Δ-61	Deletion 61
gm	Gram
Kg	Kilogram
mL	Milliliter
L	Liter
pg	Picogram
µg	Microgram
µm	Micrometer
µL	Microliter

List of Figures

List of Tables

Acknowledgements

First and foremost, I am grateful to my Almighty creator who bestowed me with the health, energy, patience and courage to come to this point today and blessed me to work under the supervision of a wonderful scientist, dedicated teacher, a true guide and above all amazing human being, Dr. Loydie A. Jerome-Majewska. It was a huge step for me to start my PhD coming all the way from Bangladesh with two toddlers. But Loydie's guidance made it possible what I have accomplished in my research last few years. She was always there to help me with the process of learning new things to become a better researcher every day. Loydie taught me how to find positivity in failures and encouraged me to think with a deeper scientific mind that helped me to move another step ahead in research. The time I spent with her in her office for our regular meetings was always precious and I learned something new every time I walked out from there. Also, our conversation on Philosophy of life is something that I will really miss. I will be forever grateful for her kind words that comforted me when I was pregnant two times during my PhD. I struggle to put into words the significant impact she has had in my life. She sowed a seed in me to dream and work for contributing to science for the rest of my life. Loydie is the best mentor I have ever had and the mentorship she provided is a gift that will go on for many lifetimes. Loydie, my time in your lab is something that I will cherish forever!

At the same time, I am deeply indebted to my co-supervisor Dr. Jacek Majewski, a very kind and wonderful person who could teach me complex science in easy ways. I am thankful to him for guiding my project with his mesmerizing depth of knowledge, especially for the RNAseq part. I will be always grateful to Jacek for referring me to Loydie's lab for my PhD.

I appreciate my supervisory committee members Dr. Collin Crist and Dr. Marie Kmita for their scholastic guidance in my project. I really feel myself lucky to have them in my committee.

I also acknowledge Dr. Aimee K Ryan and Dr. Indra Gupta for their suggestions and critical questions in the joint lab meetings that made me a better presenter over time.

Majewska lab had become my second home and people in the lab became like family. I learned several lab techniques from my senior graduate students, Dominic and Vafa in the early days of PhD. I thank Wesley for showing me paraffin sectioning. I am especially grateful to Nadine, Shruti and Yanchen for helping me with project during the pandemic and my postpartum period. I feel really lucky to have such lovely friends to work with! I also heartedly appreciate my friend Rachel for her positive thoughts about me that was always a motivation. Dr. Jean-Francois Boisclair Lachance also deserves thanks for inspiring me. The person who had the most significant role in the lab is none other than Dr. Marie-Claude Beauchamp. She was not only the person who gave me hands-on training and suggestions for many experiments but was more the dearest friend and like a sister who was always there to support me. I will be grateful to her forever for helping me in so many ways and translating the thesis abstract to French is just one of them.

I want to express my gratitude to Dr. Mitra Cowan from Transgenic Core Facility of McGill University, for doing all the microinjections for genome editing in mice.

I sincerely thank dear Mr. Ross Mackay, Student affairs advisor of the Human Genetics Department for his help since my first step at the department until today. I also appreciate Mrs. Rimi Joshi, Student affairs administrator of the department for her prompt support each time I asked for. Ross and Rimi, I really respect the way you cooperated me!

I acknowledge the funding authorities: Queen Elizabeth Scholarship, RI-MUHC and McGill Faculty of Medicine and Health Sciences for making my journey smooth.

I left behind countless well-wishers that includes family members, relatives, friends, and teachers when I took the flight from Bangladesh to Montreal. I thank all of them for inspiring

me for my PhD. My special appreciation goes to my beloved five sisters and three brothers-in-law for their continuous encouragements.

I extend my gratitude to my parents Dr. M. Shafiqul Alam and Rawshan Ara Haque, who are the reason of all the successes that I achieved in my life. I know, they counted every single day last more than five years to see me and my family again and I cannot wait to meet them as a proud daughter. Today, I also mournfully remember my late parents-in law Nargis Akhter and Md. Nurul Islam, whom I lost during my PhD. I know they would be two of the happiest people to see me as Dr. Alam.

Finally, the hardest part is to thank Dr. Abu Shadat Mohammod Noman, an incredibly kind and wonderful person I am very lucky to have as my husband. Noman, this day would never come without your unbound patience, sacrifice, support, care and love and there are no words that adequately describes my gratitude to you.

I feel the same way for my four young children; Nibras, Nora, Nuraisha and Yusuf, who deserve an immense amount of gratitude for the ways they helped me with what I am putting together today. My champs, I promise that soon I will give you more time and will take better care of you. I am sure, you will be very proud of your mom and yourselves one day!

Contribution to original knowledge

This thesis demonstrates a novel discovery that normal levels of core spliceosomal factor, SNRPB (SmB/B´), is required for proper embryonic development. It also describes the first mouse model for the rare congenital disorder Cerebrocostomandibular syndrome (CCMS). Heterozygous mutations in *SNRPB* are associated with CCMS in humans and it was thought that an overall decrease of SNRPB protein levels were responsible for the abnormalities that include mostly craniofacial and rib defects in CCMS patients. In this study, I show that reducing SNRPB levels in the whole embryo is detrimental for embryonic development before organogenesis and heterozygous removal of *Snrpb* from neural crest cells can cause abnormal craniofacial development due to aberrant splicing, primarily exon skipping. Moreover, my study revealed increased exon skipping in 13 key genes for craniofacial development and embryonic misexpression of crucial genes for facial morphogenesis: *Shh, Fgf8* and *Msx2*. Furthermore, my work in the mouse model provides supports that P53 associated cell death does not drive the craniofacial malformations in CCMS. This work has been published: ***Snrpb is required in murine neural crest cells for proper splicing and craniofacial morphogenesis.*** Dis Model Mech. 2022 Jun 1;15(6). doi: 10.1242/dmm.049544. In addition to neural crest cells, I also demonstrated for the first time that heterozygous *Snrpb* mutations in the mesodermal cell lineage causes craniofacial, cardiac and rib anomalies. Though *SNRPB* mutations were suggested to cause intramembraneous bone ossification in CCMS patients, I demonstrate that both endochondral and intramembraneous ossifications are disturbed in the *Snrpb* mutant embryos. Finally, I have demonstrated that a novel mutation of 61 base-pair in intron 2 of *Snrpb* is important in regulating SNRPB, which may lead to a better understanding of the regulation of this gene and a possible genetic detection of CCMS patients, who were not found to have mutations in *SNRPB* exons.

Format of the thesis

This thesis is in the traditional monograph style, which follows the "Guidelines for Thesis Preparation" of the Faculty of Graduate Studies and Research at McGill University. The thesis consists of six chapters. Chapter one is an introduction and literature review that presents the background material for this thesis and states the questions, hypothesis and aims of my research. Chapter two describes the materials and methods that were used in my project. Chapter three contains the results, and consists of two parts: in part A, the generation of CCMS mouse models with heterozygous mutations in *Snrpb* and their characterizations are described and in part B, the transcriptomic analysis of *Snrpb* mutants, specific for craniofacial malformations, is shown. A manuscript describing SNRPB's role in neural crest cells for craniofacial development has been published. Chapter four comprises a detailed discussion of my findings. Chapter five has the concluding summary and future directions. References mentioned throughout the thesis are in the last chapter.

Contribution of authors

Several authors have contributed variably for the results described in Chapter III

A. For results in Aim 1

The studies for *Snrpb* Δ61 mutation, *Snrpb* constitutive knock out and the mesoderm specific *Snrpb* knock out, Sabrina Alam performed all the experiments and analyzed the data. For the neural crest specific *Snrpb* knock out study, Marie-Claude Beauchamp performed 2H3 immunostaining (Figure 3.16), P53 immunohistochemistry (Figure 3.22 E-F) and the analysis, Alexia Boucher performed the proliferation and apoptosis analysis (Figure 3.19); Nadine Nzirorera reanalyzed the skeletal preparations of $Snrpb^{ncc+/-}$ mutants (Figure 3.15 A-B) in addition to Sabrina Alam. Sabrina Alam performed all other experiments done in the study.

B. For Results in Aim 2

Eric Bereke, Reinnier Padilla and Si Jing Zhang analyzed all the RNA sequencing data (Figures 3.20 and 3.21), Shruti Kumar performed RT-qPCR experiments and analyses (Figures 3.7 C and 3.22 A-D). Yanchen Dong analyzed the P53 homozygous knock down study at the postnatal stages (Figure 3.23 E), Alexia Boucher performed several *in-situ* hybridization experiments (Figure 3.25) in addition to Sabrina Alam. Sabrina Alam performed and analyzed all other experiments done in the study.

All the microinjections to introduce *Snrpb* mutations were done by Dr. Mitra Cowan, McGill Integrated Core for Animal Modeling (MICAM).

Dr. Loydie A. Jerome-Majewska coordinated all aspects of the project. Dr. Jacek Majewski supervised and coordinated the splicing portion of the work described.

CHAPTER 1

INTRODUCTION AND LITERATURE REVIEW

1.1 Cerebrocostomandibular syndrome (CCMS)

1.1.1 CCMS is a rare disorder caused by mutations in *SNRPB*

Cerebrocostomandibular syndrome (CCMS, OMIM # 117650) is a rare congenital disorder that occurs in one in a million births, where patients mostly have micrognathia and posterior rib gap defects. CCMS was first reported in 1966 by Smith *et al.* and to date, around 80 cases have been reported in literature where males and females are equally found to be affected. The syndrome is inherited in an autosomal dominant fashion with the mutation occurring in a major splicing factor gene called *SNRPB*. CCMS patients share craniofacial conditions that are like Pierre Robin sequence (PRS), which presents a triad of micrognathia, glossoptosis, and airway obstruction (Carey *et al.*, 1982; Gangopadhyay *et al.*, 2012; Logjes *et al.*, 2018; Giudice, *et al*., 2018; Baxter and Shanks, 2022). However, the classic rip gap defects make CCMS stand out as an independent syndrome.

The first report of *SNRPB* mutations in CCMS patients was published in 2014 by a combination of whole exome and Sanger sequencing. Of 14 CCMS patients with micrognathia and posterior rib gaps, one was negative for sequence or copy-number variants in the coding regions and UTRs of the *SNRPB* gene (Lynch *et al.*, 2014). Soon after that, in five unrelated French patients with CCMS, Bacrot *et al.* (2015) identified heterozygosity for four missense mutations in the *SNRPB* gene. Later, Tooley *et al.* (2016) examined 16 patients with CCMS, including eight patients who were previously studied (Lynch *et al*., 2014; Watson *et al*., 2014; Ramaswamy *et*

al., 2016) and reported *SNRPB* mutations in eight of the nine patients with no previous reports of mutation. The findings suggest that in most cases, CCMS is caused by *SNRPB* mutations.

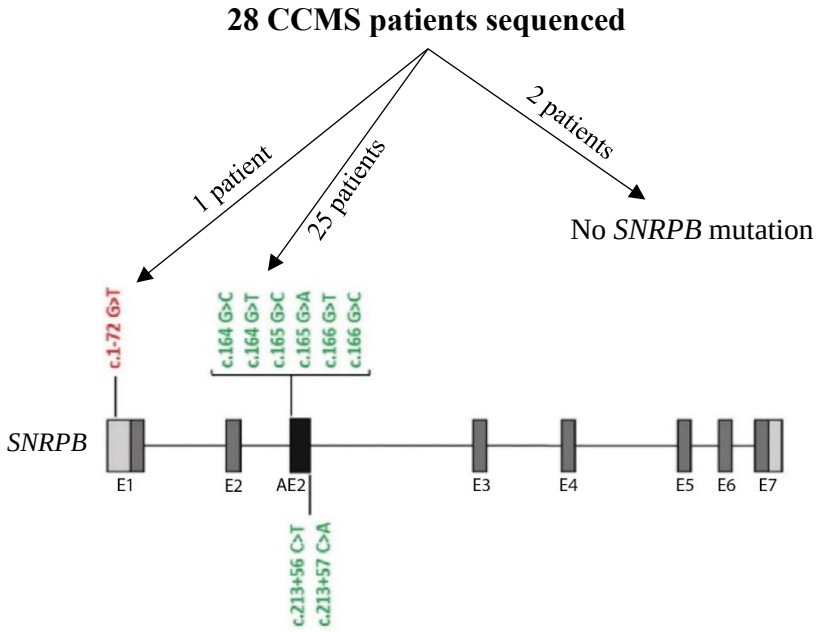

Figure 1.1: ***CCMS is caused by mutation in SNRPB; a graphical representation of all point mutations reported in the gene.*** The exons (E1-E7) of *SNRPB* are shown as rectangular boxes. The point mutations found in the majority of patients lie within the alternative exon 2 of the gene (exon in black, mutations in green fonts). One patient had a mutation in the 5'UTR shown in red font, whereas two patients had no mutation in the allele (Ref: Lynch *et al.*, 2014; Bacrot *et al*., 2015; Tooley *et al*., 2016; Beauchamp *et al*., 2020).

Almost all CCMS patients had point mutations in a highly conserved alternative exon 2 of *SNRPB,* that plays a critical role in regulating *SNRPB* levels. Mutations were mostly clustered in the exonic splicing silencer (ESS) region (Lynch *et al.*, 2014*;* Bacrot *et al., 2015;* Tooley *et al., 2016*). Only one case of CCMS, a fetus had a 5'-UTR mutation of *SNRPB* (Figure 1.1), creating a new initiation codon possibly resulting in truncated protein and a loss of function

(Lynch *et al.*, 2014). The alternative exon 2 in *SNRPB* has a pretermination codon (PTC) and its inclusion in the *SNRPB* transcript causes nonsense mediated decay (NMD) of the transcript. It was shown in patients' fibroblasts that mutations in alternative exon 2 cause an increased inclusion of this deleterious exon. This results in a rise in the levels of the transcript that goes through NMD, which is thought to lead to the overall decrease in SNRPB protein (Lynch *et al.*, 2014). However, no further reports have shown how much *SNRPB* protein is made in CCMS patients.

1.1.2 Clinical features of CCMS patients

CCMS is mainly characterized by craniofacial malformations such as a smaller mandible and costovertebral developmental anomalies (Figure 1.2). About 80-99% of patients reported so far have mandibular hypoplasia or micrognathia, cleft palate and rib anomalies such as rib gap defects, a bell-shaped thorax, and broken or discontinuous ribs, and in severe cases, complete absence of the rib cage (Lynch *et al.*, 2014, Bacrot *et al.*, 2015, Tooley *et al.*, 2016). Malformations of ribs and rib cage at birth along with micrognathia to cause respiratory distress and feeding difficulties. Respiratory difficulties lead to generalized cyanosis and potential hypoxic brain injuries that may be responsible for intellectual disability (30-79%) sometimes observed later. Patients also have anomalies involving the middle ear defects, leading to hearing loss. Cardiac defect such as aorticopulmonary septal defect (ASD), which might lead to persistent truncus arteriosus, are also reported in some CCMS patients (Table 1.1).

Intrauterine growth retardation and low birth weights are also reported in 30-79% of CCMS neonates. Those patients who survive infancy may suffer from growth retardation, scoliosis, reduced lung capacity, dental anomalies and feeding problems later in life. Though CCMS is characterized by mandibular hypoplasia and rib gap defects, CCMS patients exhibits additional organ abnormalities to a lesser extent. The severity of CCMS abnormalities is highly variable (Ibba *et al.*, 1997; Van den Ende *et al.*, 1998; James and Aftimos, 2003; Abdalla *et al.*, 2011;

Lynch *et al.*, 2014; Bacrot *et al*., 2015; Tooley *et al.*, 2016; Hameed *et al.*, 2018), a feature known as variable expressivity.

A concise list of the abnormalities seen in CCMS is given below. Though several reports have been published describing CCMS patients' abnormalities (Ibba *et al.*, 1997; Van den Ende *et al.*, 1998; James and Aftimos, 2003, Abdalla *et al*., 2011, Hameed *et al.*, 2018), the table here represents only the patients who were sequenced for *SNRPB* (Lynch *et al.*, 2014; Bacrot *et al*., 2015; Tooley *et al.*, 2016).

Table 1.1: ***Prevalence of clinical features reported in CCMS***. *****28 patients were reported by Lynch *et al.* (2014), Bacrot *et al*. (2015) and Tooley *et al.* (2016). Number of patients observed are variable as all 28 patients were not screened for every anomaly listed here. (Adapted from Beauchamp *et al*., 2020).

Anomalies in different tissues	**Number of patients with abnormalities/ number of patients observed***
Craniofacial abnormalities	
- Mandibular hypoplasia/micrognathia	27/28
- Malar hypoplasia	2/13
- Cleft palate/ bifid uvula	14/24
- Cleft lip	1/16
- Hearing loss	13/28
- Eye anomalies	1/13
Psychomotor delay	3/21
Spline and thorax defects	
- Scoliosis	11/28
- Rib anomalies	23/28
- Bell-shaped/ narrow thorax	15/24
Intrauterine growth retardation (IUGR)	6/14
Congenital heart defect (ASD)	3/16
Anal stenosis	1/13
Abnormal shaped kidney	3/16
Gastroesophageal reflux disease	4/16

Figure 1.2: ***CCMS patients mostly have craniofacial abnormalities and rib gap defects.*** CCMS patients are commonly reported with craniofacial anomalies, mainly micrognathia (smaller lower jaw), which is shown in the left two panels. The other prevalent abnormalities include rib defects that mostly include posterior rib gap defects (shown in the CT scan on the far right). The patient in the middle has both craniofacial and rib defects (Adapted from Tooley *et al*., 2016)

1.1.3 Management and prognosis CCMS

CCMS patients are treated based on their symptoms, which requires a collaborative network of health care professionals. Pediatricians, surgeons, and physicians who diagnose the disease, pulmonologists that treat abnormalities of the lungs, audiologists to assess and treat hearing problems, speech pathologists, and other health care professionals may need to work together to plan a child's treatment (www.rarediseases.org). The survival of patients with CCMS mostly relies on repeated surgical interventions. Craniofacial anomalies leading to breathing and feeding difficulties are usually immediately addressed. Hypoxia is the first issue with CCMS that can be lethal. Thus, CCMS babies with narrow rib cages and breathing difficulties are often considered for tracheostomy (Abdallah *et al.*, 2011; Ramaswamy *et al.*, 2016; Tooley *et al.*,

2016). CCMS has a very poor prognosis. Prognosis mainly depends on the severity of the anomalies. The most severe forms are often fatal within the first hours after birth. About 25% of all reported cases are fatal during the first month of life and this correlates significantly with the disease severity. However, with the advancement of surgical interventions, the life expectancy of CCMS patients is increasing. Although initial publications suggested a 50% survival rate after the first year of life, due to great strides in surgical interventions reports now suggest an 80% survival rate (Nagasawa *et al*., 2010; Tooley *et al.*, 2016). Recently, successful Ex utero intrapartum treatment (EXIT) was reported in a CCMS fetus, which would be an effective option for rescuing patients with prenatally diagnosed CCMS and preventing neonatal hypoxia (Ogasawara *et al.*, 2014).

1.1.4 CCMS is a syndrome with an unexplained molecular mechanism

SNRPB makes three transcripts. The first two, which vary only in their UTR length, encodes two protein isoforms: SmB and SmB′ (Saltzman *et al.*, 2011). The third transcript contains an alternative exon 2 of the gene and has a pretermination codon that causes it to undergo NMD. As mentioned earlier, CCMS patients have mutations in the alternative exon 2 of *SNRPB.* In fibroblast cells of CCMS patients, it was shown that there were higher levels of the third transcript, that is supposed to make no *SNRPB* protein (Figure 1.3). In fact, it was also shown through quantitative reverse transcription PCR (qRT-PCR) that mRNA expression of *SNRPB* was reduced in those patients (Figure 1.3). In another study, increased levels of the third *SNRPB* transcript were seen in leukocytes of CCMS patients, with no decrease in the two protein coding transcripts (Bacrot *et al.*, 2015). It is thought that having mutation in the alternative exon 2 thus causes an overall decrease in the level of SNRPB, by making more of the third transcript (Lynch *et al.*, 2014). However, the extent of reduction in *SNRPB* protein levels was never shown in CCMS patients.

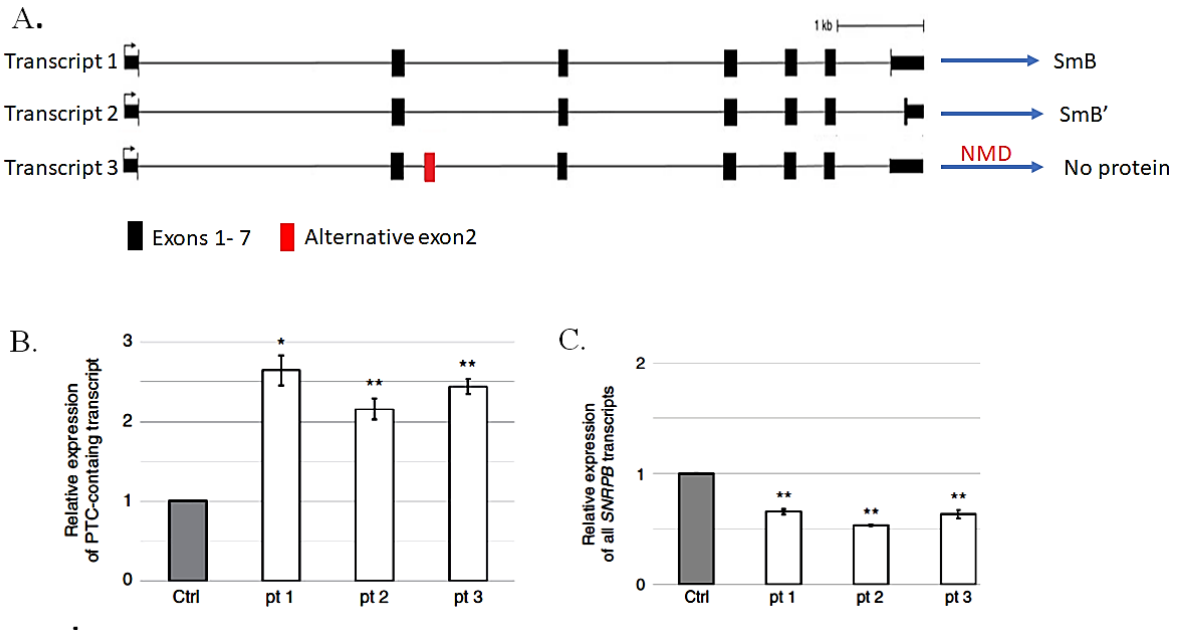

Figure 1.3: ***Mutation in alternative exon 2 of SNRPB causes increase inclusion of that exon and overall decrease of SNRPB transcript.*** (A) *SNRPB* makes three transcripts. Transcripts 1 and 2 differ in the length of their 3′ UTRs and encode SNRPB isoforms: SmB and SmB′, respectively. The third transcript includes a pre-termination codon (PTC) containing alternative exon 2 (shown as red box) that undergoes nonsense mediated decay (NMD). (B) CCMS patients produce more of the third transcripts in their fibroblasts. (C) Reduction in *SNRPB* expression at the mRNA level was also observed in those cells. (Adapted from Lynch *et al*., 2014)

It is speculated that reduction in SNRPB levels causes CCMS anomalies, but this remains to be addressed. As SNRPB is a common splicing factor that is required in all cell types, it is expected that reduction of SNRPB would affect the developmental process of different tissues or systems equally.

Thus, the following questions remain to understand CCMS etiopathology:

1. Does a reduction of SNRPB protein levels cause CCMS deformities? Do CCMS patients have *SNRPB* mutations that create null alleles?
2. If there is a general reduction of SNRPB levels in all cells, then why are craniofacial tissues and rib cages the most prevalently affected in CCMS?
3. CCMS patients are reported to have variable penetrance and expressivity of their abnormalities. What causes this variable expressivity of anomalies found in the same tissue such as in the craniofacial region?

All of these questions leave CCMS as a molecularly unexplained syndrome, which I addressed in my thesis objectives.

In the next section I will give a general background information of mRNA splicing. SNRPB is a core component of the splicing machineries and regulates alternative splicing of the pre-mRNA (Kambach *et al.*, 1999; Correa *et al.*, 2016; Liu *et al.*, 2019). Several reports demonstrated that knockdown of *SNRPB* causes aberrant splicing (Correa *et al.*, 2016; Van Alystene *et al.*, 2018; Liu *et al.*, 2019; Zhan *et al.*, 2020).

1.2 Introduction to alternative RNA splicing and splicing machinery

1.2.1 Overview of alternative splicing

Alternative splicing is the process where different combinations of splice sites within messenger RNA (mRNA) precursors can produce variably spliced mRNAs. It is a fundamental regulatory step of gene expression as the multiple mRNAs generated from a single gene can encode proteins that are variable in their sequences and activities. Though the first evidence of alternative splicing coincided with its discovery in adenovirus transcript (Chow *et al.*, 1977), alternative splicing is prevalent in higher eukaryotes and it enhances their complexity by increasing the number of unique proteins expressed from a single gene (Nilsen and Graveley,

2010). It is estimated that 95% of human genes are alternatively spliced, producing at least two alternative isoforms, demonstrating a central role of alternative splicing in normal biology (Pan *et al.*, 2008).

Four splice signals are essential for accurate splicing: 5′ and 3′ splice sites (5′ss and 3′ss), the polypyrimidine tract, and the branch site sequence (Figure 1.4). However, these signals cannot solely select the proper splice site and splicing. Regulatory sequences such as exonic splicing enhancers and silencers (ESEs and ESSs, respectively) and intronic splicing enhancers and silencers (ISEs and ISSs, respectively) (Figure 1.5) to which proteins can bind can enhance or repress splicing. There are two major splicing factor RNA binding proteins (RBPs) that modulate splicing: heterogeneous ribonucleoprotein particles (hnRNPs) and serine-arginine (SR) proteins. Based on their binding locations, these two RBPs have opposite enhancing and repressive qualities (Martinez-Contreras *et al.*, 2007; Bradley *et al.*, 2015). For example, binding of SR proteins to splicing enhancers can promote the use of suboptimal splice sites and can mediate exon inclusion. On the other hand, binding of members of the hnRNP family to splicing silencers can promote exon skipping and in addition, hnRNPs can also have the opposite effect, depending on the location of their binding sites relative to the regulated splice sites, which greatly widens their regulatory potential (Martinez-Contreras *et al*., 2007; Erkelenz *et al.*, 2013; Bradley *et al*., 2015; Geuens *et al*., 2016).

In alternative splicing, some exons are constitutively spliced—that is, they are present in every mRNA produced from a given pre-mRNA—many are alternatively spliced to generate variable forms of mRNA from a single pre-mRNA species. Alternative splicing commonly occurs in five main types: *Exon skipping,* or *cassette exon* is the most prevalent pattern (around 30%) in vertebrates and invertebrates, where an exon may be spliced out of the primary transcript or retained (Figure 1. 5). Unbalanced exon skipping is known to cause human diseases (Tazi *et*

al., 2009). However, rapidly emerging knowledge of splicing aberration in diseases along with mechanisms of splicing are opening doors for new therapeutic approaches. For example, induced exon skipping has recently emerged as a therapy to treat Duchenne Muscular Dystrophy, by converting out-of-frame mutations to in-frame mutations in *DMD* (Gushchina, 2021).

In *alternative donor site selection of 5'splice site* and *acceptor 3' splice site* splicing events, part of the exon is alternatively included or excluded in the mRNA. Alternative 3′ss exons (A3Es) and 5′ss exons (A5Es) account for ~18% and ~8% of the human and mouse conserved events, respectively (Koren *et al*., 2007). These splicing events are found to be linked to several diseases and generated by mutations causing aberrant splicing (Faustino and Cooper, 2003).

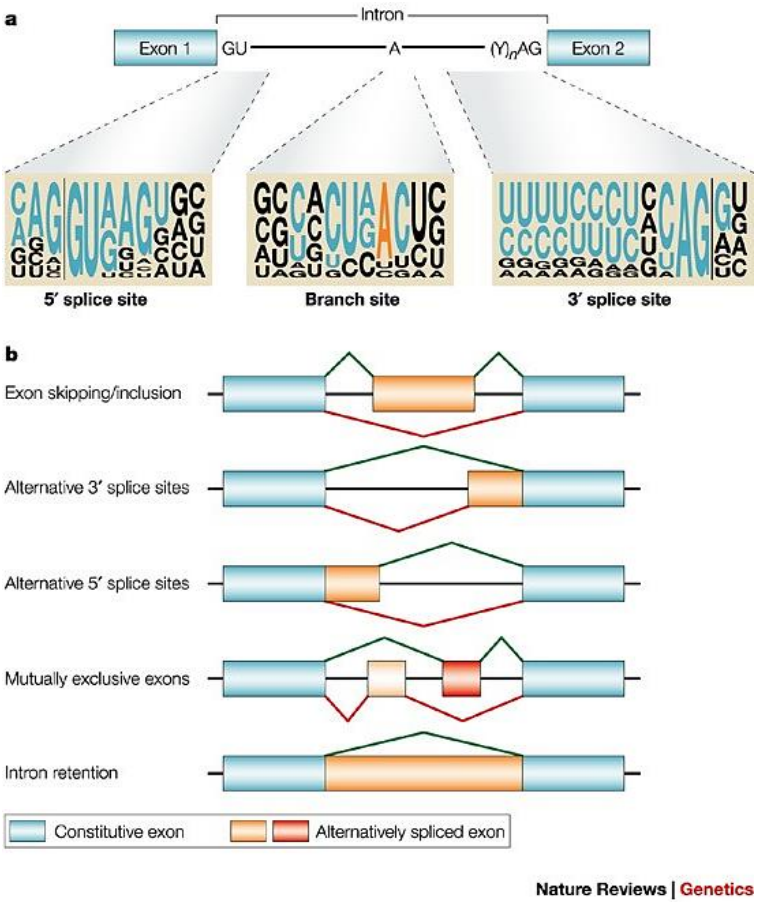

Figure 1.4: ***Different types of alternative mRNA splicing in eukaryotes.*** a. Conserved motifs at or near the intron ends showing the 5' and 3' splice sites and the polypyrimidine tract $(Y)_n$ and the A residue that serves as a branchpoint are shown in a two-exon pre-mRNA. The sequence motifs that surround these conserved nucleotides are shown below. b. Five common modes of alternative splicing. In each case, one alternative splicing path is indicated in green, the other path in red. The last type is showing intron retention corresponding to no splicing. (Adapted from Cartegni, 2002).

Another type of alternative splicing is *the mutually exclusive exon* (MXE) that represents a rare subtype (Pohl *et al.*, 2012). Mutually exclusive exons are characterized by splicing of exons that occur in a coordinated manner, where two or more splicing events are not independent. As the name "mutually exclusive" indicates, exactly one out of two exons (or one group out of two exon groups) is spliced out, while the other one is retained. MXEs are significantly

enriched in pathogenic mutations (Hatje *et al.*, 2017) and current evidence suggests that mutually exclusive exons only occur in pairs in vertebrates (Matlin *et al.*, 2005).

Finally, *intron retention*, where introns are retained in mature mRNAs, is the profound alternative splicing type in metazoans. In mammals, it was shown that as many as three-quarters of multi-exonic genes undergo intronic retention events (Merkin *et al.*, 2012; Braunschweig *et al.*, 2014; Monteuuis *et al.*, 2019). In human transcripts, it is associated with weaker splice sites, short intron length and the cis-regulatory elements.

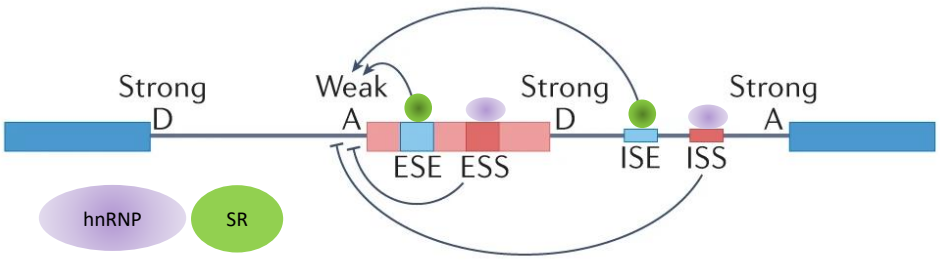

Figure 1.5: ***Schematic presentation of cis-acting elements that bind to pre-mRNA to regulate splicing.*** The enhancer or silencer sequences control the inclusion of the cassette exon (rose color) with weak or suboptimal 3'splice site (A). Promotion of the use of the weak acceptor A will result in the inclusion of the exon, whereas repression of using acceptor A will lead to inhibition of its inclusion in the transcript. The SR proteins and the hnRNPs bind to the enhancer and silencer sequences, respectively to mediate the splicing regulation. ESE, exonic splicing enhancer; ESS, exonic splicing silencer; ISE, intronic splicing enhancer; ISS, intronic splicing silencer, A, acceptor site; D, donor site; hnRNP, Heterogeneous ribonucleoprotein particles; SR, serine-arginine proteins. (Modified from Marasco and Kornblihtt, 2022)

1.2.2 Splicing requires collaborative participation of spliceosomal complexes

The splicing process requires the action of a series of large and dynamic ribonucleoprotein (RNP) complexes comprising the spliceosome (Figure 1.6). The spliceosomes are some of the most complex macromolecules in eukaryotic cells consisting of as many as 300 different proteins (Jurica *et al*., 2002). Around 99% of splicing events in humans are catalyzed by the major spliceosome that is made up of five small nuclear ribonucleoproteins (snRNPs): U1, U2, U4, U5, and U6. Each of the constituent RNP complexes are centered around a small RNA molecule (Frederick *et al.*, 2015). This RNA serves as a scaffold for a set of 'core' proteins present in each complex, as well as additional complex-specific proteins. The U1 SnRNP that attaches to the 5' splice site motif and the splicing factor SF1 that binds to the branch-point sequence just upstream of the 3'splice site initiates the splicing process. An auxiliary splicing factor named U2AF65 binds to the polypyrimidine tract and interacts with SF1. This interaction facilitates identification of the surrounding BPS by SF1 (Berglund *et al*., 1998). The U2 SnRNP displaces SF1 which is catalyzed by the RNA helicases Prp5 and Sub2. Prp5 helps with the base pairing interaction by binding to U2 and stabilizes the branch-point-interacting-stem-loop, that base pairs with the intron (Liang and Cheng, 2015). Sub2 acts to stabilize the interaction between the RNA branch point and the U2 subunit (Frederick *et al.*, 2015).

The U4, U5 and U6 tri-SnRNP forms the pre-catalytic spliceosome (Complex B). The DEAD-box helicase Prp28 catalyzes this process and releases the U1 SnRNP. The pre-catalytic spliceosome goes through a series of conformational changes forming the activated B spliceosome, where U2 and U4 subunits are released. Other RNA helicases such as Prp2 act to destabilize the RNA core of the spliceosome to catalyze the conformational change from the B complex to the C complex. The C complex subsequently causes the splicing event to occur. First, U2 associated protein complexes SF3a and SF3b are released, thus exposing the branch-point site that allows a nucleophilic attack by the branch-point 2'-OH group on the 5'SS. Then

the cross linking of U5 and U6 snRNPs happens, which is mediated by Prp8 protein. The 3'-OH of the 5' exon attacks the 3'SS, and the remaining snRNPs and associated factors are disassembled, the exons are joined together, and the intron lariat is released. Though most of the intron lariats are degraded in seconds to minutes, it was also shown that many of them are exported to the cytoplasm. In the cytoplasm, these exported intron lariats remain as stable circular molecules (Talhouarne *et al*., 2018).

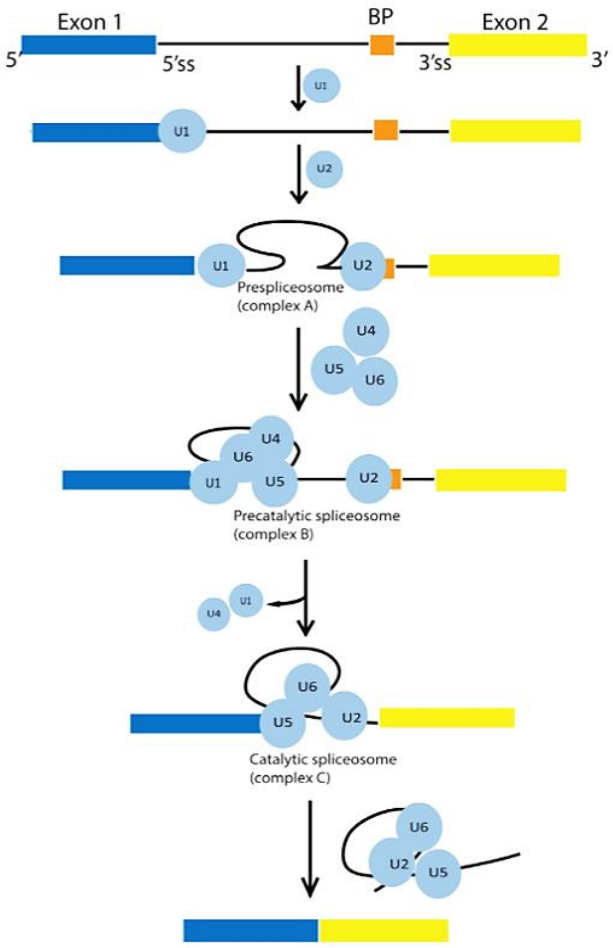

Figure 1.6: ***Simplified schematic representation of the mRNA splicing process*****.** Splicing requires participation of the small nuclear ribonucleoproteins (SnRNPs) U1-U6, shown in light blue circles. The spliceosomal proteins act in a stepwise manner to bind to specific sequences. The catalytic action of the protein complexes causes two step transesterification reactions that subsequently joins the exons, and the intron is removed as lariat at the end step of the process. (Adapted from Beauchamp *et al*., 2020)

1.2.3 Spliceosomal mutations can result in human diseases

Mutations in genes encoding for splicing proteins can cause diseases referred to as spliceosomopathies. Though splicing factors are expressed ubiquitously, in most cases of splieceosomopathies, a single tissue or cell type is predominantly affected. The range of affected tissues is as diverse as the retina, hematopoietic lineage, craniofacial skeleton, spinal cord, and limbs. Among the diseases that occur due to spliceosomal mutations, a group of them preferentially presents with craniofacial abnormalities. In these craniofacial spliceosomapathies, the skeletal elements are primarily derived from the neural crest, an embryonic cell group that contributes significantly to craniofacial development (Lehalle *et al.*, 2015; Beauchamp *et al*., 2020; Griffin and Saint-Jeannet, 2020). Although craniofacial spliceosomapathies are rare, they represent around one-third of the congenital abnormalities seen in live births mortalities (Trainor and Andrews, 2013) and fall under the umbrella of craniofacial dysostosis.

There are several craniofacial syndromes that are associated with spliceosomal mutations (Verheij *et al.*, 2009; Lines *et al.*, 2012; Bernier *et al.*, 2012; Favaro *et al.*, 2013; Wieczorek *et al.*, 2014; Xu *et al.*, 2017; Beauchamp *et al.*, 2020). Mutation in PUF60 has been linked to Verheij syndrome (Verheij *et al.*, 2009). Mutation in a component of the U5 spliceosome, *EFTUD2*, causes mandibulofacial dysostosis where patients have craniofacial malformations (Lines *et al.*, 2012). Mutations in *SF3B4*, a U2 component, are associated with Nager syndrome. Nager syndrome patients exhibit micrognathia, radial hypoplasia and limb defects (Bernier *et al.*, 2012). Similarly, mutations in exon junction core component, *EIF4A3* are known to cause Richieri-Costa-Pereira syndrome, which is also an acrofacial dysostosis disorder *(*Favaro *et al.,* 2013). Mutation of another U5 component, *TXNL4A,* causes Burn-McKeown syndrome *(*Wieczorek *et al.*, 2014). Mutation in snRNA *RNU4ATAC* can also result in head and craniofacial malformations (Farach, 2018). Moreover, mutations in accessory

proteins of the spliceosome such as *CWC27* are associated with retinitis degeneration to severe craniofacial specific syndromes (Xu *et al.,* 2017).

The proposed underlying mechanisms of spliceosomopathies is that the mutation in these splicing proteins abrogates the protein-protein or protein-RNA interactions within the spliceosomal complexes. These interrupted interactions result in the generation of aberrantly spliced transcripts, which are specifically required for one cell type or another.

1.2.4 *SNRPB* and its role in splicing machinery

1.2.4.1 SmB and SmB'

The *SNRPB* (Small nuclear ribonucleoprotein polypeptides B and B2) gene encodes the core protein for U1, U2, U4/U6, and U5 SnRNPs involved in the major splicing process. *SNRPB* produces three transcripts, the first two transcripts generate functional proteins named SmB and SmB′. These two proteins are derived from one pre-mRNA by alternative splicing (Chu and Elkon, 1991) and were shown to differ only at the carboxy terminus, where a proline-rich motif is repeated once more in SmB' (van Dam *et al.,* 1989). SmB/SmB' are essential in forming the heptameric ring of all core SnRNPs. The third annotated transcript of *SNRPB* contains a highly conserved alternatively spliced exon 2 that has a pretermination codon (PTC), thus leading to NMD of the transcript (Figure 1.3 A). The level of SNRPB in cells was thought to be maintained by the production of the third PTC containing transcript, when SNRPB is upregulated (Arneet *et al.,* 2008). Saltzman *et al.* (2011) showed that SNRPB self-regulates its expression by promoting the inclusion of the alternative exon 2 in its pre-mRNA. In HeLa cells, Saltzman *et al.* demonstrated that knockdown of SNRPB leads to more skipping of the *SNRPB* alternative exon2, suggesting a homeostatic autoregulation of SNRPB through the exclusion of the highly conserved PTC-introducing exon.

Genomic and protein analyses in chicken, two marsupials and hedgehog suggested that the ancestral form of the protein was the SmB' isoform (Gray *et al.*, 1999). The SmB/B' proteins are expressed robustly in all tissues except for postnatal brain. In the postnatal brain, SmB/B' are replaced by SmN and differentially distributed between the SnRNP components (Huntriss *et al*., 1993). In mouse fibroblast cells, Huntriss *et al*. showed that SmN expressed at low levels incorporates into U2, but SmN expressed at high levels incorporates into both U1 and U2 snRNPs and replaces SmB. Intriguingly, it was shown by Gray *et al.* (1999) that a compensatory feedback loop dramatically upregulates SmB/B' levels in response to the loss of SmN in Prader-Willi syndrome brain tissue, suggesting that these two genes encoding small nuclear ribonucleoprotein components are subject to dosage compensation.

1.2.4.2 SNRPB functions as a core component of spliceosome

SNRPB plays a role in pre-mRNA splicing as a core component of the spliceosomal U1, U2, U4 and U5 snRNPs, the building blocks of the spliceosome (Kambach *et al.*, 1999; Jurica *et al.*, 2002; Pomeranz Krummel *et al.*, 2009). It is also a component of the minor U12 spliceosome (Will *et al.*, 2004). In addition, as part of the U7 snRNP, SNRPB is involved in histone pre-mRNA 3'-end processing (Pillai *et al.*, 2001; Pillai *et al.*, 2003).

In eukaryotes, more than 20 Sm protein homologs assemble into several distinct heteroheptameric rings (Wilusz and Wilusz, 2005). Most spliceosomal snRNPs contain a common set of 7 Sm proteins (Kambach *et al*. 1999): SmB/B', SmD1, SmD2, SmD3, SmE, SmF and SmG that assemble into a ring (Figure 1.7) in a stepwise manner on the Sm site of the small nuclear RNA to form the core snRNP. In the Sm ring, SNRPB (SmB/B') has been shown to have the most efficient cross-linking in the heptamer with its adjacent SmG (Urlaub e*t. al.*, 2001). The Sm protein complexes associate with snRNA in at least two steps. The D1, D2 and E, F and G complexes associate initially with the snRNA, creating a sub core particle. This

particle provides a binding substrate for the B/B′–D3 complex, and this association completes Sm core assembly (Urlaub *et al.*, 2001).

There are two major eukaryotic Sm classes: the canonical Sm proteins and the Sm-like (Lsm) proteins. Canonical Sm proteins form heptamers that bind the major and minor uridine rich SnRNPs. Lsm proteins form two distinct heteroheptameric complexes: Lsm 2-8 or Lsm 1-7. The LSm2-8 ring forms the core of the U6 SnRNP and functions during general RNA maturation in the nucleus. The LSm1-7 ring functions during mRNA degradation in the cytoplasm. It is involved in recognizing the 3' uridylation tag and recruitment of the de-capping machinery (Bouveret *et al.*, 2000; He and Parker, 2000).

Figure 1.7: ***Schematic diagram of canonical Sm ring.*** *SNRPB* encoded SmB/ B' is one of the seven core proteins required to form the ring.

Sm proteins do not contain established RNA binding motifs and studies did not detect efficient crosslinking of Sm proteins to mRNAs. The RNA interaction surface and binding specificity of the Sm proteins are suggested to be determined by interactions among the Sm protein complexes (Hermann *et al*., 1995; Raker *et al*., 1996; Urlaub *et al.*, 2001; Lu *et al.*, 2014).

1.2.4.3 Depletion of SNRPB in cells: what we know so far

There are several studies to date in various cell lines which demonstrate the effect of *SNRPB* knockdown on splicing and gene expression. In glioblastoma cell lines, RNA sequencing of *SNRPB* knocked-down cells revealed differential expression of genes that were involved in RNA processing, DNA repair, and chromatin remodeling (Correa *et al.*, 2016). Splicing was abrogated in the glioblastoma cell line upon *SNRPB* knockdown and skipped exons (SE) and

retained introns (RI) were among the highest of differentially regulated events. In addition, more than 20 % of the core spliceosome components were differentially expressed and almost 60 % of the spliceosome components presented splicing alterations. Correa *et al*. also showed that *SNRPB* depletion could inhibit glioblastoma cell growth.

In hepatocellular carcinoma cell line it was shown that *SNRPB* played a key role in variant formation via alternative splicing regulation (Zhan *et al.*, 2020). Downregulation of *SNRPB* was shown to inhibit epithelial-mesenchymal transition (EMT) in liver cancer cells in another study (Li *et al*., 2022). In a non-small cell lung cancer cell line, knockdown of *SNRPB* was shown to regulate RAB26 by causing NMD of the transcript through intron retention (Liu *et al.*, 2019). In cervical cancer cells, *SNRPB* knockdown using shRNA (short hairpin RNA) markedly reduced cell proliferation, migration, and invasion. Moreover, increased apoptotic cell death and upregulated P53 were detected in cervical cancer cells with *SNRPB* knockdown. Knockdown of *SNRPB* in neuronal cell lines was also shown to cause upregulation of P53 targets in association with abnormal splicing of *Mdm2* and *Mdm4*; two upstream regulators of P53 activity (Van Alystene *et al.*, 2018).

A more recent study of morpholino mediated Snrpb knockdown was done in *Xenopus* embryos. The morphant embryos had abnormal cartilages formed from neural crest cells. It was demonstrated that Snrpb knockdown causes abnormal neural crest cell formation (Park *et al.*, 2022). However, no animal study has been done to show how SNRPB depletion affects splicing, gene expression, or its consequences in embryonic development.

1.3 Craniofacial development

In my study, a substantial part of the work was done to understand the role of *SNRPB* in craniofacial development and how its mutation causes abnormal head and face development that recapitulates CCMS anomalies. Therefore, in this section of the introduction, I will briefly introduce craniofacial development and how different cell types are involved in orchestrating the development of the craniofacial complexes.

1.3.1 Overview of craniofacial development

Craniofacial development is a unique and complex process that occurs during the first 10 weeks of human gestation (Diewert, 1985). The process starts once the anterior–posterior axis of the embryo is established and requires interactions amongst diverse cell populations. Several distinct signaling pathways and intricate morphogenetic movements of the ectoderm, mesoderm, and endoderm germ layers are required for proper craniofacial development. It requires crucial steps such as neural tube closure together with correct development of the skull, midline patterning, neural crest generation and migration, and outgrowth, patterning, and differentiation of the facial primordia and the pharyngeal arches. The five pairs of pharyngeal arches in human are indispensable transient structures that first appear at the end of the fourth week of gestation and develop throughout the fifth week (Graham, A., 2003). Each pharyngeal arch is covered on the outside by a layer of ectoderm and inside with a layer of endoderm, mesoderm and neural crest derived mesenchyme, is situated in between.

Cells from the germ layers form five primordia in the early embryo that are known as the frontonasal prominence (FNP, that includes the medial and lateral nasal prominences), paired maxillary (MX), and paired mandibular (MD) prominences (Figure 1.8). In a developing embryo, these prominences gradually grow and fuse toward the midline to form the nose, lips and jaws, creating the philtrum, with fusion being completed by 10 weeks. Hindrance in the development and growth of any of these processes can significantly affect craniofacial

development and results in several human syndromes. Notedly, craniofacial development is very similar between human and mice, which makes mice an ideal model to study craniofacial development and disorders.

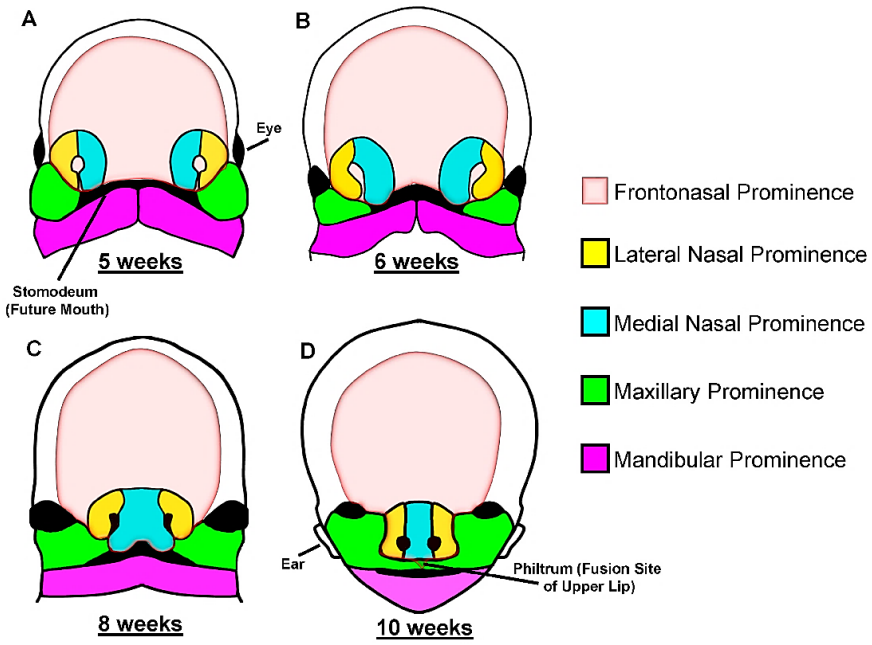

Figure 1.8: ***Human facial development during early gestation requires formation of five facial prominences.*** The frontonasal prominence, two maxillary prominences and two mandibular prominences form, grow and fuse over time at the midline by 10 weeks. Similar processes also occur in mice craniofacial development. (Adapted from Sebastian Dworkin *et al*., 2016).

In addition to the three germ layers, a transient, migratory, and multipotent cell population called neural crest cells (NCCs) significantly contributes to craniofacial development (Tan and Morriss-Kay, 1985; Hall, 1999; Cordero *et al.*, 2011; Achilleos and Trainor, 2012). The importance of NCCs in craniofacial development is well recognized as they give rise to the majority of the facial mesenchyme and later the craniofacial skeleton such as the majority of

the bones, cartilages and connective tissues in the cranial region. The embryonic head is populated by the mix of two robust mesenchymal populations of dual origin, the mesodermal and neural crest cells (Cibi *et al.*, 2019; M. C. McKinney *et al.*, 2020 and Gabrel G. *et al.*, 2021).

The formation of the bones in the head occurs in two different processes: 1) intramembranous bone formation, where direct differentiation of mesenchymal condensations turns into osteoblasts and 2) endochondral bone formation, where chondrocytes derived from mesenchymal cells produce a framework of cartilaginous tissue that is subsequently replaced by osteoblasts and bone matrix. The bones of the neurocranium (brain base) are composed of bones of dual origin (Figure 1.9). The viscerocranium bones (facial skeleton) derived from NCCs are mostly formed via intramembranous ossification (with exceptions such as the skull base). The paraxial mesoderm-derived bones are mostly formed through endochondral ossification. Craniofacial skeletal development is very similar between mice and human from these two cell populations.

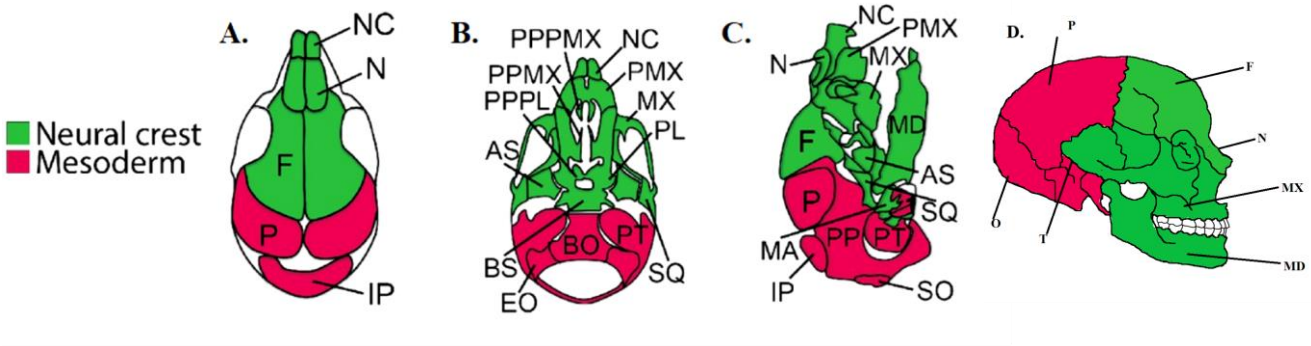

Figure 1.9: ***Mammalian craniofacial skeleton is of dual origin of neural crest cells and mesodermal cells.*** The dorsal (A), ventral (B) and sagittal (C) view of mouse skull showing bones that are a contribution of both neural crest cells and mesoderm cells. Similar bones and origins are present in human craniofacial skeleton (D). AS, alisphenoid; BO, basioccipital; BS,

basisphenoid; EO, exoccipital; F, frontal bone; IP, interparietal; MD, mandible; MX, maxilla; N, nasal; NC, nasal capsule; P, parietal bone; PL, palatine; PMX, premaxilla; PPMX, palatal process of maxilla; PPPL, palatal process of palatine; PPPMX, palatal process of premaxilla; PT, petrous part of temporal bone; SO, supraoccipital; SQ, squamous; O, Occipital; T, Temporal bone (Modified from Cibi *et al.*, 2019 and Galea *et al.*, 2021)

1.3.2 Role of NCCs in craniofacial development

A significant event for craniofacial development occurs when multipotent NCC cells emerge at the border of the neural plate when the neural tube closes. They are induced in the ectoderm at the interface between the neuroepithelium and the prospective epidermis at all levels of the antero-posterior axis of the developing embryo. Although derived from the ectoderm, NCCs are referred to as a "fourth germ layer" for their contribution in embryonic development (Hall, 2000). Lineage tracing experiments in vertebrates showed that specific subpopulations of NCCs migrate as a wave of cells to the frontonasal prominences and pharyngeal arches and give rise to the entire mandible, visceral skeletons and cranial nerves (Noden 1988, Lumsden *et al.*, 1991; Couly *et al.*, 1993; Trainor and Tam, 1995; Hall 1999; Le Douarin and Kalcheim, 1999; Santagati and Rijli, 2003). Their extensive migration occurs by first separating from the neuroepithelium, a process called delamination, which is facilitated by the epithelial-to-mesenchyme transition (EMT) (Theveneau and Mayor, 2012). The EMT and delamination of NCCs require significant cellular mechanisms including reorganization of the cytoskeleton and cell-cell adhesion changes (Clay and Halloran, 2011).

NCCs migrate ventro-laterally throughout the embryo and later differentiate into multiple cell types (Achilleos and Trainor, 2012). NCCs are classified into distinct axial groups based on their origin in the axial level- cranial, cardiac, vagal, trunk and sacral-which give rise to

different structures based on their differentiation potentials. The cranial neural crest cells, which are unique to vertebrates (Le Douarin and Dupin 2003), as mentioned give rise to most of the bone and cartilage of the head and face (Figure 1.10), cranial ganglia, smooth muscle, connective tissue, and pigment cells. The cardiac neural crest cells contribute to heart development by forming the cardiac septa, cardiac neurons, and glia. The vagal and sacral neural crest cells give rise to the enteric neurons and glia. The trunk neural crest cells form the sensory neurons and glia, autonomic neurons, chromaffin cells, and melanocytes that cause pigmentation in the skin (Dupin and Somer, 2012).

NCCs are subdivided into Hox-positive versus Hox-negative cells (Creuzet *et al.*, 2002). Hox-gene expression is primarily associated with the caudal pharyngeal arch populations of NCCs. Only Hox-negative NCCs are capable of generating the skeletal components of the face (Couly *et al.*, 1998, Couly *et al.*, 2002; Le Douarin *et al.*, 2004). These Hox-negative NCCs that colonize in the first pharyngal arch gives rise to skeletal components such as Meckel's cartilage, maxillae, and dentary bones. The cranial region of Meckel's cartilage forms the middle ear bone called the stapes, whereas the proximal region forms the two other middle ear bones, the malleus and the incus. The Hox-positive second pharyngeal arch forms a continuous cartilage known as hyoid cartilage, which is the origin of several structures such as the styloid process of the temporal bone, the stylohyoid ligament, and the lesser horn of the hyoid bone.

The expression of *Hoxa2* is maintained through late stages in branchial arch 2, a pattern that has been conserved in mouse, chick, frog and zebrafish (Couly *et al.*,1998; Kanzler *et al.*,1998; Pasqualetti *et al.*,2000). The importance of negative influence of *Hox* genes in the development of the first pharyngeal arch derivatives was shown by the fact that the null mutation of *Hoxa2* in mice results in the duplication of first branchial arch structures such as the incus, malleus, and Meckel's cartilage (Rijli *et al.*, 1993; Kanzler *et. al,* 1998). *Hoxa2* is not only required for proper patterning of the neural crest cells but also it plays role to inhibit intramembranous and

endochondral ossification (Rijli *et al.*, 1993; Kanzler *et. al*, 1998). It was also shown in chick embryos that *Hoxa2* gain-of-function into the *Hox*-free neural crest domain in the first branchial arch suppresses lower jaw and frontonasal structure formation (Grammatopoulos *et al.*,2000; Creuzet *et al.*, 2002). Similar findings were reported in *Xenopus* by overexpression of *Hoxa2* in the first branchial arch (Pasqualetti *et al.*, 2000). In addition, morpholino mediated knockdown of *Hoxa2* resulted in homeotic transformation of hyoid to jaw (Baltzinger *et al*., 2005). Unlike *Hoxa2*, *Hoxb2* is not required for second arch patterning in mouse and zebrafish (Rijli *et al.*,1993; Baltzinger *et al.*, 2005). In contrast, morpholino-induced knockdown experiments in zebrafish showed a functional redundancy between *Hoxa2* and *Hoxb2* in branchial arch 2 patterning (Hunter and Prince, 2002). In zebrafish, *Hoxa2* and *Hoxb2* are expressed in the second arch through late developmental stages.

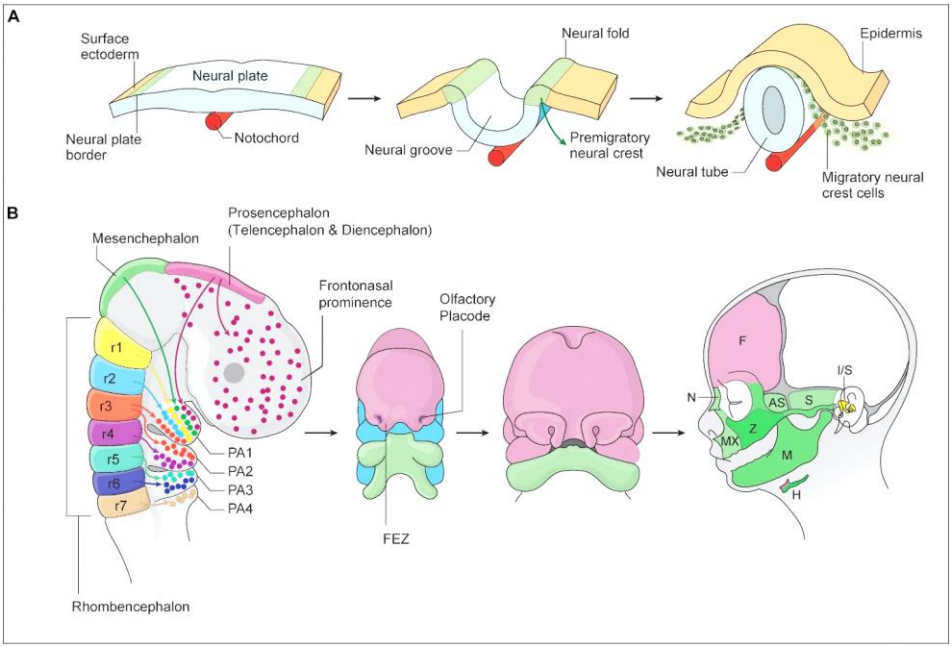

Figure 1.10: ***Cranial neural crest cells form, migrate and differentiate to several craniofacial structures.*** **(**A) Neural crest cells are induced when the two halves of the neural plate is elevated to form the neural tube. The cells undergo EMT, migrate and colonize the frontonasal

prominences, and pharyngeal arches. (B) Cranial NCCs are generated from prosencephalon (diencephalon and telencephalon), mesencephalon, and rhombencephalon regions. They travel ventro-laterally to their destination to the facial prominence and pharyngeal arches where they participate in morphogenesis to form the structures of the face. AS, alisphenoid bone; F, frontal bone; FEZ, frontonasal ectodermal zone; FNP, frontonasal prominence; H, hyoid bone; I/S, incus and stapes; M, mandible; MX, maxilla; N, nasal bone; PA, pharyngeal arches; r, rhombencephalon; S, squamosal; Z, zygomatic bone. (Adapted from Fritriasari and Trainor, 2021)

1.3.3 Signals in mammalian neural crest cell ectomesenchymal differentiation

In craniofacial development, the establishment of the ectomesenchymal lineage within the cranial neural crest is of great significance. NCCs that are early-migratory turn into the skeletal and connective tissue of the face and pharyngeal region, whereas later-migrating NCCs

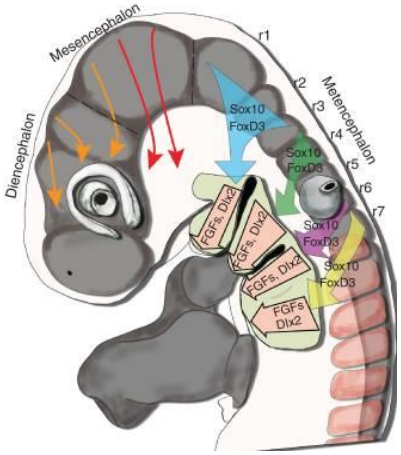

Figure 1.11: ***Neural crest cell delamination and differentiation.*** Neural crest cells migrate from their location. Orange and red arrows show migration of NCCs from the diencephalon and mesencephalon, respectively. Blue, green, pink and yellow arrows show Sox10 and FoxD3 expressing cells migrating from the rhombomeres to the pharyngeal arches. Peach color arrows show NCCs in the pharyngeal arches expressing ectomesenchymal markers such as FGFs and Dlxs. (Source: Bhatt *et al.*, 2013)

primarily adopt a neural fate (Bhatt S. *et al*., 2013). Upon delamination and migration, NCCs express the migratory neural crest cell marker, *Sox10* which is also a glial determination factor (Britsch *et al*., 2001). S*ox10* expression in NCCs is initiated as the cells dissociate from the neural tube. The expression is maintained during neural crest cell migration and the expression is continued in the glial and melanocyte lineages. However, in many NCC derivatives, *Sox10* expression is turned off (Pusch *et al.*, 1998). In the glial precursor NCCs, the transcriptional repressor, *FoxD3* is exclusively expressed (Thomas and Erickson, 2009). NCCs entering the pharyngeal arches express ectomesenchymal differentiation markers such as *Dlx2*, *Dlx5* and FGFs (Figure 1.11) (Blentic *et al.*, 2008). By contrast, those NCCs that do not enter the arches persist in their expression of early neural crest markers. Dlx5 factors are important to mediate localization of ectomesenchymal subpopulations within the pharyngeal arches and by doing so define where skeletogenic condensations will arise (Gordon *et al.* 2010). In addition, *Dlx5* acts as a mediator to promote *Runx2* expression in myogenic cells (Lee *et al,* 2003). Targeted inactivation of *Dlx5* and *Dlx6* genes in mice results in abnormal craniofacial and axial cartilage and bone development (Robledo *et al.*, 2002). Furthermore, *Dlx1/2/5/6* mutants have revealed these genes' function in collectively regulating regional identity along the proximodistal axis of the pharyngeal arches and specifying their specific cranioskeletal derivatives (Qiu *et al.*, 1987;Qiu *et al.*, 1995; Robledo *et al.* 2002; Depew *et al.* 2002). Moreover, *Dlx* gene expression are known to distinguish mandibular and the maxillary patterning. From murine experiments it was suggested that *Dlx1/2* regulate maxillary development as homozygous mutants of *Dlx1/2* shows abnormal development of the upper jaw (Jeong *et al.*, 2008). In contrast, *Dlx5/6* is suggested to confer the mandibular fate. Simultaneous inactivation of *Dlx5* and *Dlx6* (*Dlx5/6*$^{-/-}$) results in homeotic transformation of the lower jaw into upper jaw (Depew *et al.*, 2002). Jeong *et al.* (2008) showed branchial arch expression patterns of the genes downstream of *Dlx5/Dlx6* were downregulated in both *Dlx5* and *Dlx6* homozygous mutants.

i. Fibroblast growth factors (FGFs)

Some of the most studied signaling molecules involved in craniofacial development are the fibroblast growth factors (FGFs). FGF signaling has been shown to be involved in the establishment of NCCs to become the ectomesenchymal lineage in both chick and zebrafish (Blentic *et al.*, 2008). This signaling is known to play a key role in determining the fate of neural crest cells towards a skeletogenic type. For example, FGF2 was involved in both chondrogenic and osteogenic differentiation of the cranial neural crests *in vitro* (Sarkar *et al.*, 2001). *FGF8* is another well studied molecule that established the importance of cell type interactions and a determinant of cell fate during craniofacial development. It is expressed in the pharyngeal ectoderm, and its downstream signaling is mediated through the *Fgfr1* receptor that is expressed in the NCCs. *Fgf8* can induce *Sox9* expression by the NCCs, which is a determinant of chondrogenic lineage of the NCCs (Mori-Akiyama *et al.*, 2003). FGF8 secreted from the paraxial mesoderm enhances the specification of neural crest fate by upregulating the expression of *Zic5*, *Msx1*, *Pax3*, *Snail2*, *Zic1*, and *FoxD3* in *Xenopus* (Sato *et al.*, 2005) and mouse (Monsoro-Burq *et al.*, 2003; Kubota and Ito, 2000). Loss of FGF signaling has been shown to cause abnormal craniofacial skeletal development in several mouse studies (Jin and Chen 2014). Recently, it was shown that mutations of *Fgfr1* and *Fgfr2* in neural crest cells caused agenesis and/or reduction in medial and proximal structures of facial skeletons (Ray *et al.*, 2020).

Mutations that disrupt FGF signaling cause congenital craniofacial disorders such as craniosynostosis (Muenke and Schell, 1995; Reardon and Winter 1995; Chan and Thorogood 1999; Moosa and Wollnik, 2016). Pathogenic variants of *FGFR1, 2* and *3* are associated with Crouzon, Pfeiffer, Jackson-Weiss, Apert, Beare-Stevenson and Muenke syndromes (Reardon *et al.*, 1994; Wilkie *et al.*, 1995; Muenke *et al.*, 1994; Jabs *et al.*, 1994; Meyers *et al.*, 1996).

Some of these syndromes such as Apert, Crouzon, or Pfeiffer syndromes are caused by overactivation of the FGF receptors (Anderson *et al*., 1998).

ii. Sonic Hedgehog

Sonic Hedgehog (Shh), a well-recognized morphogen with a broad role in organogenesis, has also been shown to play an important role in NCC fate specification. At early stages of development, *Shh* expression is present throughout the axial mesendoderm and plays an essential role in bilateral patterning (Dale *et al.*, 1997). Later, it is expressed in the epithelium of facial primordia (Echelard *et al.*, 1993). The transcriptional target of SHH, *Ptch1* is expressed in the developing face region where there is a high density of cranial neural crest cells, suggesting the signal transduces in the NCCs (Jeong *et al.*, 2004). As *Shh* is expressed in the ventral forebrain neuroepithelium, the oral ectoderm, and the pharyngeal or foregut endoderm (Jeong *et al*., 2004) but is absent from the neural crest-derived mesenchyme (Ahlgren *et al.*, 2002), it suggests that NCCs themselves do not express *Shh*.

The role of *Shh* in determining skeletal fates of the NCCs has been shown by the sustained treatment of Shh that leads to the formation of chondrocytes and osteoblasts by the progenitor cells (Dupin *et al*., 2010). Loss of *Shh* signaling in NCCs is known to cause craniofacial morphogenesis disorders in mice and zebrafish (Wada *et al.*, 2005, Veistinen *et al.*,2012). Furthermore, the conditional disruption of Hedgehog signaling by removing Smoothened (a hedgehog receptor) in NCCs has been shown to cause extensive reduction and loss of craniofacial structures (Jeong *et al.*, 2004).

Expression of *Shh* from endoderm regulates the pharyngeal arch patterning by maintaining key differentiation genes such as *Fgf8* and *Sox9* in the first pharyngeal arch, in mice (Haworth *et al*, 2006, Yamagishi *et al.*, 2006). *Shh* expression in the facial ectoderm is very important as it induces proliferation and outgrowth of the underlying NCC-derived mesenchyme. *Shh*

expression is induced at the cephalic ectoderm and forms a boundary with the *Fgf8* expressing cells, forming a distinct region called the frontonasal ectodermal zone (FEZ). FEZ acts as a signaling center that regulates proximodistal extension and dorsoventral polarity of the upper face (Hu *et al.*, 2003; Hu and Marcucio, 2009). SHH and FGF8 have strong synergistic effects on chondrogenesis *in vitro* (da Costa, 2018) and are sufficient to promote outgrowth and chondrogenesis as shown *in vivo* in chick embryos (Abhzanov and Tabin, 2008).

In human, *SHH* mutations are associated with several craniofacial abnormalities (Roessler *et al.*, 1996; Abramyan, 2019). Insufficient SHH signaling due to loss of function mutation cause diseases such as holoprosencephaly (HPE), hypotelorism and cyclopia, whereas grain of function mutations result in Greig cephalopolysyndactyly syndrome (GCPS), diprosopus and hypertelorism (Roessler *et al.* 1997; Vortkamp *et al.*, 1991; Wild *et al.*, 1997).

iii. Transforming growth factors (TGFs)

Transforming growth factor-β (TGF-β) ligands are expressed in a time- and tissue-specific manner and are important in regulating the formation of various craniofacial structures (Chai *et al*., 1994). From both *in vitro* and *in vivo* studies, TGFs are known to function as important switches mediating ectomesenchymal versus neural fate of the NCCs. TGFβ signaling modulation in mice NCCs does not prevent their migration into the pharyngeal apparatus but made these cells unable to acquire non-neural cell fates resulting in craniofacial defects that resemble human syndromes such as DiGeorge syndrome (Wurdak *et al.*, 2005). It has been demonstrated that TGFβ signal inactivation results in persistent *Sox10* expression, and perturbed generation of mesenchymal derivatives, which eventually leads to defective skeletal morphogenesis. Thus, negative regulation of *Sox10* by TGFβ signaling promotes the generation of mesenchymal progenitors from neural crest (NC) stem cells (John *et al*., 2011). Both *Tgfβ1* and *TgfβII* signaling act as crucial switches to induce ectomesenchymal fates by reducing *Sox9*

expression in the pharyngeal arch NCCs (Wurdak *et al.*, 2005). The importance of TGFβ transduction in neural crest cells for craniofacial development has been demonstrated by abrogation of *Smad4* in NCCs. *Smad4* is a transcriptional effector that mediates signaling responses to the TGFβ family in various biological processes ranging from embryonic development to adult tissue homeostasis (Masuyama, N. 1999; Chu, G. *et al.,* 2004; Wu and Hill, 2009; Guglielmi, L., 2021). On ligand binding, receptor-regulated SMADs (R-SMADs) SMAD1/5 and SMAD2/3 are phosphorylated by activated type I receptors and form complexes with SMAD4 that translocate in the nucleus to regulate target gene expression (Derynck and Feng, 1997; Watanabe, M. *et al.*, 2000; David and Massagué, 2019). In mice, *Smad4/Wnt1-Cre* mutants displayed several craniofacial and cardiac defects (Nie *et al.,* 2008). Both frontonasal processes and the mandibular arch were hypoplastic and failed to fuse in the midline, the trigeminal ganglia were hypoplastic and ectomesenchymal patterning in the first pharyngeal arch was altered (Nie *et al.,* 2008).

iv. Muscle segment homeobox genes

Transcriptional regulators such as *Msx1* and *Msx2* that control cellular proliferation and differentiation during embryonic development play a role in fate determination of cranial NCCs (Satokata *et al.* 2000; Han 2007). In humans, *MSX1* variants are associated with diseases that include orofacial clefting *(*Liag *et al.,* 2016). *Msx1* and *Msx2* are strongly expressed in migrating NCCs, and expression continues during their colonization in the facial prominences and branchial arches. In mice, *Msx1/Msx2* single or double mutants exhibit several craniofacial anomalies (Satokata and Maas, 1994; Satokata *et al.* 2000; Ishii *et al*., 2003; Han 2007). *Msx1* mutant mice show palatal defects and abnormalities of the tooth, nasal, frontal and parietal bones, and of the malleus in the middle ear (Satokata and Maas, 1994) whereas *Msx2* null mutation causes ossification defects in the skull (Ishii *et al.,* 2003). It was found that *Msx1/Msx2* double mutant mice do not show defect in NCC migration into the frontal bone

primordium, but they show defective differentiation of the frontal mesenchyme and establishment of the frontal primordium resulting in frontal bone development defects (Han, 2007). This suggests a role of *Msx1* and *Msx2* genes in the osteogenesis of the NCC lineages.

1.3.4 Role of ectodermal cells in craniofacial development

One of the first crucial steps in craniofacial development occurs when the head ectoderm is subdivided into non-neural and neural regions. The ectoderm is essential for normal craniofacial development by inducing and then collaborating with the underlying cranial neural crest cell populations (Mouri and Jacobson, 1990; Selleck *et al.*, 1995; García-Castro *et al.*, 2002; Le Douarin *et al.*, 2004; Van Otterloo *et al.*, 2022). Facial surface ectodermal cells not only form the epidermis such as skin and hair but also, provide signals that direct appropriate growth, patterning, and morphogenesis of the craniofacial regions. Reciprocal signaling interactions among the surface ectoderm, brain and neural crest control craniofacial morphogenesis (Marcucio *et al.*, 2005; Schneider and Helms, 2003).

The ectoderm is a critical source of Wnt signaling that is required for continued facial outgrowth and patterning. Removing Wnt/β-catenin signal from the ectoderm has been shown to cause craniofacial shape changes and skeletal defects in mice (Reid *et al.*, 2011; Reynolds *et al.*, 2019). One potential mechanism by which Wnt signaling causes phenotypic variation in the facial region is via its role in the patterning of the frontonasal ectodermal zone (FEZ) (Marcini *et al.*, 2021).

Transcription factors that are expressed strongly in the facial ectoderm are also known to be important for proper craniofacial development. Mutations in *IRF6* and *GRHL3* (Peyrard-Janvid *et al.*, 2014) and *TRP63* (Bamshad and Michael, 2016) have been known to cause orofacial clefting in human syndromes. More recently, it was demonstrated that removal of two members of the AP-2 transcription factor family, AP-2α and AP-2ß, within the early embryonic ectoderm

in mice leads to major alterations in the craniofacial development (Van Oterloo *et al.*, 2022). In those mutants, clefts in both the upper face and mandible, accompanied by fusion of the upper and lower jaws in the hinge region complex were seen.

One of the important roles of ectoderm as a signaling center during craniofacial morphogenesis is the FEZ formation. Removing *Shh* from the ectoderm has been shown to inhibit facial primordia growth in chick and resulted in craniofacial abnormalities seen in human, such as facial clefts (Hu and Helms, 1999), highlighting its role in proper facial development. It has also been shown in *Shh* null mutant mice that the neural crest cells die significantly and the branchial arch structures are lost (Ahlgren and Bronner-Fraser, 1999).

Neural ectoderm is also a source of patterning information for the middle and upper face, as has shown in the zebrafish model. For example, loss of neuroectodermal *Shh* prevented neural crest cells from aggregating into condensations and eventually from forming skeletal elements, that were also previously reported abnormal in mice (Helms, 2005).

Transplantation experiments in birds provided the crucial findings of the requirement of proper FEZ formation in the ectoderm to collaborate with the neural crest cells for facial development (Hu *et al*., 2003; Hu and Marcucio, 2009). For example, when regions of facial ectoderm were transplanted to ectopic sites in the avian face, the developmental fate of underlying frontonasal neural crest cells was altered and resulted in a duplication of upper beak structures in chick (Hu *et al*., 2003).

1.3.5 Role of mesodermal cells in craniofacial development

Upon head specification, development of the craniofacial complex requires intercellular mechanisms of two different origins: the cranial neural crest cells (CNCCs) and the mesodermal cells (Noden 1978; Schneider, 1999; Jiang *et al.*, 2002; Noden and Trainor, 2005 Cibi *et al.*, 2019; M. C. McKinney *et al*., 2020 and Galea *et al.*, 2021). While both the NCCs

and the mesoderm contribute to the formation of the same structures in the head, they remain segregated. Bones of mixed origin such as the basisphenoid bone arise due to fusion of the neural crest cell derived lateral and mesoderm derived medial basisphenoid cartilage (Noden 1983). The presence of a neural crest–mesoderm interface hinders cell movement and thus prevents the mixing of different connective tissue precursors as shown by transplantation studies in chick (Noden 1978; Schneider, 1999; Jiang *et al.*, 2002; Noden and Trainor, 2005). Detailed analysis of NCC migration using NCC lineage marker and Dil labelling of mesodermal cells demonstrated distinct skeletal structure formations in mouse skull from those two cell populations, except for the interparietal bone that is of mixed origin (Jiang *et al.*, 2002).

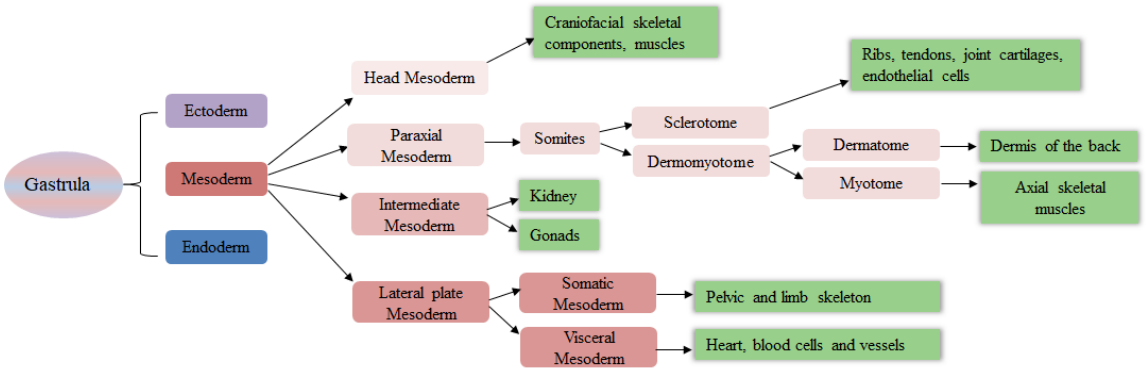

Figure 1.12: ***A schematic representation of mesoderm derivatives in embryonic development.*** Mesoderm significantly contributes to craniofacial development forming the cranial skeleton and muscles. Mesodermal subtypes generate embryonic derivatives (in green boxes).

Mesoderm is generated at the onset of gastrulation that is initiated at approximately embryonic day (E) 6.5 of mouse gestation, and at the beginning of the third week of pregnancy (Moore *et al.*, 2020). Once generated, mesodermal cells migrate from the primitive streak of the gastrula and develop into different mesoderm specific cell types. For craniofacial development, early migrating mesodermal cells form the head mesenchymal cell lineages (Moore *et al.*, 2020*;* Dox

et al., 2012). The different mesoderm subtypes are specified along the mediolateral axis as paraxial mesoderm, lateral plate mesoderm and intermediate mesoderm (Figure 1.12), depending on the gradient activities of BMPs (Tani *et al.*, 2020). Each of the mesodermal cell lineage subtypes forms specific structures and connective tissues upon differentiation. Head mesoderm-derived mesenchymal cells give rise to the connective tissue and skeletal elements of the caudal part of the cranium and the dorsal part of the neck. Mesodermal cells in the pharyngeal arches initially form a mesodermal core, which is surrounded by cranial neural crest cells. (Noden and Trainor, 2005). The interactions of mesodermal and neural crest cells during head morphogenesis were shown spatiotemporally by labelling and time-lapse imaging of those two cell populations (McKinney, 2020). Distinct signalling such as *Bmp4* or *Fgf8* could act to build the synergy of these cell types to collaborate formation of craniofacial skeletons and muscles.

1.3.6 Role of endodermal cells in craniofacial development

One of the key essential structures in craniofacial development are the endoderm-derived pharyngeal pouches that appear as out-pockets between the pharyngeal arches. The pouches give rise to tissues of the hearing components such as the middle ear cavity and eustachian tube. They also form palatine tonsils, thymus, parathyroid glands, and parafollicular cells of the thyroid (Grevellec and Tucker, 2010). The pharyngeal arches are composed externally of ectoderm and lined internally by endoderm, enveloping a mesenchymal core composed of NCCs and mesoderm. The juxtaposition of the endoderm and ectoderm forms an internal cleft and an external pouch, respectively, that separates each arch from its neighbor. Proper pharyngeal pouch formation is essential for correct formation of the individual pharyngeal arch. Failure in development of the pharyngeal pouches has clinical consequences such as DiGeorge syndrome (also known as III-IV pharyngeal pouch syndrome**)**, where a microdeletion of

choromosome 22q11.2 results in impaired development of the pharyngeal pouch system (Robinson, 1975; Raatikka *et al.*, 1981; Kobrynski and Sullivan, 2007).

Using time-lapse microscopy in zebrafish it was demonstrated that pharyngeal pouches form when clusters of endoderm cells migrate laterally, and it was also shown that *Fgf8* and *Fgf3* play essential roles in regulating the segmentation of the pharyngeal endoderm into pouches (Crump *et al.*, 2004). When *Fgf8* was inactivated and *Fgf3* was knocked down with morpholinos in zebrafish, the migration of endodermal cells was disrupted, pharyngeal pouches failed to form, and the pharyngeal arch derived cartilages were severely reduced. In mice, *Fgf8* mutants had a smaller or absent third and fourth pharyngeal pouch with abnormal pharyngeal arch development (Abu Issa *et al.*, 2002). The bending of endodermal epithelium is a significant step of pouch formation and genes like *Ripply3* have been shown to play a role in the process in mice (Tsuchiya *et al.*, 2018). In zebrafish, signals from the early endoderm pattern the facial primordia and have a profound influence on the morphogenesis of the middle and lower face (Crump *et al.*, 2004).

A substantial information about the role of endodermal cells in cranioskeletal patterning came from the experiments performing ablation and grafting of defined endodermal regions in birds (Couly *et al.*, 2002). In this study, removal of foregut endoderm caused absence of neural crest cell derived facial skeletons in chick, whereas transplantation and rotation of different endodermal regions from quail to chick indicated endoderm instructs neural crest cells as to the size, shape and position of all the facial skeletal elements that include both cartilage and membrane bones. Patterning of the hyoid cartilage, specification of the shape and orientation of the nasal and mandibular skeleton by the neural crest domain are conferred by the cues provided by the foregut endoderm as demonstrated in chick (Ruhin *et al.*, 2003). In addition, it was later demonstrated that Shh signaling from the foregut endoderm patterns skeletal cartilage in chick embryos (Brito *et al.*, 2006; Benouaiche *et al.*, 2008).

1.4 Question, hypothesis, and objectives of the research

In light of what is known about CCMS, how splicing occurs, and the way craniofacial development occurs, I posed a question which led me to the hypothesis and aims of my PhD.

1.4.1 Question

As mentioned earlier, *SNRPB* is a core component of major SnRNPs (U1, U2, U4, U5 and U6) and is predicted to be widely expressed. Mutations in alternative exon 2 of *SNRPB* are suggested to create *SNRPB* hypomorphic alleles that result in malformation in specific tissues, such as the craniofacial and the costovertebral regions. Thus, we ask the question, "*Does reduction in* SNRPB *disrupt splicing of tissue-specific transcripts during development resulting in characteristic features of CCMS?"*

1.4.2 Hypothesis

My hypothesis is that *"During development, there are tissue-specific transcripts that are mis-spliced due to* SNRPB *reduction, to result in specific abnormalities found in CCMS. Those affected transcripts can be uncovered using a mouse model with reduced levels of* SNRPB*".*

1.4.3 Aims and Objectives

To test my hypothesis, I had set the following aims of my research.

1. Develop a mouse model for CCMS. My objective is to make a mutation in *Snrpb* to reduce *Snrpb* expression and to characterize if reduction of SNRPB in mice can model CCMS.
2. Then, I aim to find the genes and/or pathways that are affected in specific malformations, such as craniofacial abnormalities in the generated *Snrpb* mutant mouse model.

CHAPTER II

MATERIALS AND METHODS

All antibodies, chemicals and most mouse lines used in this study are commercially available.

2.1 Mouse lines

2.1.1 Commercially available mouse lines used in the study

All procedures and experiments were performed according to the guidelines of the Canadian Council on Animal Care and approved by the animal Research Institute of McGill University Health Centre (RI-MUHC).

Wild-type CD1 animals were purchased from the Jackson Laboratory. The following mouse lines of C57Bl/6J genetic background were purchased from The Jackson Laboratory: mT/mG *Gt(ROSA)26Sor*$^{tm4(ACTB-tdTomato,-EGFP)Luo}$*/J, stock# 007676* (Soriano, 1999); *Wnt1-Cre2 (*B6.Cg-*E2f1*$^{Tg(Wnt1-cre)2Sor}$*/J,* mouse strain: 022501; Lewis *et al*., 2013) and *β-actin-Cre (stock #* 019099) Lewandoski *et al*., 1997) . The *Trp53*^{tm1brn} mouse line, also on C57BL/6 background, with *LoxP* sites flanking exons 2-10 of the *Trp53* gene was purchased from The Jackson Laboratory (*Trp53*$^{LoxP/+}$) (stock #008462) (Marino *et al*., 2000). The *R26R* strain [*Gt (ROSA)26Sor*^{tm1Sor} mice (Muzumdar *et al*., 2007) were on a mixed C57BL/6J;129/S4 genetic background and a kind gift from Dr Nagano (Department of Obstetrics and Gynecology, McGill University, Montreal, Canada). The *Mesp1-Cre* transgenic mice were of C57BL/6(B6) /CBA background (Saga *et al*., 1999) and were a generous gift from Dr. Jean-Francois Cloutier (Department of Neurology and Neurosurgery, McGill University). All the lines, once in house, were maintained on a CD1 mixed genetic background.

2.1.2 Mouse lines generated through CRISPR/Cas9 genome editing technique

2.1.2.1 Generation of the del-61 (Δ61) and del-46 (Δ46) alleles and maintenance of the mouse lines

Using CRISPR/Cas9-mediated homology-directed repair, I aimed to insert *LoxP* sequences in introns 1 and 2 of *Snrpb*, to flank exon 2 with *LoxP* sequences. A pair of guide RNAs (gRNAs) (Sequences in Table 2.1) were designed using the online services of Massachusetts Institute of Technology (http://crispr.mit.edu). Efficient guide RNAs were selected based on previous references (Xu *et al*., 2015). The microinjections were performed at the McGill Integrated Core for Animal Modelling (MICAM). In the first round of microinjection, there were no successful events with 2 males born from the microinjection. In the second round, there were 7 animals born (5 males, 2 females). In those animals, 3 males had deletion alleles in intron 2. The deletions were followed for transmission in the G1 offspring. I then sequenced the mutant bands for each deletion from the G1 offspring by Sanger sequencing and aligned them with UCSC genome database. I found one deletion, specifically a 61 base-pair long sequence spanning within intron 2. The deleted sequence was 3'GACGAAGGAAGATATGTCTTGGTGGCCAACGGTCCCATTTAAATCAAAAGCAG GAGAGCAA-5'. The other mutant allele was a shorter deletion of 46 base pair around the same region of intron 2: 3'-CGAAGGAAGATATGTCTTGGTGGCCAACGGTCCCAT TTAAATCAAA-5'. Thereafter, I backcrossed each of the animals for at least five generations with wild-type CD1 animals to establish the *Snrpb* Δ-61and Δ-46 mutant mouse lines to remove any potential off-target effect from CRISPR editing. The heterozygous mutant animals from each line were mated to produce homozygous mutant embryos and pups.

2.1.2.2 Generation and establishment of *Snrpb* conditional mutant mouse lines

I used a CRISPR/Cas9-mediated homology-directed repair strategy to insert *LoxP* sequences in intron 1 and intron 3 to flank exons 2, alternative exon 2 and 3. The designed guide RNAs were purchased from Integrated DNA technologies. Repair templates were ordered as PAGE-purified Ultramer® DNA Oligo (Integrated DNA Technologies) and re-suspended in ddH_2O. Microinjection with single-strand DNA template, gRNAs (Sequences in Table 2.1) and Cas9 mRNA was performed at MICAM. Injected embryos (BL6/C3H genetic background) were transferred into uteri of pseudo pregnant foster mothers (CD1, Charles River Laboratories). Upon birth, the insertion was confirmed in two animals (one male and one female) by Sanger sequencing from the G1 animals. Then I generated homozygous animals with *LoxP* sequences in intron 1 from those G1 mice. Intron 1 homozygous *LoxP* G2 animals were then used for the second round of microinjection (BL6/C3H genetic background) to insert *LoxP* into intron 3. From this microinjection, Sanger sequencing was done from the DNA of G1 male offspring from a founder and a WT CD1 female. In this animal, it was confirmed that both *LoxP* sequences in intron 1 and intron 3 were intact. Thereafter, I backcrossed the animals for at least five generations to establish the *Snrpb* conditional mutant mouse line and to remove any potential off-target effect from CRISPR editing, and backcrossing was continued for animals used.

2.1.2.3 Oligos for CRISPR/Cas9 injections

I synthesized the guide RNAs using the GeneArtTM Precision gRNA SynthesisKit (ThermoFisher Scientific) according to the manufacturer's protocol: Briefly, a DNA template for each of the guide RNAs was assembled by PCR reaction using primers containing the corresponding spacer sequence. The guide RNA DNA templates were then transcribed *in vitro* into RNA using an NTP mix, TranscriptAidTM Enzyme Mix and reaction buffer (Thermo Fischer Scientific) and incubated at 37^{o}C for 3 hours. The transcribed guide RNA was then

purified using the GeneJETTM RNA Purification Micro Columns (ThermoFisher Scientific). The guide RNA DNA templates were verified for proper assembly by 4% agarose gel electrophoresis before use for *in vitro* transcription. To confirm the presence and verify the purity of the generated guide RNA prior to use for microinjections, Urea PAGE was performed using 12.5% polyacrylamide gel.

Repair templates designed for inserting the *LoxP* sequences had at least 50 base-pair of homologies to the targeted sequence on both 5' and 3' sides of the *LoxP* sequence. The repair template for intron 1 had sequences for *EcoRI* after the 5' region of homology, while the repair template for intron 3 had *EcoRV* sequences inserted after the *LoxP* sequence (Table 2.1).

Table 2.1: ***Guide and oligo sequences used for microinjections (A) and primers used to generate gRNAs (B).***

A.

Guide sequence for intron 1	Sequence 1: 5' CTAGGCTGAAGCTGGGCGAT 3' Sequence 2: 5' GCAGAAGTCTAGGCTGAAGC 3'
Guide sequence for intron 2	Sequence 1: 5' GAGCAAGGTTTGCTGGACGA 3' Sequence 2: 5' GTCCCATTTAAATCAAAAGC 3'
Guide sequence for intron 3	Sequence 1: 5' AATATGGCCTGAGGCCATAT 3' Sequence 2: 5' ACTTTAACGCCCATGCCCAG 3'
Repair template sequences for intron 1	5' CAATTTCCAACTGTCTTCCACACAGTCTTT ACCTGAGACTCTTCCTATCGCCCAGCTGAATTC ATAACTTCGTATAGCATACATTATACATTATAC GAAGTTATTCAGCCTAGACTTCTGCCAGGTAACC TGCTAGTCTCCCTTCCCTTAAAAAAGTCATC 3' (Eco RI site *LoxP* sequence)
Repair template sequences for intron 3	5'TACAGAACTGCTGGGTAACCAATATGGCCTC AGGCCATATTGATTAGGATTCCTCTGATAACTTC GTATAGCATACATTATACGAAGTTATGATATCGG CATGGGCGTTAAAGTCACAAATTCTAGCTGTCTC TCCACTCACTGGCAAGGTAGC 3' (*LoxP* sequence Eco RV site)

B.

For intron 1, guide sequence 1	Forward: TAATACGACTCACTATAGCTAGGCTGAAGCTGGGCGAT Reverse: TTCTAGCTCTAAAACATCGCCCAGCTTCAGCCTAG
For intron 1, guide sequence 2	Forward: TAATACGACTCACTATAGGCAGAAGTCTAGGCTGAAGC Reverse: TTCTAGCTCTAAAACGCTTCAGCCTAGACTTCTGC
For intron 2, guide sequence 1	Forward: TAATACGACTCACTATAGGAGCAAGGTTTGCTGGACGA Reverse: TTCTAGCTCTAAAACTCGTCCAGCAAACCTTGCTC
For intron 2, guide sequence 2	Forward: TAATACGACTCACTATAGGTCCCATTTAAATCAAAAGC Reverse: TTCTAGCTCTAAAACGCTTTTGATTTAAATGGGAC

2.1.2.4 T7 endonuclease assay

To assess the efficiency of guide RNAs, T7 endonuclease assay (Sakurai, T. *et al.*, 2014) was performed on PCR products of the DNA extracted from animals born from microinjection. Briefly, a 20ul reaction was set up according to the manufacturer's protocol for T7 endonuclease I (New England Biolabs; NEB): 10ul PCR product, 2ul 10X NEB Buffer 2, and 8ul ddH2O. The reaction mixture was incubated in a thermocycler to denature and re-nature the PCR product using the following program: 95^{o}C 5 min, ramp of -2^{o}C/sec to 85^{o}C and hold for 5 secs, ramp of -0.1^{o}C/sec to 25^{o}C and hold for 5 sec and infinite hold at 4^{o}C. Next, 0.75ul of T7 endonuclease I (NEB) was added to the reaction mixture and incubated at 37^{o}C for 30 mins. The T7-treated samples were analyzed on a 2% agarose gel to check if there were fragments generated from endonuclease digestion of indels.

2.2 Generation of constitutive and tissue-specific *Snrpb* mutant (*Snrpb*$^{+/-}$) embryos

2.2.1 Generation of *Snrpb*$^{+/-}$ mutant embryos

Snrpb$^{+/-}$ mutants were generated by crossing *Snrpb*$^{LoxP/+}$ mice with *β-actin-Cre*$^{Tg/+}$ mice. Upon *β-actin Cre* activation, one allele of *Snrpb* had exons 2 - 3 removed from all cells in the mutant embryos. One-fourth of the embryos were expected to be heterozygous mutants from this and all other matings with *Cre* lines. PCR genotyping was done to confirm the genotype of the embryos (see section 2.4).

2.2.2 Generation of neural crest cell-specific *Snrpb*$^{+/-}$ mutants

To generate embryos and animals with neural crest-specific *Snrpb* heterozygosity, *Wnt1-Cre2*$^{Tg/+}$ animals were mated with *Snrpb*$^{LoxP/+}$ mice. Embryos obtained from these matings were *Snrpb* heterozygous mutant in the neural tube, neural crest cells and their derivatives; all other cells were *Snrpb* WT.

2.2.3 Generation of mesoderm-specific *Snrpb*$^{+/-}$ mutants

To generate embryos and animals with mesoderm-specific *Snrpb* heterozygosity, *Mesp1-Cre*$^{Tg/+}$ animals with *Snrpb*$^{LoxP/+}$ mice were mated. Embryos obtained from these mating were *Snrpb* heterozygous mutant in mesodermal cells and their derivatives, while all others were *Snrpb* WT.

2.3 Collection of embryos

The male and female animals were put in the same cage in the late afternoon. In the following morning females were checked if they were plugged. The day of plug was considered E0.5. On the day of dissection, pregnant females were euthanized through isoflurane euthanasia, embryos were removed from their extraembryonic membranes and the yolk sacs were collected for genomic DNA extraction and genotyping. All embryos were assessed for morphological abnormalities, viability was checked by the presence of a heartbeat, and somite number was counted for embryos between E8.5 and E10.5.

2.4 Genotyping of mice and embryos

i. Δ-61 and Δ-46 mutants: Genomic DNA was extracted from mouse tails or yolk sacs by alkaline lysis (Hou *et al*., 2017). *T*he WT, Δ-61 and Δ-46 alleles were amplified (Primer sequences in table 2.2) using the following PCR program: 30 s 95°C, 30 s 62°C, 30 s 72°C for 35 cycles followed by an elongation step of 10 min at 72°C. This PCR product was run on a 2% agarose gel to visualize the WT (292 bp) and mutant (Δ-61, 231 bp; Δ-46; 246 bp) amplicons.

ii. **Constitutive and conditional mutants**: For identifying the conditional allele (with *LoxP* sequences), primers for intron 1 *LoxP* or intron 3 *LoxP* were used (Primer sequences in table 2.2). The following PCR conditions were used: 30 secs 95°C, 30 secs 62°C, 30 secs 72°C for 35 cycles followed by an elongation step of 10 mins at 72°C. For detecting the intron 1 *LoxP*,

the PCR amplified a WT (347 bp) and a mutant (387 bp) amplicon. For the intron 3 *LoxP* detections, the WT and mutant band was 207 bp and 247 bp, respectively. For detection of exon 2 to exon 3 deletion after Cre-recombination, a three-primer PCR was done that amplified from intron 1 to intron 3 (using primers F2, F3 forward and R3 reverse from table 2.2). From this PCR, the wild-type alleles of 207 base pair (spanning in intron 3) was amplified in the wild-type embryos. The heterozygous mutants produced a wild-type (207 bp) and a mutant band (320 bp) that was generated upon Cre-recombination (sequence from intron 1 *LoxP* to intron 3 *LoxP* where exon 2, intron 2, alternative exon 2 was deleted).

Table 2.2: ***List of primers used for genotyping Snrpb alleles. The sequences are in 5' to 3' direction.***

For	Forward Primer	Reverse primer
Δ-61, Δ-46	F1: GATCCTGTGTGACTGTGATGAG	R1: GGAGAACATGAGAGCCCTTTAC
Intron1 *LoxP*	F2: CCCGAGACAGACACAACATAAG	R2: GCTTTGAAGGTCCCGATGAA
Intron3 *LoxP*	F3: TCTGGGTACTTTGGTGCAAG	R3: GCCTGTATAACATCCCTGGTG

iii**. Genotyping of commercially available lines:** For the commercially available lines, namely R26R, *Wnt1-Cre2*, mT/mG and *β-actin-Cre*, genotyping was performed as detailed on The Jackson Laboratory website: protocol #29915 (*R26R*), #25394 (*Wnt1-Cre2*), #20368 (mT/mG), #33618 (*β-actin-Cre*), respectively. For *Mesp-1* genotyping *(Saga et al, 1999)*, primers are used in combination with internal control primers. The primer list for *Cre* genotyping is given below with band sizes.

Table 2.3: ***List of primers used for genotyping commercially available lines used in the study. The sequences are 5'to 3' direction.***

For	Forward Primer	Reverse primer	Band Size
Wnt1-Cre2	Mutant: CAGCGCCGCAACTATAAGAG	CATCGACCGGTAATGCAG	~475 bp
	Internal control: CAAATGTTGCTTGTCTGGTG	GTCAGTCGAGTGCACAGTTT	200 bp
β-actin-Cre	Mutant: GTCCTTACCCAGAGTGCAGGT	Common: TGCAATCCCTTGACACAGA	187 bp
	Wild-type: ACCAGTTTCCAGTCCTTCTGG		241 bp
Mesp1-Cre	Mutant: TGCCACGACCAAGTGACAGCAATG	ACCAGAGACGGAAATCCATCGCTC	400 bp
	Internal control: CAAATGTTGCTTGTCTGGTG	GTCAGTCGAGTGCACAGTTT	200 bp
R26R	Common: AAAGTCGCTCTGAGTTGTTAT	Mutant: GCGAAGAGTTTGTCCTCAACC	300 bp
		Wild-type: GGAGCGGGAGAAATGGATATG	603 bp
mT/mG	Mutant: TAGAGCTTGCGGAACCCTTC	Common: CTTTAAGCCTGCCCAGAAGA	128 bp
	Wild-type: AGGGAGCTGCAGTGGAGTAG		212 bp

2.5 Postnatal fitness observation of *Snrpb* Δ-61mutants

Animals (N: wild-type=10, heterozygous=29, homozygous=18) that were born were followed at birth and onward. Animals that became sick and died were recorded, for each genotype and

the sex was noted. Dead animals were checked for any abnormal lesions, growth, or any other sign of diseases. The ones that were very sick were dissected (N=4) to look at internal organs and any sign of abnormalities. For blood analysis, intracardiac blood was collected via cardiac puncture immediately from euthanized animals. Blood was collected in EDTA tubes.

2.6 Wholemount *in situ* hybridization and preparation of embryos for embedding

Embryos were collected and fixed in 4% PFA. They were washed and kept in PBS solution at 4°C until use. They were then dehydrated using a graded methanol series for wholemounts. Wholemount RNA *in situ* hybridization was performed as previously described (Revil and Jerome-Majewska, 2013). For cryo-embedding, fixed embryos were first cryoprotected in 30% sucrose overnight in a rocker at 4°C, embedded in Sheldon Cryomatrix (Thermoscientific) and stored at minus 80°C until sectioning.

2.7 Cartilage staining of embryos

To investigate cartilage formation, embryos were stained with Alcian Blue (Regeur and Lyons, 2014). Embryos were put to fix in Bouin's solution on a rocker at room temperature for 2 hours followed by several washes with 0.1% ammonium hydroxide in 70% ethanol, until the embryos looked white. The embryos were then incubated in 5% acetic acid solution twice for 1 hour each. They were then stained with 0.05% Alcian Blue (Fisher scientific) in 5% acetic acid solution for 2 hours. Embryos were rinsed with 5% acetic acid and then 100% methanol, respectively, two times each for 1 hour. The embryos were then cleared in BABB (1 benzyl alcohol: 2 benzyl benzoate) solution and once cleared, the cartilages were analyzed under a light microscope (Leica Mz6 Infinity1 stereomicroscope).

2.8 Skeletal staining and analyzing of embryos

For skeletal staining, the skin was removed from frozen E17.5 embryos and neonatal pups and stained as described by Wallin *et al*. (1994). Briefly, after evisceration, they were fixed in 100%

ethanol for 24 hours and then put in 100% acetone for another 24 hours. They were then kept at 37°C on a rocker in the staining solution of alizarin red and Alcian blue for 3-4 days. Then they were washed with water and then put in a series of potassium hydroxide (KOH) and then KOH in glycerol to remove excess tissue. Once the tissues were cleared and the skeletons were exposed, they were examined under the microscope and were kept stored in 50% glycerol in KOH.

In the skeletal preparations, the head bones and cartilages were analyzed, the limbs and fingers were checked, and the ribs were inspected for any defects. The ear cartilages and bones were also looked at including the middle ear structures such as the malleus, incus and stapes. For the neural crest-cell specific mutants, I used Infinity Analyze program to measure the mandible length from the incisor to the articular surface of the condyloid process from the photograph taken by Leica MZ6 Infinity1 stereomicroscope. Measurements were taken three times per sample and the average was used for statistical analysis. In mutants in which the processes of the mandibles were not properly formed, the incisor to the proximal end of the mandible were measured.

2.9 Wholemount X-gal staining of embryos

Embryos were first fixed in 4% paraformaldehyde for approximately 45 minutes. They were washed in the detergent rinse solution (0.02% Igepal, 0.01% sodium deoxycholate, 2 mM $MgCl_2$ in 0.1 M phosphate buffer pH 7.5) 3 times, each 15 minutes. They were then immersed in freshly prepared 1 mg/ml X-gal staining solution (0.02% Igepal, 0.01% Sodium Deoxycholate, 5 mM Potassium Ferricyanide, 5 mM Potassium Ferrocyanide and 2 mM $MgCl_2$ in 0.1 M phosphate buffer pH 7.5) overnight at 37°C in the dark. Embryos were washed in PBS and post-fixed in 4% paraformaldehyde in PBS at 4°C overnight, on a rocker. For sectioning post-staining, embryos were embedded in Sheldon Cryomatrix (Thermoscientific)

and stored at minus 80°C. Images of the sectioned (thickness 15 µm) embryos were taken under Leica M205FA stereomicroscope and ImageJ was then used to quantify the X-gal-stained area. From the top of the neural tube until before the heart was considered for the staining quantification of the craniofacial area.

2.10 Phosphotungstic acid staining for CT scan

Embryos were fixed overnight in 4% paraformaldehyde at 4°C in a rocker and then washed with PBS. After a series of dehydration steps according to a protocol described previously (Lesciotto *et al*., 2020), embryos were stained in 0.7% phosphotungstic acid (PTA). The protocol was modified as embryos were not embedded in wax for scanning. A pre-scanning was done to confirm complete penetration of the PTA in embryos. If the penetration was not complete, the embryos were placed back in the PTA solution. For stages E12.5, E 14.5 and E17.5 it required around two, three and more than 5 weeks, respectively of continued PTA staining for full penetration. Pre-scanning was repeated meanwhile and once all the structures were visualized in the pre-scan, embryos were rehydrated in a series of methanol washes and CT scanning was done at 20-µm thickness.

2.11 Immunofluorescence and TUNEL assay

Immunofluorescence experiments were performed on 10-µm-thick sections according to standard protocols (Zakariyah *et al*., 2012). Primary antibody used was anti-PH3 (Ser10) (06-570, Millipore; 1:200 dilution) and Alexa Fluor 568 (A-11004, ThermoFisher Scientific; 1:500 dilution) secondary antibody was used. For identifying cells undergoing apoptosis, TUNEL assay was performed using a Cell Death Detection Kit, TMR Red (12156792910, Roche). For quantification of fluorescence signal, particle analysis on ImageJ was used. For TUNEL and PH3 quantification, four embryos were analyzed per genotype. The head regions of at least four sections were counted per embryo.

2.12 Immunohistochemistry

Embryos were sectioned at 10-μm thickness for immunohistochemistry as previously described (Beauchamp *et al*., 2021; Hou *et al*., 2017). Anti-P53 primary antibody (2524, Cell Signaling Technology; 1:250 dilution) or anti-neurofilament primary antibody (2H3, Developmental Studies Hybridoma Bank; 1:150 dilution) was used. The secondary antibody that was provided with the VECTASTAIN® Universal Quick HRP Kit was used and visualized with diaminobenzidine (DAB). To look at P53 expression, 3 embryos per genotype and at least 3 sections per embryo were tested. For 2H3, wholemount staining of 2 embryos per genotype was done.

2.13 Western blot

Individual E11.5 embryos were snap-frozen and lysed in RIPA buffer (25 mM Tris·HCl pH 7.6, 10% glycerol, 420 mM NaCl, 2 mM $MgCl_2$, 0.5% NP-40, 0.5% Triton X-100, 1 mM EDTA, protease inhibitor) on ice. Embryos were then sonicated and centrifuged at 13000rpm for 20 minutes at 4°C. Protein lysates from the supernatant were then measured according to standard methods using a DC protein assay kit (Bio-Rad, Mississauga, Ontario, Canada). Proteins were denatured at 95°C for 5 minutes with Laemmli buffer [0.1% 2-mercaptoethanol, 10% glycerol, 2% Sodium dodecyl-sulphate (SDS), 63 mM Tris-HCl (pH6.8)]. 50μg of protein was resolved on 12% polyacrylamide gel. They were then transferred to PVDF membranes (Bio-Rad, Cat#1620260) overnight at 4°C at 20 volts. After blocking the membrane in 5% milk for one hour at room temperature, all membranes were probed with primary antibody overnight at 4°C (*SNRPB* 1:1000, Santa Cruz, cat#sc-374009). The membranes were then incubated at room temperature with horseradish peroxidase-conjugated secondary antibody (Cell Signaling), and antigen-antibody complexes were detected using the ECL system (ZmTech Scientifique, Montreal, Quebec, Canada). The β-actin protein band (1: 5000, Cell signaling)

was used as a loading control to normalize the level of the protein of interest. The blot was cut after transfer and the antibody incubations were performed simultaneously for both SNRPB and β-actin, in two split blots. Images of the protein bands were taken with Bio-Rad's ChemiDoc MP System and were digitally analyzed using Image Lab software. The experiment was repeated at least 3 times with different biological samples.

2.14 RT-PCR

Total RNA was isolated from whole embryos using TRIZOL. The extracted RNA was treated with DNase I (NEB; according to the manufacturer's protocol). The reaction mix was incubated at 37°C for 10 minutes, then added 1 µl of 0.5 M EDTA to stop the reaction and heat inactivation was done at 75°C for 10 minutes. The RNA was then used for reverse transcription with the iScript cDNA synthesis kit (Bio-rad, Cat. #170–8890), according to the manufacturer's protocol. The following conditions were used for cDNA synthesis: 5 min 25°C, 30 min 42°C, 5 mins 85°C. RT-PCR for *Smad2*, *Pou2f1* and *Rere* were performed under the same PCR conditions: 5 mins 95°C, (30 secs 95°C, 30 secs 55°C, 30 secs 72°C) 35 cycles, followed by an elongation step of 5 mins at 72°C. The primers for RT-PCR, are listed below.

Table 2.4: ***Primers Used for RT-PCRs, sequences are 5' to 3' direction.***

For	Forward primer	Reverse primer
Snrpb AE-2 transcript	TTTGCAGGCAGCATTTCC	CTCGCTTCTCTTCCCTTTCT
Mdm2 Exon 3 skipping	GATCACCGCGCTTCTCCTGC	GATGTGCCAGAGTCTTGCTG
Mdm4 Exon 7 skipping	TGTGGTGGAGATCTTTTGGG	CACCTGCTGCATGCAAAATC
Smad2 Exon 3 skipping	GAGCAGAATGGACAGGAAGAA	TCAGTTCTTTTTCTGGGATTGG
Pou2f1 Exon 4 skipping	GGTCTGGACTTTCAGAAACAGC	GAATGGCTGACTGCACTGAA
Rere Exon 4 skipping	GGCCAAACACACCGTATTTC	AGAGTTCCCGATTCTTGATGAC

2.15 RNA isolation for RNAseq

E9.0 embryos were placed in RNA later (Invitrogen) immediately after dissection prior to RNA isolation. After genotyping, heads of two somite-matched embryos from different litters were pooled. RNA extraction was done using a Qiagen RNeasy kit, following the manufacturer's protocol (manufacturer). RNA quantity and quality was checked using ND2000 before sending for RNA sequencing. Three WT and three heterozygous pools (2 embryo heads per pool) were used for RNAseq analysis. Embryos were sex determined by PCR (McFarlane *et al.*, 2013). Each wild-type pool had one male and one female embryo, two mutant pools had only female embryos and one mutant pool had one male and one female embryo. Primers used for sex determination PCR: forward GATGATTTGAGTGGAAATGGAAA TGTGAGGTA, reverse CTTATGTTTATAGGCATGCACCATGTA. The following PCR conditions were used: 2 mins 94°C, (30 secs 94°C, 30 secs 57°C, 30 secs 72°C) 34 cycles, followed by an elongation step of 5 mins at 72°C.

2.16 RNAseq analysis

Sequencing libraries were prepared by the McGill Genome Centre (Montreal, Canada), using a TruSeq Stranded Total RNA Sample Preparation Kit (TS-122-2301, Illumina, San Diego, CA, USA) by depleting ribosomal and fragmented RNA, synthesizing first- and second-strand complementary DNA (cDNA), adenylating the 3′ ends and ligating adaptors, and enriching the adaptor-containing cDNA strands by PCR. The libraries were sequenced using an Illumina NovaSeq 6000 PE100 sequencer, with 100 nucleotide paired end reads, generating between 109 and 230 million reads per sample. The sequencing reads were trimmed using CutAdapt (Martin, 2011) and mapped to the mouse reference genome (mm10) using STAR (Dobin *et al*., 2013) aligner (version 2.6.1d), with default parameters, and annotated using the Gencode (Harrow *et al*., 2006) M2 (version M2, 2013) annotation. Htseq-count [part of the 'HTSeq' (Anders *et al*., 2015) framework, version 0.13.5] was used for expression quantification.

To perform differential splicing analysis, rMATS 4.0.2 (Shen *et al*., 2014) was used, and detected splicing events were filtered by systematically excluding those with a mean of inclusion junction counts lower than 5 in either WT or heterozygous samples. To identify a significant DSE, an absolute inclusion level difference cut-off of more than 0.05 was used and a Benjamin–Hochberg multiple testing correction with an FDR cut-off of less than 0.1 was used. The rationale for relaxing the FDR cut-off here was to obtain a large dataset enriched for alternative splicing events in order to observe general tendencies, such as increased propensity for exon skipping or intron retention in the mutants. To characterize 3′ SS sequences, LaBranchoR (Paggi and Bejerano, 2018), a BP prediction tool based on a deep-learning approach was used, which uses a bidirectional long short-term memory network model to identify relevant BPs upstream of DSEs. The BPs and their surrounding area consensus motifs were generated using WebLogo 3.0 (Crooks *et al*., 2004).

For differential expression analysis (DEA), DESeq2 (Love *et al*., 2014) package was used, and a list of significant DEGs was derived using an FDR cut-off of less than 0.05 with no additional restriction on the absolute log2 fold change (Log2FC) (to allow for detection of even minor expression changes). For Kyoto Encyclopedia of Genes and Genomes (KEGG) pathway analyses, the combined list of up- and down-regulated genes from DEA was used as input to gProfiler2 (Raudvere *et al*., 2019) package (ghost function), and all the detected genes from DEA were used as background.

A differential analysis of transposable element (TE) and long non-coding RNA (lncRNA) expression was also carried out, to investigate whether *SNRPB* deficiency may result in deregulation of the non-coding transcriptome. Those analyses did not uncover any differences in the mutant embryos (data not shown). Spliced Transcripts Alignment to a Reference (STAR) was used to map the processed reads with modified options: —outFilterMultimapNmax 100

—winAnchorMultimap Nmax 100 —outMultimapperOrder Random —alignSJoverhangMin 8 —outFilterMismatchNmax 999 —alignIntronMin 20 —alignIntronMax 1000000 —alignMatesGapMax 1000000, with mouse annotations from the University of California, Santa Cruz RepeatMasker (Gencode M1) and lncRNA (Gencode M1) to guide mapping. The mapped lncRNA and TE reads were respectively quantified with salmon (Patro *et al*., 2017) and TElocal (Jin *et al*., 2015) softwares. Differential lncRNA and TE expression analyses were performed using DESeq2, with the TE and lncRNA read counts being normalized using protein-coding gene expression size factors, and differentially expressed lncRNA and TEs selected based on an FDR cut-off of less than 0.05 and an absolute Log2FC of greater than 0.5 to increase detection signal.

2.17 RT-qPCR

RT-qPCR was performed using Advanced Universal SYBR® Green Supermix. Experiments were performed in biological duplicates to ensure technical replicability. Target genes were normalized with a normalization factor as calculated by geNorm software (Vandesompele *et al*., 2002). Three housekeeping genes – *B2m, Gapdh* and *Sdha* – were used for generation of the normalization factor as previously reported (Vandesompele *et al*., 2002).

Table 2.5: ***Primers Used for RT-qPCR. Sequences are in 5' to 3' direction.***

For	Forward Primer	Reverse primer
Trp53inp1	AAGTGGTCCCAGAATGGAAGC	CTGGGAAGGGCGAAAACTCT
Ccng1	TTCCAAGATAAGTGGCCGAGA	AGTGCGTCCAGACACAATCC
Phlda3	CATGTCAGCTTCTCTGTCCACTT	CTGGTTGGCTCCTTCCATGAT
B2m	ATGCTATCCAGAAAACCCCTCAA	GCGGGTGGAACTGTGTTACG
Gapdh	ATGACATCAAGAAGGTCCTG	CATACCAGGAAATGAGCTTG
Sdha	GCTGTGGCCCTGAGAAAGATC	ATCATGGCCGTCTCTGAAATTC
Snrpb	GCTGCTGGCAGAGGAAT	TCCTGCAATACTGGCTGTG

2.18 Quantification and statistical analysis

Quantitation of the X-gal-stained embryo sections, TUNEL sections and PH3 stained sections were performed using ImageJ software (National Institutes of Health, Bethesda, MD, USA). Statistical analyses were conducted using Prism 8.0 software (GraphPad, San Diego, CA, USA). Chi-square test or non-parametric Mann–Whitney U-test analysis was performed using GraphPad Prism. For survival analysis, Log-rank (Mantel-Cox) test analysis was done. *P value* <0.05 was considered significant.

CHAPTER III

RESULTS

A. RESEARCH FINDINGS OF AIM 1

3.1 A novel 61 base-pair intronic deletion of *Snrpb* regulates SNRPB level and models Cerebrocostomandibular syndrome (CCMS) in mice at a low penetrance

3.1.1 Identification of *Snrpb* alleles with a 61 base-pair (Δ61) and 46 base-pair (Δ46) intronic deletions near alternative exon 2

To generate a conditional mutant mouse model that can be used to reduce levels of *Snrpb* and uncover its role in embryonic development, I targeted introns 1 and 2 to insert *loxP* sequences. The guide RNAs and repair templates were injected into zygotes at the McGill Integrated Core for Animal Modeling (MICAM). From two rounds of microinjections, I received 11 animals (9 males, 2 females) which I genotyped to look for insertions. There was no insertion in the targeted introns 1 and 2 in any of those 11 mice. But I found 3 founder males, who had two different size smaller bands in intron 2. To know the deletion sequence, I cloned the smaller size bands from two founders. The wild-type band was of expected size (292 bp) (Figure 3.1 A). I also cloned the wild-type band and sequencing of the clone confirmed it the expected *Snrpb* wild-type band. For the smaller bands, sequencing revealed one was a 231bp sequence that had a 61-bp deletion in intron 2. The other band was a 246 bp sequence with a shorter 46-bp deletion intron 2, overlapping the 61-bp (Figure 3.1 B). As the location of the deletions in intron 2 were close to the alternative exon 2 that regulates *SNRPB*, I bred each of the founder males having the two different deletions with wild-type CD1 females and observed for phenotypic abnormalities in the offspring.

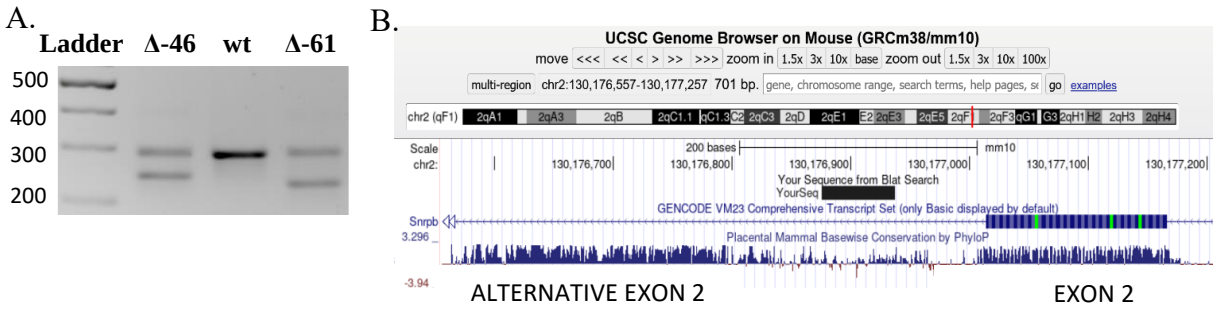

Figure 3.1: ***61-bp and 46-bp intronic deletion occurred in intron 2 of Snrpb.*** **(**A) The lower mutant bands for *Snrpb* Δ46 and *Snrpb* Δ61 mutants were extracted, cloned and confirmed by sanger sequencing as two different size deletions in intron 2. (B) Location of the 61 base-pair deletion that is near the alternative exon 2 of *Snrpb* in UCSC genome browser.

3.1.2 A subset of *Snrpb* Δ61 heterozygous and homozygous mutant embryos and pups at birth were found abnormal with craniofacial, limb and rib defects

I observed that a subset of Δ61 heterozygous (*Snrpb*$^{\Delta 61/+}$) mice was abnormal at birth (P0) (n=13/159). Abnormal P0 animals had abnormal craniofacial phenotypes like microcephaly where the head looked smaller with a shorter snout and mandible (Figure 3.2 A). Of the abnormal pups, some (n= 7/13) had died shortly after birth. To investigate embryonic development of the Δ61 mutants, I then dissected pregnant females and found similar abnormalities such as microcephaly, micrognathia, short snout and smaller ear in about six percent of heterozygous and homozygous mutant embryos (n=8/135) (Figure 3.2 B). Mutant pups also had shorter limbs and finger defects such as clinodactyly and polydactyly (Figure 3.2 C).

As *SNRPB* mutation in CCMS patients is known to cause skeletal abnormalities, to examine if the intronic mutation I generated in *Snrpb* causes cartilage and bone formation defect, I stained embryonic day (E) 14.5 with Alcian blue and E17.5 embryos with Alcian blue and Alizarin

red. At E14.5, cartilage formation was found abnormal in the head of two homozygous mutants (2/11). One *Snrpb*$^{\Delta 61/\Delta 61}$ mutant has severely reduced cartilages in the head with a very short Meckel's cartilage (Figure 3.2 D). The other homozygous mutant had a slightly reduced head cartilage and the proximal portion of the Meckel's cartilage was wavy (Figure 3.2 E). The severely affected mutant had extreme reduction in rib cartilage whereas in one heterozygous mutant the proximal location of lower ribs was wavy. Finger clinodactyly was seen in 5 of the 11 mutants (Figure 3.2 F). The findings of reduced, absent and deformed cartilages suggest that chondrogenesis is hampered in this mutant model.

At E17.5, we found an extra rib pair in around 17% of heterozygous (n=3/17) and 43% of homozygous (n=7/16) mutants (Figure 3.2 G). A wild-type embryo was also found to have an extra pair of ribs (n=1/10). In the sternum, one heterozygous mutant (n=1/17) had reduced ossification centers, suggesting there might be an ossification delay (Figure 3.2 H). In the fingers, two homozygous mutants had clinodactyly (Figure 3.2 E) (n=2/16). In the head, I found reduced ossification in frontal, parietal and interparietal bones in one heterozygous and two homozygous mutants (n=3/33) (Figure 3.2 I). Taken together, the data suggest that ossification is impaired in some *Snrpb* Δ61 mutants.

Though at low penetrance, a significant proportion of Δ61 heterozygous (n=15/306) and homozygous (n=11/168) mutant embryos had morphological and skeletal abnormalities while compared to the wild-type littermates (n=160, which includes two smaller embryos) (T-test,p=.007). In contrast, *Snrpb* Δ46 mutants were normal with the exception of one embryo that was found dead at E14.5 and had a smaller head, jaw and abnormal ear (N=1/158).

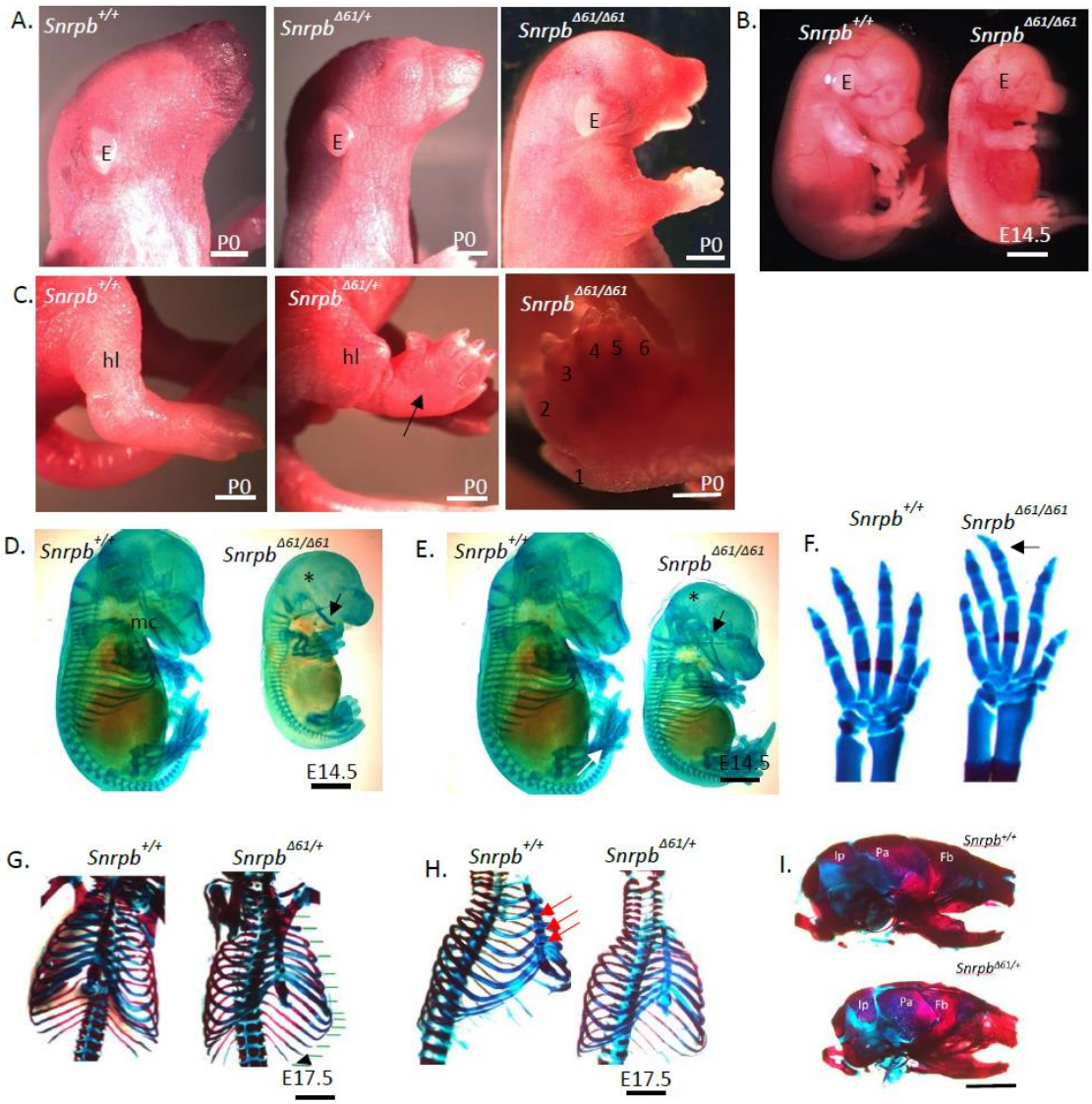

Figure 3.2: ***A 61-bp intron 2 deletion in Snrpb causes abnormal development in mice.*** (A) P0 mutants at birth showing craniofacial abnormalities such as microcephaly, shorter snout and smaller jaw in the heterozygous and homozygous mutants. (B) Similar craniofacial abnormalities were found at embryonic stage E14.5. (C) *Snrpb*$^{\Delta 61/+}$and *Snrpb*$^{\Delta 61/\Delta 61}$ mutants showing abnormal hind limb (black arrow) and polydactyly, respectively. (D-E) Showing skeletal anomalies such as abnormal Meckel's cartilage (black arrows), limbs, and ribs and head cartilages (asterisks) in the mutants. (F) A E17.5 mutant embryo showing clinodactyly of the middle finger (arrow). (G) Extra pair of ribs in the *Snrpb*$^{\Delta 61/+}$ mutant at E18.5 (black arrowhead). (H) Absence of ossification centers in the sternum one of the deletion mutants. (I)

Reduced ossification in the mutant head bones compared to control littermate. E, Ear; mc, Meckel's cartilage; Fb, frontal bone; Pb, Parietal bone; Ip, interparietal bone. Scale bar=500 µm

3.1.3 *Snrpb* Δ61 heterozygous and homozygous mutant pups are significantly smaller and die over time

I found that *Snrpb*$^{\Delta 61/+}$ and *Snrpb*$^{\Delta 61/\Delta 61}$ pups weighed less than their wild type littermates at birth and onward (Figure 3.3 A, B). Additionally, when we followed five litters of animals born form heterozygous animal matings, *Snrpb*$^{\Delta 61/+}$ and *Snrpb*$^{\Delta 61/\Delta 61}$ alleles were found in Mendelian segregation (n= wt: *Snrpb*$^{\Delta 61/+}$: *Snrpb*$^{\Delta 61/\Delta 61}$ = 10:29:18; chi-square test, p value= 0.323) at birth. However, a significant proportion of heterozygous mutants (41%, n=12; Log rank test, p value=.02) and homozygous mutants (34%, n=6; Log rank test, p value= .04) died or had to be euthanized between four and 48 weeks of life, suggesting that this mutation reduced fitness (Figure 3.3 C). In contrast, no mutants for 46 bp intronic deletion had died (n=0/31). The common external signs of sickness seen in *Snrpb* Δ61 mutants included being pale, hunched and dehydrated, coats were turning rough, seizure and bloated abdomen. Autopsy of dead mutant animals (n=4, 2 homozygous and 2 heterozygous mutants) showed lesions in their lungs and spleens (Figure 3.3 D). Two of the 29 heterozygous mutant mice had developed cataract, and two others had circling behavior in the cage, which is often associated with inner ear defects (Lee *et al*., 2001). These findings suggest that the 61 base-pair intronic deletion results in morphological defects in embryos and causes postnatal abnormalities, which could be because of disrupted *Snrpb* mRNA expression and or protein levels.

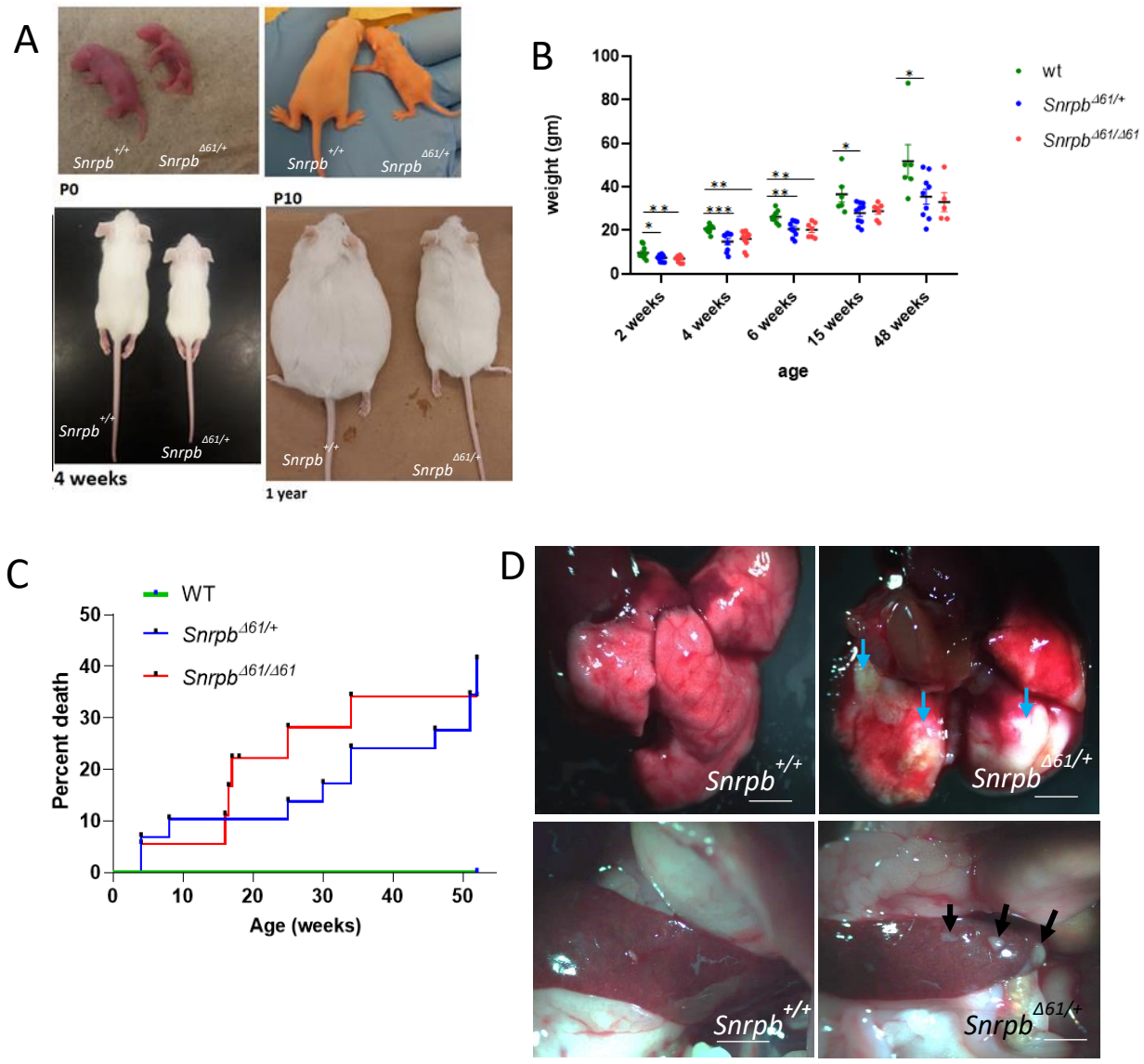

Figure 3.3: ***Wild-type Snrpb is required in postnatal period in mice.*** (A, B) The Δ61 mutants were smaller compared to the controls at birth and onward. The weight was significantly reduced in the mutants (multiple t-test). (C) A significant proportion of Snrpb$^{\Delta 61/+}$ and Snrpb$^{\Delta 61/\Delta 61}$ animals die over time (N: wt=0/10; *Snrpb*$^{\Delta 61/+}$=12/29; *Snrpb*$^{\Delta 61/\Delta 61}$=6/18). (D) Abnormal lesions in the lung (blue arrows) and spleen (black arrows) were found in the sick mutants.

3.1.4 Blood analysis of mutants did not reveal any significant changes in the complete and differential blood count

Since animals with the *Snrpb* Δ61 mutation were becoming pale, sick and dying over time, I collected blood from wild-type (n=3), heterozygous mutant (n=3), and homozygous (n=3) mutant adult animals. Blood analysis was done to find any pathological indications in blood parameters that might be associated to their sickness or death. The complete blood count (CBC) was done and the number of different cells such as white blood cells (WBC), red blood cells (RBC), platelets, neutrophils, eosinophil, monocytes were counted for any significance difference among the genotypes. As the sick animals showed paleness, to test for presence of anemia, the level of hemoglobin, hematocrit, mean corpuscular volume (MCV), mean corpuscular hemoglobin *(*MCH) and mean corpuscular hemoglobin concentration (MCHC) were also checked in the samples. However, no significant difference was seen among the wild-type and the mutant animals in different parameters of the complete blood test (Figure 3.4).

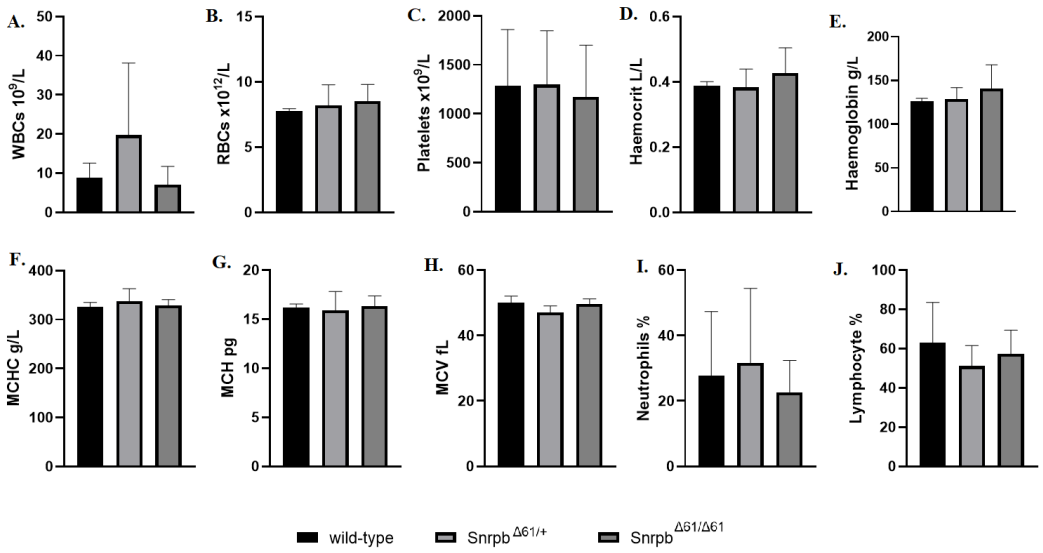

Figure 3.4: ***Blood parameters analysis in wild-type and Snrpb Δ61 mutant animals.*** No significant difference was found between adult wild-type and *Snrpb*$^{\Delta 61/+}$ or *Snrpb*$^{\Delta 61/\ \Delta 61}$ mutants' blood parameters (A-J). Error bar indicates standard deviation (SD).

3.1.5 An increase in the inclusion of alternative exon 2 and a decrease in SNRPB level was seen in a proportion of *Snrpb* Δ61 heterozygous and homozygous mutant embryos

I postulated that the Δ61 deletion increases the inclusion of the PTC containing exon 2, thereby reduces the protein level of SNRPB. I looked at both transcript and protein of the mutants by RT-PCR and western blot, respectively. For RT-PCR, I used primers from exon1 to exon 4 to amplify the transcripts with the alternative exon 2 in wild type (n=5), $Snrpb^{\Delta 61/+}$ (n=6) and $Snrpb^{\Delta 61/\Delta 61}$ (n=5) mutant embryos. I found an increase in the proportion of E11.5 $Snrpb^{\Delta 61/+}$ (2/6) and $Snrpb^{\Delta 61/\Delta 61}$ (3/5) mutant embryos with inclusion of alternative exon 2 when compared to wild type (1/5) (Figure 3.5 A, B). The difference was not significant.

As I hypothesized that the increased inclusion of alternative exon 2 would lead to a decrease in SNRPB protein level in the *Snrpb* Δ61 heterozygous and homozygous mutants, I performed western blots of E11.5 whole embryos to look at the protein level. These western blot analyses revealed a reduction in SNRPB levels in $Snrpb^{\Delta 61/+}$ (n=3/8) and $Snrpb^{\Delta 61/\Delta 61}$ mutant embryos (n=3/9) (Figure 3.5 C, D). In addition, a group of both heterozygous and homozygous mutant embryos had a lower level of SNRPB than the lowest level seen in the control embryos (under the green dashed line in Figure 3.5 D).

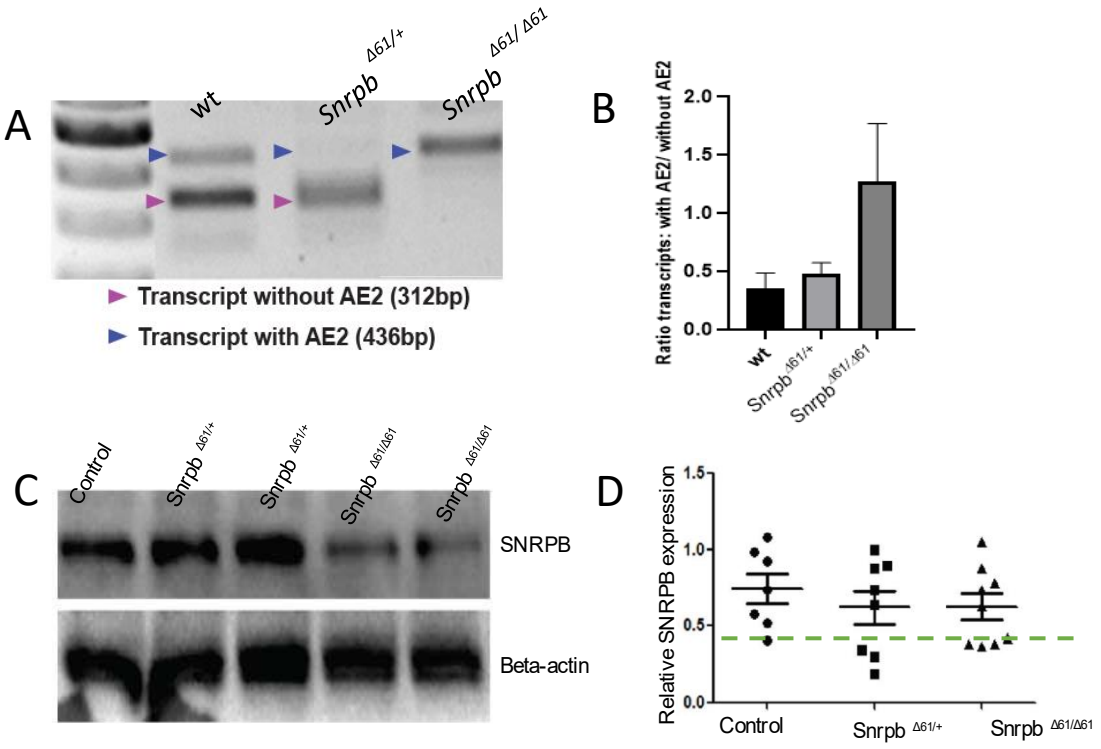

Figure 3.5: ***The intronic 61 bp sequence is important for*** **SNRPB** ***level regulation.*** (A) A subset of the *Snrpb*$^{\Delta 61/+}$ and *Snrpb*$^{\Delta 61/\Delta 61}$ embryos produce the alternative exon 2 containing transcript. (B) Graph showing a statistically non-significant (unpaired t-test) increased ratio of the alternative exon 2 containing transcript in the mutants (N: wild-type (wt)=5, *Snrpb*$^{\Delta 61/+}$=6, *Snrpb*$^{\Delta 61/\Delta 61}$=5) and (C, D) A non-significant decrease in SNRPB protein was seen in a proportion of the heterozygous and homozygous Δ61mutants.

Though the *Snrpb*-Δ61 mouse model recapitulates CCMS abnormalities, the low penetrance at which these defects are found limits our ability to use this model to study the role of SNRPB in embryonic development. Furthermore, our findings suggest that sequences in intron 2 are important for regulating expression of *Snrpb.* Therefore, I modified my approach and used CRISPR/Cas9 to introduce *LoxP* sequences in introns 1 and 3, without disrupting intron 2.

Generation of mice with *LoxP* sequences in intron 1 and 3:

CRISPR/Cas9 injections were performed in two steps to generate conditional mutant mice. From the first round of microinjection, I targeted intron 1 to insert *LoxP* sequence by injecting the guide RNA used before for intron 1 with newly designed oligo template. I received 15 mice (8 males, 7 females) on BL6/C3H genetic background. Of the 15 mice, two males and two females had PCR products that with possible *LoxP* insertion. I digested each of the PCR product with the restriction enzyme (*Eco*RI) included in the oligo template and found the expected band sizes, which was an indication of a potential *LoxP* insertion. Then the mutant bands from the genotyping PCR were sequenced by Sanger sequencing (Figure 3.6 A-C). All of them had *LoxP* sequences inserted in intron 1. Each of the founders was then mated to wild-type C3H animals to see if the *LoxP* is transmitted to the offspring. Three founders transmitted the *LoxP* to the F1 animals confirming germline insertion of the sequence.

For inserting the second *LoxP* sequence in *Snrpb* intron 3, homozygous F2 males were generated on C3H genetic background and sperm from one male was used to fertilize oocyte of females of BL6/C3H genetic background. 13 pups (4 males, 9 females) from this round of microinjection were screened by PCR. Of them, two males and two females had insertions in intron 3. The PCR product was digested with *Eco*RV as restriction site for *Eco*RV was included in the repair template after the *LoxP* sequence to facilitate screening. The mutant band from the genotyping PCR were sequenced by Sanger sequencing (Figure 3.6 D-F).

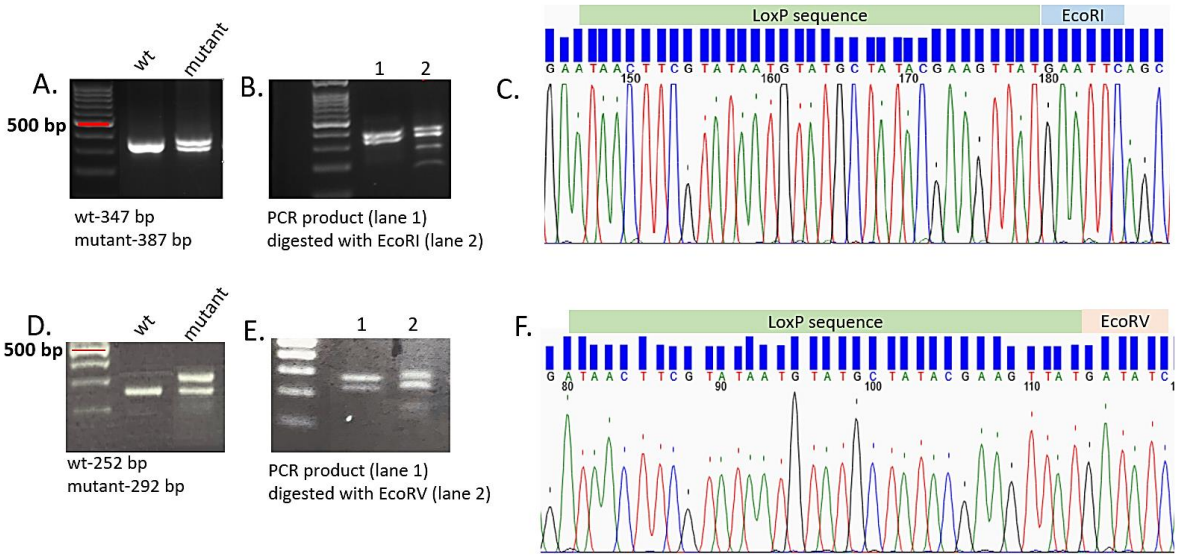

Figure 3.6: ***Sanger sequencing confirms LoxP insertion in Snrpb intron 1 and 3.*** Genotyping PCR (A, D), restriction enzyme digestion of the PCR products (B, E) and sequencing of the mutant bands (C, F) confirmed *LoxP* insertion in *Snrpb* intron 1 and intron 3, respectively.

3.2 *Snrpb* constitutive heterozygosity causes embryonic lethality in mice before organogenesis

As the CCMS patients are heterozygous for *SNRPB* mutation, I first aimed to make constitutive heterozygotes ($Snrpb^{+/-}$) mice by mating $Snrpb^{loxP/+}$ animals with *β-actin-cre* mice. (Figure 3.7 A). From this mating, I did not find any $Snrpb^{+/-}$ animals at postnatal day 0 (P0) or weaning (P21), indicating that these mutants died before birth (n=22, 3 litters, *chi-square* P value=0.04) (Table 3.1A).

To determine when $Snrpb^{+/-}$ embryos die, I dissected pregnant females (mating: *β-actin-*$cre^{tg/+}$ x $Snrpb^{loxP/+}$) from E6.5 – E10.5 (Table 3.1B). I found that $Snrpb^{+/-}$ embryos were abnormal from E7.5 and were undergoing resorption by E9.5. All mutants were found dead by E10.5

(Figure 3.7 D-J). At E8.5, one-third of the *Snrpb*$^{+/-}$ mutants (n=3/9) developed heart, somites, and neural folds. However, they were smaller when compared to the control embryos, and the forebrain, midbrain, and hindbrain were not formed. The remaining E8.5 *Snrpb*$^{+/-}$ mutants (n=6/9) arrested earlier and only headfolds could be seen in those embryos. At E9.5, most of the mutant embryos (n=5/6) had no identifiable structures (Figure 3.7 H) and one embryo (n=1/6) developed outside of the yolk sac had heart and neural folds (Figure 3.7 I). By E10.5, I found only one deformed dead mutant embryo. Thus, constitutive heterozygous deletion of *Snrpb* caused embryonic lethality before organogenesis.

I used RT-PCR to confirm that *Cre*-mediated deletion of the *Lox*P-flanked region generated a shorter *Snrpb* transcript of expected size of 527 bp (Figure 3.7 B). A smaller PCR product below the wildtype 791 bp transcript was seen in the mutants and was found to be nonspecific to *Snrpb.* A statistically significant 70% reduction in mRNA levels of *Snrpb* in E8.5 *Snrpb*$^{+/-}$ embryos were found (p= 0.0052, two-tailed t-test) (Figure 3.7 C). Thus, deletion of exons 2 – 3 of *Snrpb* leads to a significant reduction in *Snrpb* level in heterozygous mutant embryos. I postulate that the level of functional protein expressed by a single wild-type allele of *Snrpb* was insufficient for embryonic growth and survival post-implantation.

Table 3.1: ***Mendelian segregation table for Snrpb heterozygous mutants at weaning (A) and different stages of embryonic development (B).***

A.

Animals crossed	***Snrpb*** $^{L/+}$	***Snrpb*** $^{L/+}$***; beta actin*** $^{tg/+}$	***Snrpb*** $^{+/+}$***; beta actin*** $^{tg/+}$	***Snrpb*** $^{+/+}$	**Total genotyped**
Snrpb $^{L/+}$ x *Beta actin-Cre* $^{Tg/+}$	6	0	7	9	22

B.

Stage	***Snrpb*** $^{L/+}$	***Snrpb*** $^{L/+}$***; beta actin*** $^{tg/+}$ **(abnormal/dead)**	***Snrpb*** $^{+/+}$***; beta actin*** $^{tg/+}$	***Snrpb*** $^{+/+}$	**Total genotyped (#not typed resorptions)**
E6.5	8	8	5	5	26 (0)
E7.5	3	5 (5)	2	4	14 (0)
E8.5	12	9 (9)	19	12	52 (1)
E9.5	2	6 (6)	2	2	12 (2)
E10.5	3	1 (1)	4	2	10(0)
Total	**28**	**29 (21)**	**32**	**25**	**114**

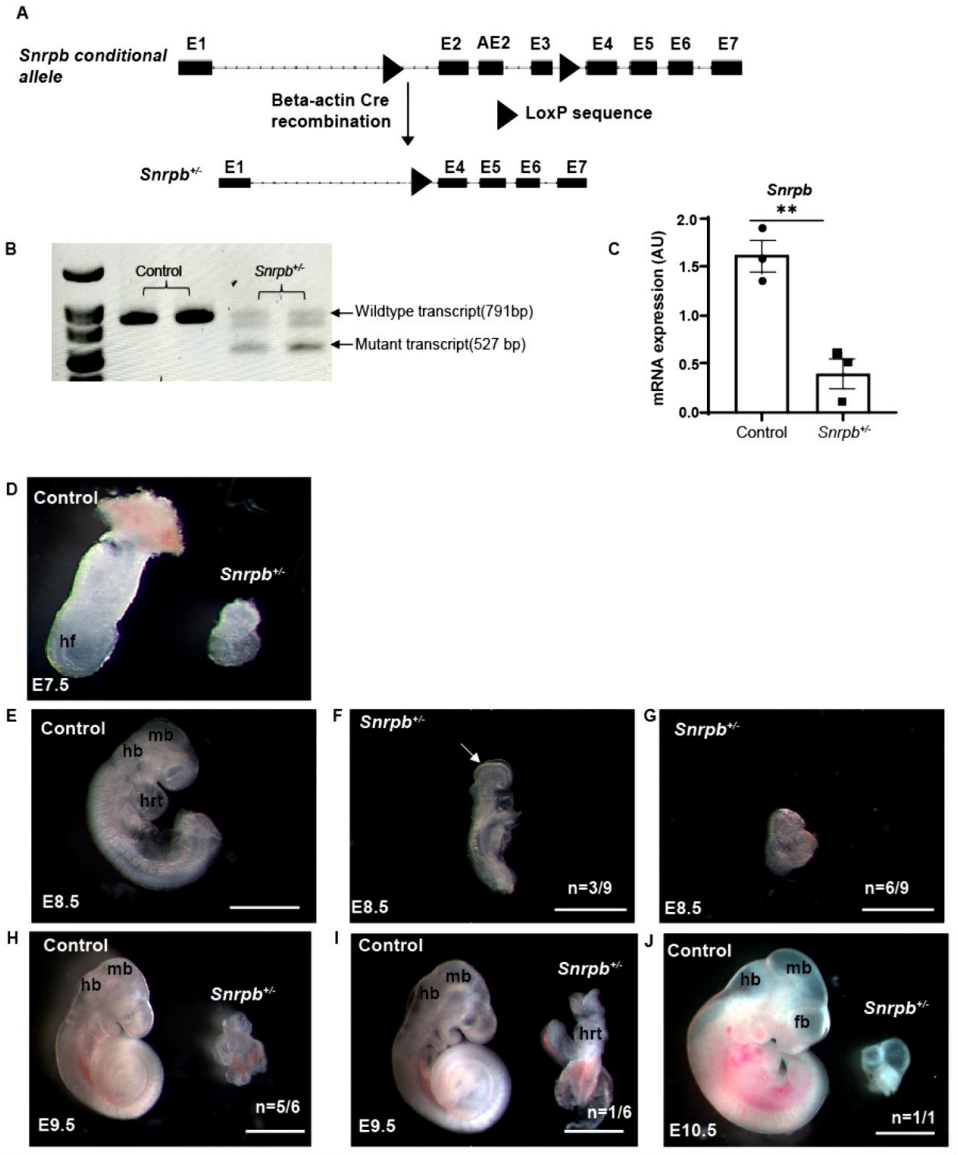

Figure 3.7: ***Snrpb heterozygosity causes embryonic lethality before organogenesis.*** (A) Generation of *Snrpb*$^{+/-}$ allele by mating *Snrpb*$^{loxP/+}$ mice with *Beta-actin Cre*$^{tg/+}$ mice. (B) *Snrpb*$^{+/-}$ embryos produce a shorter transcript of 527 bp (primers amplified E1-E6) (C) A 70% reduction of *Snrpb* the *Snrpb*$^{+/-}$ mutants found by RT-qPCR. (D) Abnormal *Snrpb*$^{+/-}$ embryo at E7.5. (E-G) A control embryo at E8.5 showing normal embryonic development while the *Snrpb*$^{+/-}$ mutants were abnormal. (H-I) Abnormal *Snrpb*$^{+/-}$ mutants compared to the control littermates (on the left). (J) One deformed mutant embryo was found at E10.5. mb, midbrain; hb, hindbrain; fb, forebrain; hrt, heart; hf, headfold; nf, neural fold. Scale bar= 500 µm. (Adapted from Alam *et al.*, 2022)

Snrpb constitutive heterozygous embryos died before organogenesis. Thus *Snrpb*$^{+/-}$ mutants could not be used to study how reduced SNRPB causes specific tissue anomalies in CCMS. Thus, I decided to use tissue-specific *Cre* lines to remove *Snrpb* from specific cell types during development. Since ribs are derived from the mesoderm and rib gaps are one of the most prevalent defects found in CCMS patients (Lynch *et al.,* 2014; Bacrot *et al*., 2015; Tooley *et al.,* 2016), I first describe mice with loss of *Snrpb* in the mesodermal cells and their derivatives.

3.3 *Snrpb* is required in mesodermal cell lineages for proper embryonic development and survival

3.3.1 *Snrpb* mesoderm-specific heterozygous mutants have embryonic abnormalities and die before birth

Mesp1 is expressed in the nascent mesodermal cells at early gastrulation (from E6.5) and cells that exit the primitive streak (Saga *et al.,* 1996). To remove *Snrpb* from mesodermal cells and their lineages, I mated *Mesp-1 Cre* mice with *Snrpb* conditional *(Snrpb*$^{LoxP/+}$) mice. To determine if the resulting *Snrpb*$^{mes+/-}$ pups are born, I allowed the pregnant females from these matings go to term and followed the pups until weaning. I found that all pups that were born survived until weaning and when genotyped, no mutants (*Snrpb*$^{mes+/-}$) were found (n=0/30, *Chi-square* p value= .0079) (Table 3.6). To investigate if *Snrpb*$^{mes\ +/-}$ embryos are abnormal and when they die before birth, I dissected the pregnant females from E9.5 to E17.5 (Table 3.2). At E9.5, I recovered 38 mutants of which five were abnormal. Two mutants had narrow frontonasal prominence and a smaller pharyngeal arch 2 with an enlarged heart (Figure 3.8 A, right). The remaining three mutants had an otic vesicle with an irregular shape when compared to control. At E10.5, I found three of the five *Snrpb*$^{mes+/-}$ mutants did not have an epicardium

(Figure 3.8 B, right). Until this stage, the somites looked normally formed in the mutants. At E12.5, out of nine mutants, three were normal looking and four were resorbed. The remaining two *Snrpb*$^{mes+/-}$ mutants had abnormal heart (Figure 3.8 C, right). At E13.5, I found two mutants, one had a smaller lower jaw and slight edema in the back (Figure 3.8 D), while the other one looked phenotypically normal. By E14.5, the phenotypes became fully penetrant and all the *Snrpb*$^{mes+/-}$ mutants (n=9) were either resorbed (n=5) or morphologically abnormal (n=4) (Figure 3.8 E). The abnormal embryos had extensive subepidermal edema in the back suggestive of a cardiac or vasculature defect and had a smaller lower jaw. They looked overall smaller than the control embryos. By E17.5, I found only one resorbed mutant in a total of 14 embryos. These preliminary data suggest that the *Snrpb*$^{mes+/-}$mutants die by 17.5 and that no mutants survive to birth when one allele of *Snrpb* is removed from the mesodermal cells and their derivatives.

Table 3.2: ***Mendelian segregation table for mesoderm specific Snrpb heterozygous mutants at different stages of embryonic development and birth***. **Chi-square* test p value was statistically significant at P0. ^= abnormal; $^{\Delta}$ = dead/resorbed.

Stage	***Snrpb*** $^{L/+}$	***Snrpb*** $^{L/+}$***; Mesp1-Cre*** $^{tg/+}$ **(abnormal/dead)**	***Snrpb*** $^{+/+}$***; Mesp1-Cre*** $^{tg/+}$	***Snrpb*** $^{+/+}$	**Total genotyped**	**Not typed**	**# Litters**
E9.5	24	38 (5^)	27	37	126	5(4 resorbed)	9
E10.5	9	5(3^)	3	9	26	-	2
E12.5	5	9 (2^, 4$^{\Delta}$)	7	7	28	-	2
E13.5	2	2(1^)	7	4	15	3(resorbed)	2
E14.5	5	9 (4^, 5$^{\Delta}$)	5	11	30	-	2
E17.5	4	1(1$^{\Delta}$)	2	7	14	-	1
P0*	12	0	7	11	30	-	3
Total	**61**	**64**	**58**	**86**	**249**	**8**	**21**

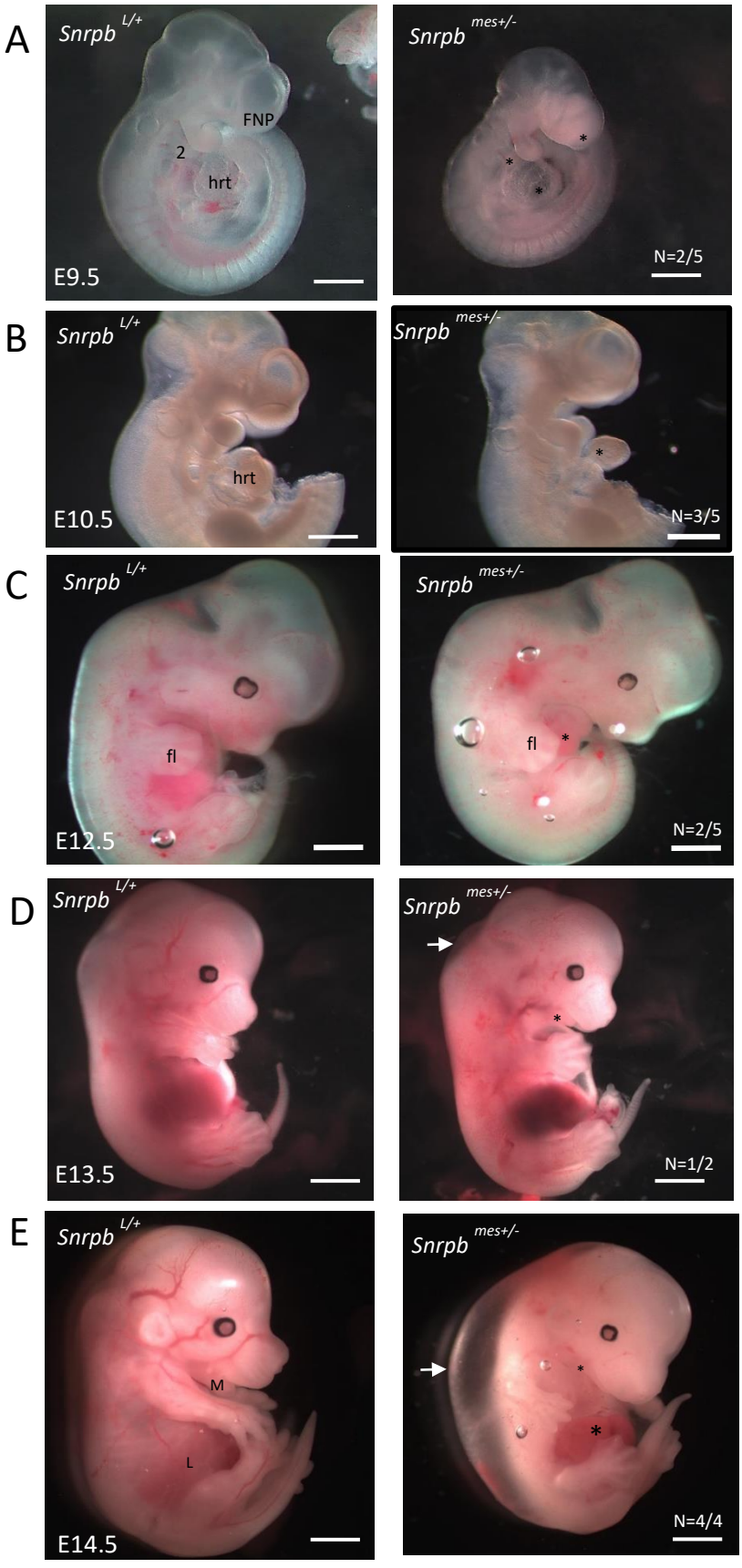
A
Snrpb L/+
FNP
2
hrt
E9.5
Snrpb mes+/-
N=2/5
B
Snrpb L/+
hrt
E10.5
Snrpb mes+/-
N=3/5
C
Snrpb L/+
fl
E12.5
Snrpb mes+/-
fl
N=2/5
D
Snrpb L/+
E13.5
Snrpb mes+/-
N=1/2
E
Snrpb L/+
M
L
E14.5
Snrpb mes+/-
N=4/4

Figure 3.8: ***Mesoderm-specific Snrpb heterozygous mutants have embryonic abnormalities*****.** (A) E9.5 *Snrpb*$^{mes+/-}$ mutant shows abnormal development of frontonasal prominence, smaller pharyngeal arch 2 and a larger heart compared to the control embryo. (B) Abnormal E10.5 *Snrpb*$^{mes+/-}$ mutant. (C) At E12.5, two of the five mutants had an open abdominal cavity with abnormal heart formation. (D) At 13.5, a *Snrpb*$^{mes+/-}$ mutant embryo showing a smaller jaw (black asterisk) and a slight swelling dorsal subepidermal swelling (arrow). (E) At 14.5, all mutants had a smaller jaw and head, with extensive edema in the back (arrow) and exposed liver the liver (black asterisk). At this stage, mutants were all smaller than the controls. For all the stages except P0, the *Chi-square* test p-value was not significant for Mendelian segregation analysis. Black asterisks on the mutant embryos in each panel show abnormal structures. The left panel shows a control embryo. FNP, frontonasal prominence; 2, pharyngeal arch 2; hrt, heart; M, mandible; fl, forelimb; L, liver. Scale bar= 500 µm

3.3.2 Cartilages derived from both mesoderm and neural crest cells (NCCs) are reduced in the E14.5 *Snrpb*$^{mes+/-}$ mutant embryos

To look at the skeletal development in the *Snrpb*$^{mes+/-}$ mutants, I stained the E14.5 embryos with Alcian blue. The staining revealed significant reduction in the cartilages in the craniofacial region and abnormal formation of the ribs. In the head, squamosal cartilage was markedly reduced in the mutants (n=3/3) (Figure 3.9). The cochlear cartilage of the auditory capsule of inner ear was also reduced in all three mutants analyzed (Figure 3.9A). Ventral analysis of the head cartilage revealed the hypophyseal cartilage, which forms part of the basisphenoid bone, was hypoplastic in the mutants (Figure 3.9 A, B). Intriguingly, I found, Meckel's cartilage, which is completely derived from the neural crest cells (NCCs) was smaller, and wavy in the *Snrpb*$^{mes+/-}$ mutant embryos (n=3/3) (Figure 3.9 A, B). However, the other frontal face cartilages such as nasal cartilage were not compromised in the mutants (Figure 3.9 A, B).

The ribs and the limbs which are derived from mesodermal cell lineages, more specifically from paraxial mesoderm, have gaps in CCMS patients. Therefore, I analyzed cartilage formation in those structures in *Snrpb*$^{mes+/-}$ mutants. I found the rib cartilages were irregularly spaced in the mutants (n=3/3), when compared to the control littermates (Figure 3.9 C). Ventral analysis of the ribs revealed that lateroventral extension of the ribs was shorter than those of the wild-type embryos (Figure 3.9 D). In addition, the primordium of the sternum was not formed in the mutants and the limbs were shorter in *Snrpb*$^{mes+/-}$ embryos.

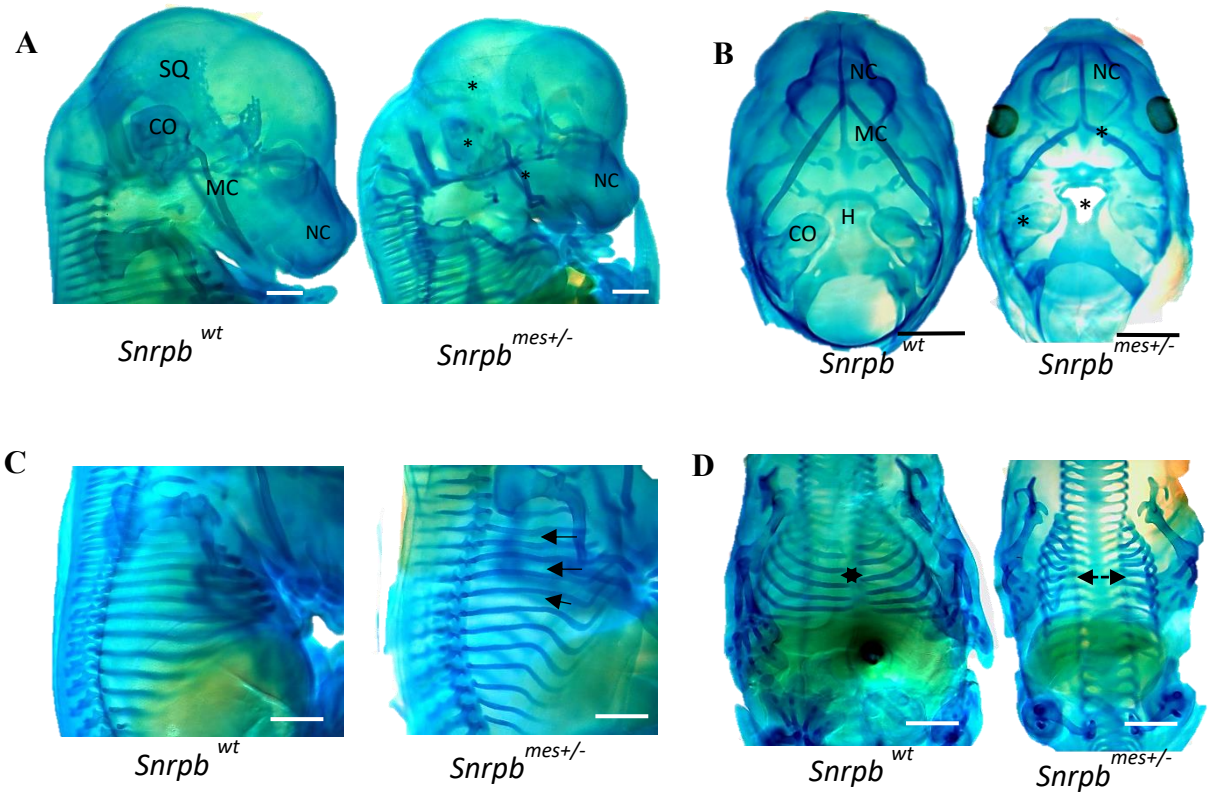

Figure 3.9: ***Cartilage development was abnormal in the Snrpb***$^{mes+/-}$ ***mutants.*** (A) Head cartilages showing that they were affected in the mutant embryos such as the parietal cartilage and the cochlear cartilage was greatly reduced (sagittal view). (B) Skull showing abnormal development of the hypophyseal cartilage that is derived from neural crest cells. The center of the cartilage was not formed resulting in a hole in the middle (ventral view). (C) Ribs in the

Snrpb$^{mes+/-}$ mutants show irregular spacing (arrows) compared to the pattern in the wild-type (sagittal view). (D) In the mutants, narrower rib cages were formed and ventrolateral growth of ribs failed to occur (ventral view). The ventral ends of bilateral ribs had more spaces in between (shown in black arrow spacing). The black asterisks show abnormally formed structures in the mutants. SQ, squamosal cartilage; NC, nasal cartilage; MC, Meckel's cartilage; CO, cochlear cartilage; H, hypophyseal cartilage. Scale bar=500 μm

3.3.3 Abnormal pattern of *Sox10* expression was found in the E9.5 *Snrpb*$^{mes+/-}$ mutant embryos

Once generated, NCCs migrate dorsoventrally to various destinations and differentiate to form craniofacial structures. Transcription factor *Sox10* expression is initiated in the early undifferentiated migratory neural crest cell population. The expression subsides once they reach the pharyngeal arch, except for the glial lineages. To look at *Sox10* expression, I immunoassayed the *Snrpb*$^{mes+/-}$ E9.5 embryos with *Sox10* by wholemount immunofluorescence. My preliminary data showed that the pattern of the Sox10 expressing neural crest cells in the craniofacial region was abnormal in the mutants (n=3) when compared to the control E9.5 embryos. In the controls (Figure 3.10 A), I saw the normal projection of Sox10 expression toward the upper region of the eyes. Sox10 expressing NCCs in this region form the ophthalmic nerves of cranial ganglia upon differentiation. The expression of *Sox10* continues in the NCC derivatives that form the trigeminal nerves. However, I did not see such expression in the mutants (n=3/3) (Figure 3.10 B). In the pharyngeal arches, Sox10 was expressed at the distal region of the second pharyngeal arch in the wild-type embryos (n=3), whereas the expression was more limited to the proximal portion in the *Snrpb*$^{mes+/-}$ mutants, with less expression at the distal part (white asterisk in pa2 of Figure 3.10 B). Moreover, Sox10 expression within the otic vesicle was reduced when compared to what was seen in the wild-

type embryos. Finally, one mutant embryo (n=1/3) had ectopic *Sox10* expression in the frontonasal prominence. These preliminary data demonstrate mesoderm-specific *Snrpb* mutation causes misexpression of *Sox10,* which might be potentially associated with abnormal behaviors of NCCs in the *Snrpb*$^{mes+/-}$ mutants. However, it will need further investigation to understand the fate of the NCCs in *Snrpb*$^{mes+/-}$ mutants.

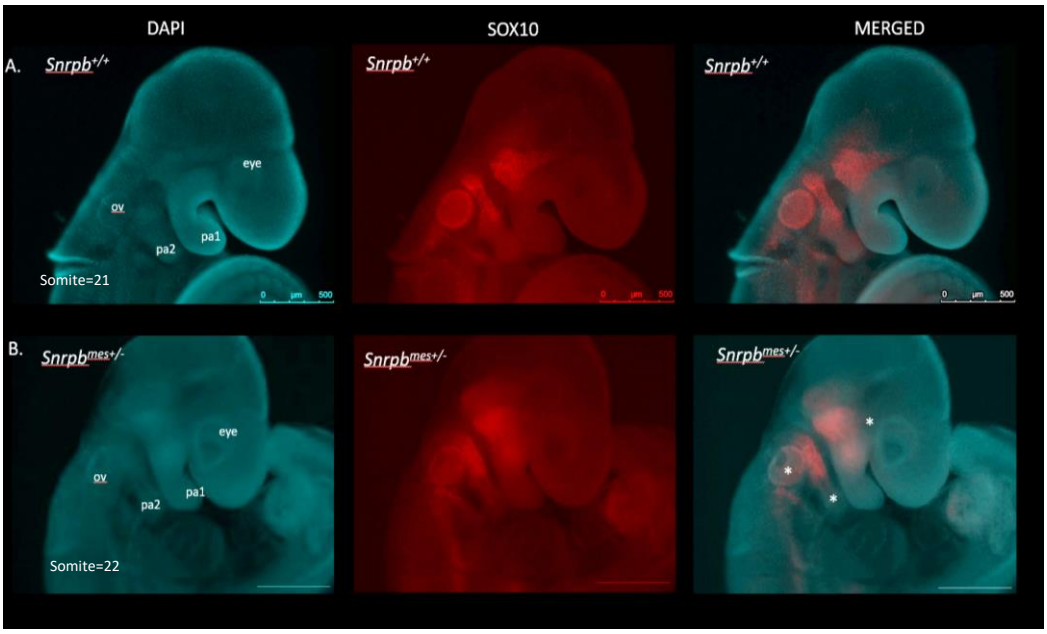

Figure 3.10: ***Abnormal Sox10 expression in the E9.5 Snrpb$^{mes+/-}$ embryos*** *(n=3).* While in the wild-type embryo (A), the neural crest cells expressing Sox10 projected toward the upper eye region, such expression was absent in the mutant (asterisk) (B). The expression pattern was more toward the distal portion of the second pharyngeal arch in wild-type embryos, whereas expression was more limited to the proximal location of the *Snrpb*$^{mes+/-}$ mutants (asterisk). ov-otic vesicle; pa1-pharyngeal arch 1; pa 2-pharyngeal arch 2. Scale bar= 500 µm

CCMS is characterized by craniofacial defects that resembles Pierre Robin Sequence (PRS), where patients have mandibular dysmorphology, glossopteris and respiratory obstructions and in some cases, cleft palate (Carey *et al.*, 1982; Gangopadhyay *et al.*, 2012; Logjes *et al.*, 2018; Giudice *et al*., 2018; Baxter and Shanks, 2022). The micrognathia in PRS syndrome are known to occur due to reduced neural crest cells in the first pharyngeal arch. As neural crest cell derivatives give rise to the jaws and skeletal elements of the face, I attempted to phenocopy the craniofacial defects found in CCMS in mice by heterozygous removal of *Snrpb* from the NCCs. My results from this part of the work are described below.

3.4 *Snrpb* heterozygosity in neural crest cells causes abnormal brain and craniofacial development in mice that mimics CCMS

3.4.1 Pups born with heterozygous *Snrpb* mutation in NCCs had craniofacial abnormalities and died shortly after birth

I used the *Wnt1-Cre2* transgenic mice to remove *Snrpb* in the neural tube and NCCs ($Snrpb^{ncc+/}$) to examine its role during craniofacial development. No $Snrpb^{ncc+/-}$ mutant pups were found on postnatal day (P)1(n=0/48) and P21 (n=0/30) (for both stages chi-square p value >.0001). At birth (P0), I recovered five heterozygous $Snrpb^{ncc+/-}$ pups from six litters (n=47). Most of them had no visible milk spots (Figure 3.11 A), indicating that they failed feed (n=4/5). Of them, one $Snrpb^{ncc+/-}$ pup was morphologically normal, while the rest had abnormally shaped heads, short snouts, and small outer ears (n=4) (Figure 3.11 B, C).

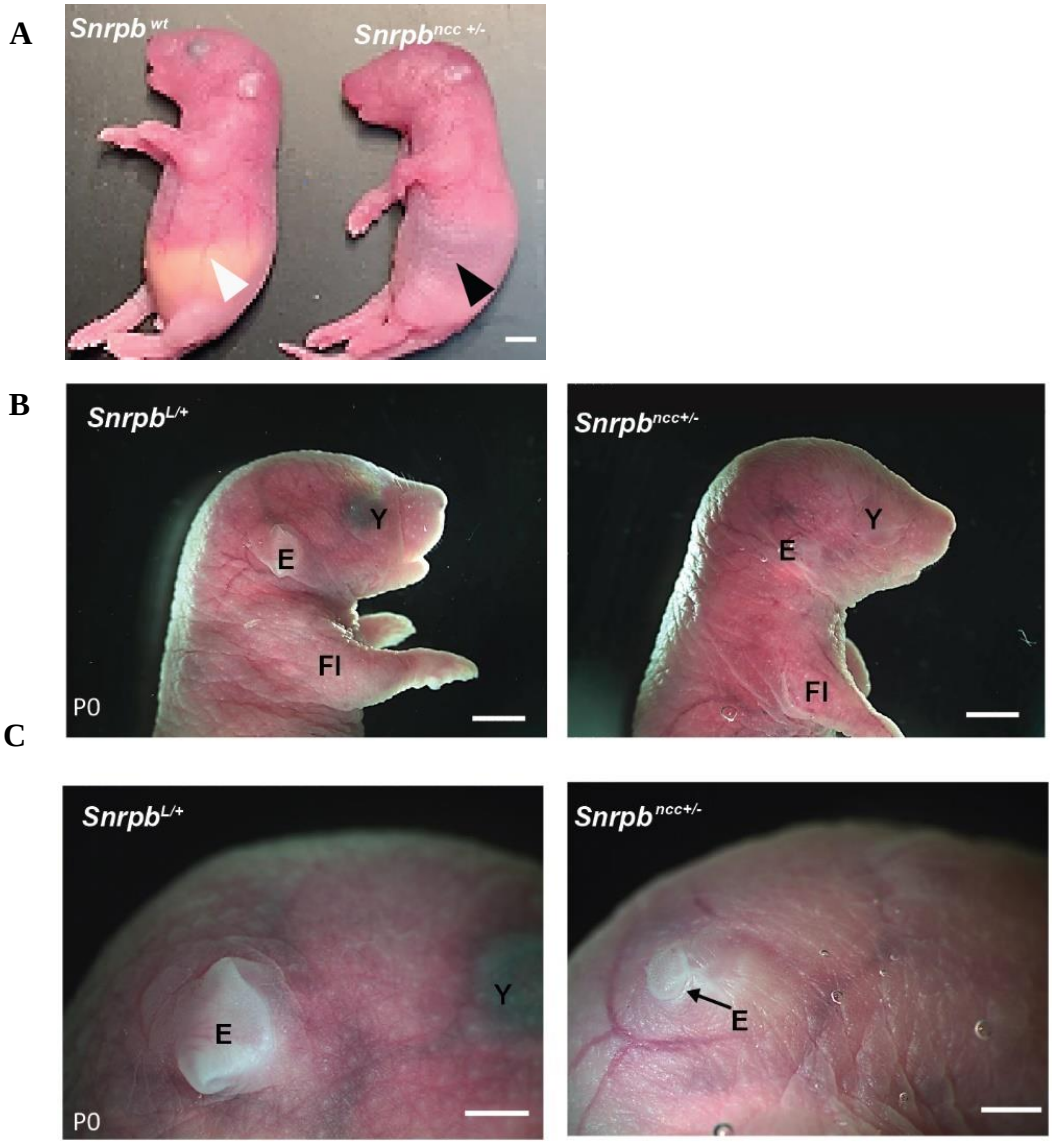

Figure 3.11: *Snrpb*$^{ncc+/-}$ *pups have craniofacial defects at birth.* (A) *Snrpb*$^{ncc+/-}$ mutant pups lack milk spot in their stomach (black arrowhead), which is visible in the *Snrpb* wild-type littermate (white arrowhead). (B) P0 *Snrpb*$^{ncc+/-}$ pups have an abnormally shaped head, micrognathia and abnormal outer ears. (C) Higher magnification showing a hypoplastic pinna in the *Snrpb*$^{ncc+/-}$ mutant (black arrow). E, ear; Y, eye; Fl, forelimb. Scale bar= 500 µm (Adapted from Alam *et al.*, 2022)

3.4.2 Wild-type levels of *Snrpb* are required in the neural crest cells from E9.5 and onward for normal development of the head and face

To determine when *Snrpb* is first required in neural crest cells for embryonic survival and craniofacial development, I collected and analyzed embryos from E9.0 to E17.5. *Snrpb*$^{ncc+/-}$ embryos were found at the expected Mendelian ratio until E17.5, when significantly fewer mutant embryos were found (n=12/100; p value <0.025, chi-square test) (Table 3.3 A). At E14.5 and E17.5, 43% and 25% of *Snrpb*$^{ncc+/-}$ embryos were dead and undergoing resorption, respectively. Thus, a significant number of *Snrpb*$^{ncc+/-}$ embryos die between E14.5 and birth. I found that, at E9.0, *Snrpb*$^{ncc+/-}$ embryos with 13 or fewer somites were indistinguishable from control (*Snrpb*$^{+/+}$ or *Wnt*$^{tg/+}$) littermates (Table 3.3 B; Figure 3.12 A). However, at E9.5, 35% of *Snrpb*$^{ncc+/-}$mutants (n=18) exhibited hypoplasia of the midbrain and hindbrain. At E10.5, 74% of mutant E10.5 embryos (n=43) also showed hypoplasia of the frontonasal, maxillary and mandibular prominences, and the pharyngeal arches, and smaller midbrain and hindbrain (Table 3.3 B; Figure 3.12 B, C). E11.5 *Snrpb*$^{ncc+/-}$embryos (n=12) could be sorted into three groups based on their shared phenotypes. I assigned the 17% of embryos that were morphologically normal and indistinguishable from controls to group 1/normal (n=2); the 17% of mutants with hypoplasia of the developing brain, face and head to group 2 (n=2); and the remaining 66% to group 3 (n=8). Abnormalities found in group 3 included hypoplasia of the midbrain, swelling in the forebrain, subepidermal swelling, absence of the frontonasal and the maxillary prominences, and a hypoplastic mandibular arch (Table 3.3 B; Figure 3.12 D). At E12.5, 25% were morphologically normal (n=4/16; group 1) and 12% mutant embryos were resorbed (n=2/16). Morphologically abnormal mutants at this stage were classified as group 2 (19%; n=3/16) or group 3 (25%; n=4/16). Mutants in group 2 exhibited clefts in the frontonasal prominence and the mandible, while those in group 3 had hypoplasia of the midbrain, an abnormal forebrain, and cleft of the hypoplastic frontonasal and maxillary prominences (Table

3.3 B, Figure 3.12 E). A fourth phenotypic group constituting 19% of *Snrpb*$^{ncc+/-}$ embryos was found (n=3/16) at E12.5. Embryos in this group showed an absence of the ventral portion of the head and face, edema in the head and a hypoplastic mandibular arch (Table 3.3 B; Figure 3.12 E, rightmost image). At E14.5, morphologically normal, group 1 *Snrpb*$^{ncc+/-}$embryos comprised 8% of live mutant embryos (n=1). Mutant embryos in group 2 (n=3) had a hypoplastic pinna, a dome-shaped head and nasal clefts; and those in group 3 (n=4), showed hypoplasia and cleft of the frontonasal, maxilla and mandibular regions, and subepidermal edema (Table 3.3 B; Figure 3.12F). *Snrpb*$^{ncc+/-}$embryos in group 4 (n=4) showed the most severe abnormalities (Table 3.3 B, Figure 3.12 F), and were missing the ventral portion of the head and face. At E17.5, I did not find any phenotypically normal group 1 embryos. Half of the mutant embryos found alive were classified as group 2 (n=6), and the remainder were in groups 3 (n=4) and 4 (n=2) (Table 3.3B; Figure 3.12 G). Thus, both wild-type alleles are required in the neural crest cells from E9.5 onwards for normal development of the head and face.

Table 3.3: *Snrpb$^{ncc+/-}$ embryos in different phenotypic groups and Mendelian segregation at different embryonic stages.* (A) Number of *Snrpb$^{ncc+/-}$* mutant (*Snrpb $^{L/+}$; Wnt-Cre $^{Tg/+}$*) embryos of different stages classified into four groups. Group 1 is normal mutants whereas Group 2 to 4 had increasing phenotypic severity. (B) Mendelian segregation of the mutants at different stages. The number in the parentheses are the genotyped dead embryos or resorptions. Parental genotypes were *Snrpb$^{L/+}$* and *Wnt1-Cre $^{Tg/+}$*. *Chi square test shows significance (P < .05). (Adapted from Alam *et al.*, 2022)

A.

Stage	Group 1	Group 2	Group 3	Group 4	Resorbed mutants	Total genotyped
E9.0	21	0	0	0	2	23
E9.5	33	18	0	0	1	52
E10.5*	14	43	0	0	1	58
E11.5	2	2	8	0	0	12
E12.5	4	3	4	3	2	16
E14.5	1	3	4	4	9	21
E17.5	0	6	4	2	4	16

B.

Stage	*Snrpb$^{L/+}$ (resorbed)*	*Wnt-Cre $^{Tg/+}$ (resorbed)*	*Snrpb $^{+/+}$ (resorbed)*	*Snrpb $^{L/+}$;Wnt-Cre $^{Tg/+}$/ Snrpb $^{ncc+/-}$ (resorbed)*	*Total genotyped*
E9.0	16	16	18(1)	23 (2)	73
E9.5	46	52(3)	56	52(1)	206
E10.5	31(2)	39	42	58(1)	170
E11.5	10	12	13	12	47
E12.5	14	8	12	16 (2)	50
E14.5	17	19	16	21(9)	73
E17.5	37	20	27(1)	16(4) *	100
Total	**171**	**166**	**184**	**198**	**719**

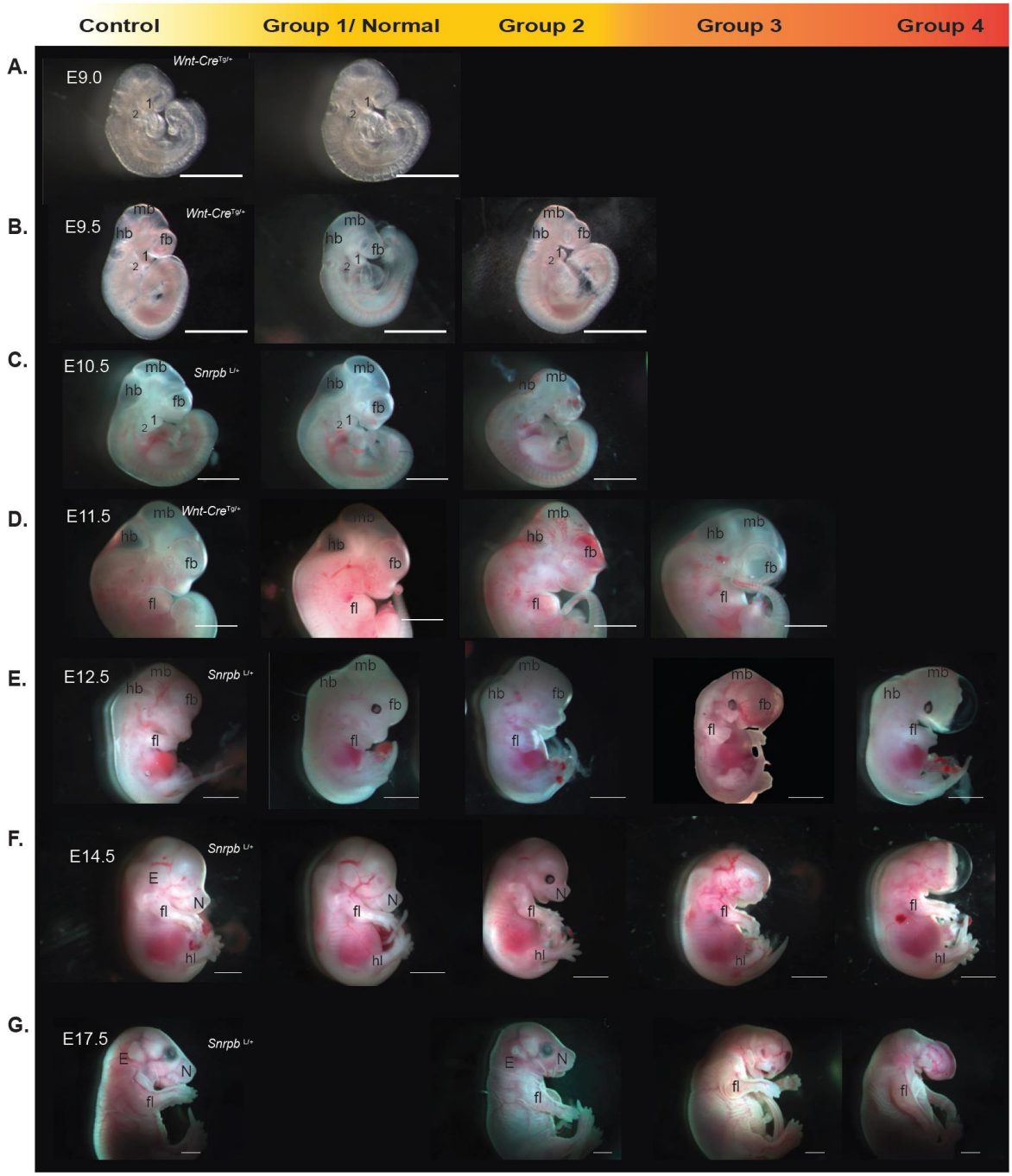

Figure 3.12: *Snrpb*$^{ncc+/-}$ *embryos show craniofacial malformations of varying expressivity from E9.5 onward.* (A-G) Depending on the phenotyping severity embryos were classified into groups. Mutant embryos that could not be distinguished from control littermates were grouped as group 1/ normal mutants. E, ear; N, nose; Y, eye; fl, forelimb; hl, hindlimb; fb, forebrain; mb, midbrain; hb, hindbrain; 1/ 2, pharyngeal arch 1 and 2; respectively. Scale bar= 500 µm (Adapted from Alam *et al.*, 2022)

3.4.3 *Snrpb* heterozygous neural crest cells cause abnormal craniofacial skeletal development of the mutant embryos and pups

3.4.3.1 Skeletal analysis of the P0 pups revealed defects in craniofacial bone development

To investigate the skeletal development in the five newborn (P0) pups that I recovered, I stained them with Alcian blue and Alizarin red. I found that the morphologically normal *Snrpb*$^{ncc+/-}$ pup of group 1, had a curved but closed premaxilla (n=1/1; Figure 3.13 A, far right). Furthermore, though one of the morphologically abnormal group 2 pups had a cleft in the premaxilla and was missing the palatine shelves (n=1/4), no bony palate defects were found in the remaining mutant pups (n=3/4) (Figure 3.13A). Skull defects were found in both group 1 and group 2 *Snrpb*$^{ncc+/-}$ pups. These defects included reduced size of the squamous part of the temporal bone (n=3/5), heterotopic ossification in the frontal suture (n=1/5), and a hypoplastic and asymmetric basisphenoid (n=3/5) (Figure 3.13 A). Defects were also found in the mandible and middle ear. Meckel's cartilage and the lower jaw which forms around it were asymmetric in most of these mutants (n=5/5). Specifically, the angular process was asymmetric in the group 1 mutant with 1 a wider angular process on one side (n=1/1) and in three of the group 2 mutants (n=3/4) (Figure 3.13 B). The articular surface cartilage was also absent or hypoplastic in group 1(n=1/1) and group 2 (n=2/4) mutants (Figure 3.13B). Additionally, the condyloid and the angular processes of the jaw were shortened bilaterally in one group 2 mutant (n=1/4). Middle ear defects such as absent, or abnormally shaped tympanic ring, and presence of ectopic ossification was found in group 1 and group 2 mutants (n=5/5; Figure 3.13 C). These data suggest that the mutants that that were not severely abnormal, still had craniofacial skeletal anomalies which might contribute to their death.

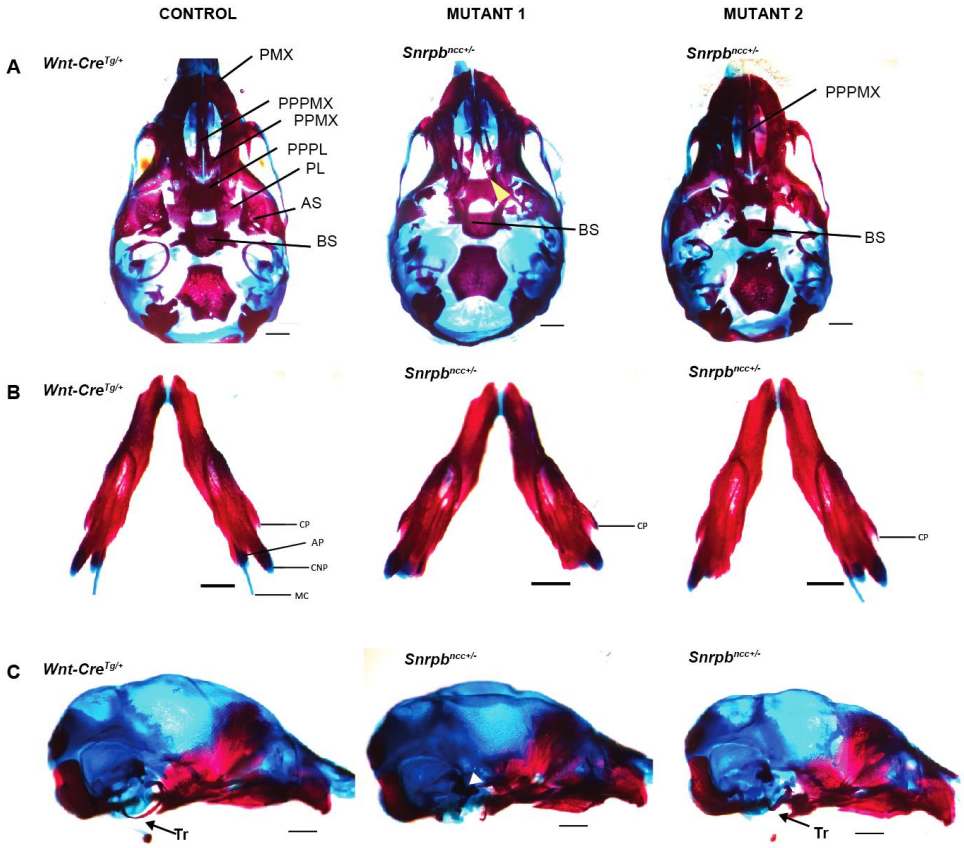

Figure 3.13: ***Craniofacial skeletal malformations in newborn Snrpb$^{ncc+/-}$ mutants.*** Representative images of P0 control and *Snrpb$^{ncc\ +/-}$* pups stained with Alcian blue and Alizarin red. (A) Ventral views showing normal closed palate and normal bones in the head of the control but a bony palate cleft (yellow arrowhead) and abnormal basisphenoid in a group 2 mutant (mutant 1). A group 1 mutant (mutant 2) with a closed bony palate, but abnormal alisphenoid, basisphenoid and hypoplastic tympanic ring is shown. (B) Representative images of abnormal mandibles of two *Snrpb$^{ncc+/-}$* mutants, compared to a control mandible. (C) Representative images of lateral views showing normal craniofacial bones and tympanic ring (arrow) in a control pup and abnormal middle ear bones (white arrowhead) and tympanic ring in the mutants. BS, basisphenoid bone; AS,alisphenoid bone; PL,palatine; PPPL, palatal process of palatine; PMX, premaxilla; PPPMX, palatal process of premaxilla; PPMX, palatal process of maxilla; Tr, tympanic ring of ear; AP, angular process; CP, coronoid process; CNP, condyloid process. Scale bar=500 µm (Adapted from Alam *et al.*, 2022)

3.4.3.2 Craniofacial cartilages at E14.5 are smaller, missing, ectopic or duplicated in the *Snrpb*$^{ncc+/-}$ mutants

To investigate the cartilage development in the mutants, I stained E14.5 embryos with alcian blue. At this stage, the normal mutant embryo (n=1) I recovered from dissections had indistinguishable cartilages from that of the controls. However, in E14.5 *Snrpb*$^{ncc+/-}$ embryos belonging to groups 2 and 3 (n=7), the squamosal cartilage was hypoplastic (Figure 3.14 A, B). Mutant embryos in these two groups also showed clefts of the nasal and pre-maxillary cartilage as well as hypoplastic Meckel's cartilage. Those heterozygous mutants belonging to group 4 had absent neural crest cell-derived cartilage that are normally found on the ventral surface of the head and face (Figure 3.14 A. B, far right). Furthermore, although the mandible formed in E14.5 *Snrpb*$^{ncc+/-}$ embryos in groups 2 and 3, it was still abnormal and smaller. I found some ectopic cartilages were formed in some of the mutants (n=4 of 7) (Figure 3.14 C) that I could not identify conclusively.

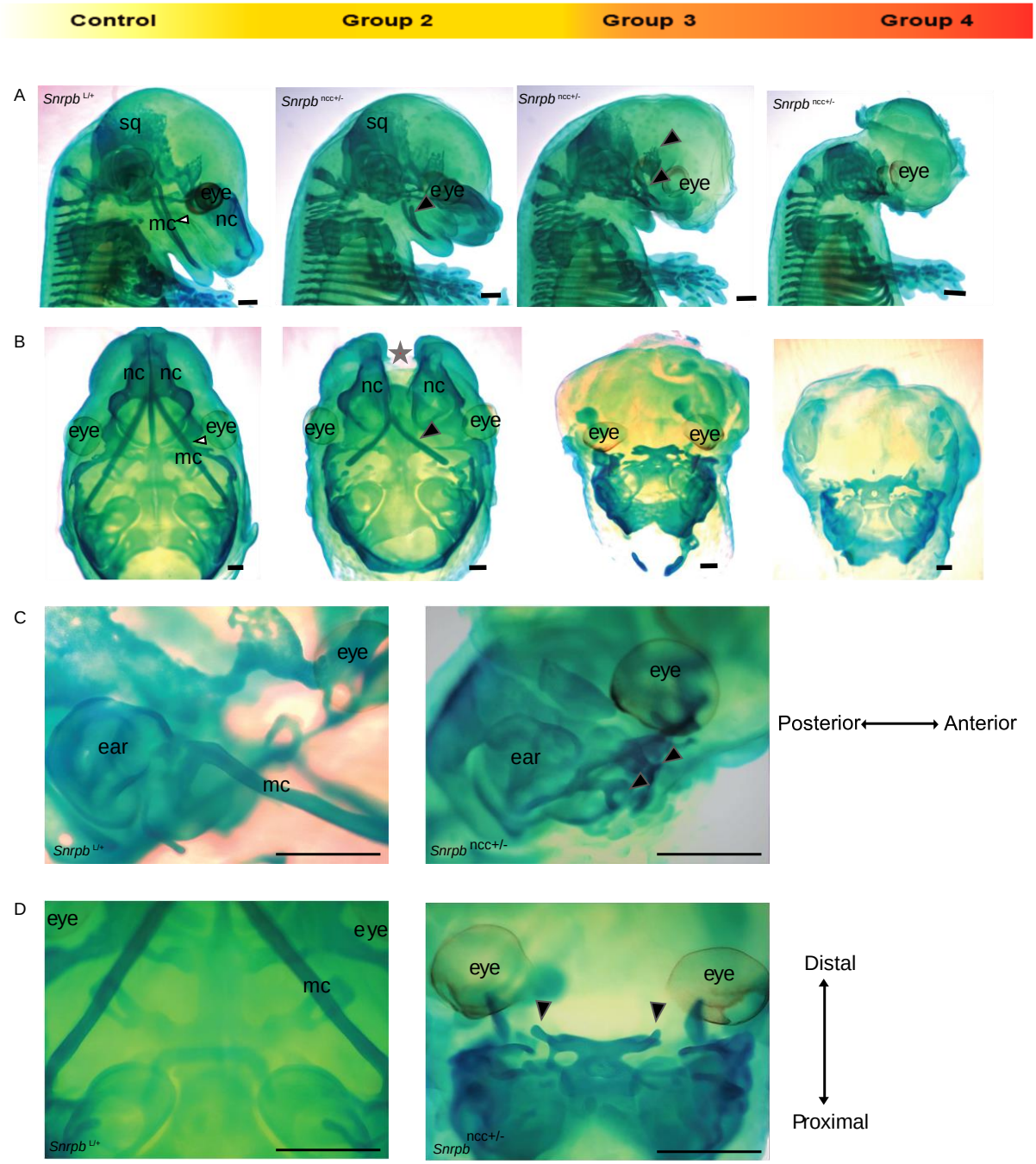

Figure 3.14: ***E14.5 Snrpb$^{ncc+/-}$ mutants show hypoplastic and loss of craniofacial cartilages.***

(A) Representative images showing sagittal views of a wild-type embryo with normal development of head, nasal and Meckel's cartilage (white arrowhead); a group 2 *Snrpb$^{ncc+/-}$* mutant with a shorter and discontinuous Meckel's cartilage (mc) (black arrowhead); a group 3 mutant with reduced head cartilage (black arrowhead), ectopic cartilage in the maxillary prominence (black arrowhead), and an absent nasal cartilage; a group 4 mutant with absent

anterior craniofacial cartilages. (B) Representative images showing ventral views of the head of a wild-type, control, embryo with symmetrical Meckel's cartilage (white arrowhead) and nasal cartilage; in the group 2 mutant Meckel's cartilage is truncated and asymmetrical (black arrowhead) and the nasal cartilage is clefted (black asterisk); in group 3 and 4 mutants, ventral cartilages are missing. (C) and (D) Higher magnification of the ear (lateral view) and cranial base (ventral view) of control and a group 3 *Snrpb*$^{ncc\ +/-}$ mutant indicating ectopic cartilages found in a subset of mutants (n=4/7), arrowheads. mc, Meckel's cartilage; nc, nasal cartilage; sq, squamosal cartilage. Scale bar= 500 µm. (Adapted from Alam *et al*., 2022)

3.4.4.3 *Snrpb*$^{ncc+/-}$ mutants were found to have both endochondral and intramembranous bone ossification defects

Skeletal bones are formed from either cartilage through the endochondral ossification process, or through a more direct process called the intramembranous ossification process, that does not require any cartilage intermediate. To investigate ossification in the *Snrpb*$^{ncc+/-}$ mutants, I stained E17.5 mutants with Alizarine red and Alcian blue. Both parietal and interparietal bones were hypoplastic in groups 2 and 3, whereas in group 4 mutants, they were not formed (Figure 3.15 A). In addition to interparietal bone deformities, other neural-crest-derived bones such as the temporal and alisphenoid bones were missing, while the frontal and nasal bones were hypoplastic in groups 2 and 3 (n= 5) (Figure 3.15 B). These mutants also showed nasal clefts and palate abnormalities, and the mandible was also abnormal (Figure 3.15 B, C). The zygomatic arch also failed to form in group 3 mutants (Figure 3.15 B). In all groups of the mutants, I also saw a hypoplastic basisphenoid bone, which is a derivative of both mesoderm and neural crest cells (Figure 3.15 B). When analyzing the mandibles, I found that the mandible formed in groups 2 and 3 E17.5 *Snrpb*$^{ncc+/-}$ embryos were both asymmetrical and bilaterally smaller when compared to that of controls (Figure 3.15 D, T-test, $p<.0001$). Distal ends of the

jaws were abnormally shaped, while the proximal elements of the mandible such as the coronoid, condylar, and angular processes were not found in mutants (Figure 3.15 C). Additional defects found in mutant embryos included a missing tympanic ring, hypoplasia, or absence of the hyoid, and missing tracheal cartilages. Like at E14.5, I also found ectopic bones in the middle ear (n=4 of 7) (Figure 3.15 E).

From the analysis of the skeletal components, I concluded that in *Snrpb*$^{ncc+/-}$ mutants, NCCs can form cartilages, whose development is disrupted due to the mutation. I also found deficiencies in ossification of bones that are derived from both intramembranous and endochondral processes. Intriguingly, I found that skeletal components that are derived from mesodermal cell lineages are also abnormal in *Snrpb*$^{ncc+/-}$ mutants, suggesting that interaction between the two cell types are perturbed by removing one *Snrpb* allele in NCCs.

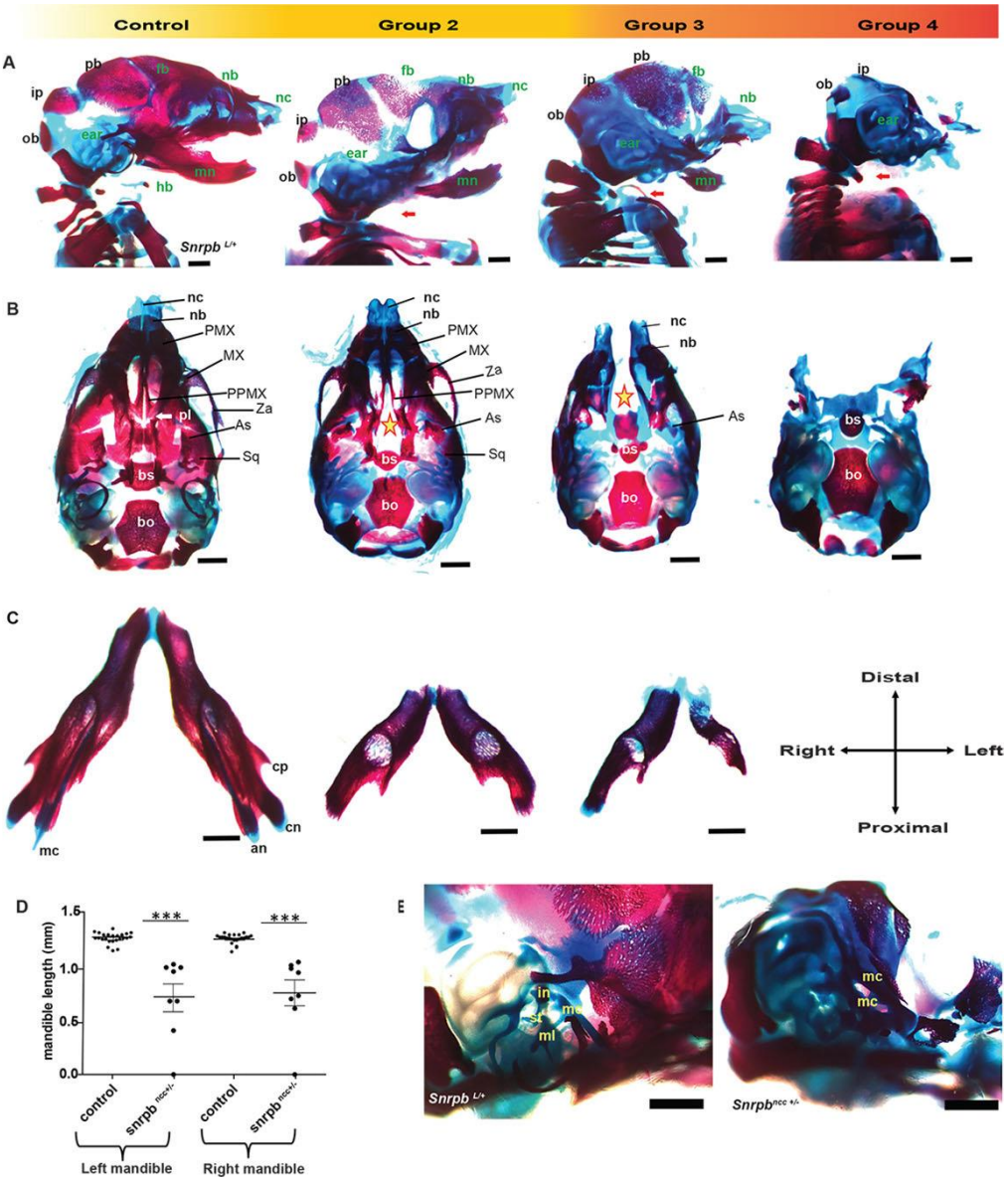

Figure 3.15: ***Abnormal craniofacial skeletal development was seen at E17.5 with hypoplastic or missing cartilages and bones.*** (A, B) Representative images of Alcian Blue and Alizarin Red-stained E17.5 normal (*Snrpb*^{wt} or *Snrpb*$^{L/+}$) and *Snrpb*$^{ncc+/-}$ mutant embryos showing craniofacial abnormalities of varying penetrance. (A) Sagittal view showing hypoplasia or absence of neural crest cell-derived bones (labeled in green font) in *Snrpb*$^{ncc+/-}$ mutants. The missing hyoid bone and tracheal cartilage are indicated by red arrows. (B) Ventral view of the skull showing palatal and maxillary clefts (stars) in group 2 and 3 *Snrpb*$^{ncc+/-}$ mutants, respectively. (C) Representative images of the lower jaw of a normal embryo and two

Snrpb$^{ncc+/-}$ mutants, showing asymmetric mandibles with no discernable angular, coronoid or condylar processes. (D) Both left and right mandibles are significantly shorter in Snrpb$^{ncc+/-}$ embryos (***P<0.0001, unpaired, two-tailed t-test), compared to control embryos. (E) Representative higher-magnification images of the inner ear of a control and *Snrpb*$^{ncc+/-}$ embryo. an, angular process; As, alisphenoid bone; bo, basioccipital bone; bs, basisphenoid bone; cn, condylar process; cp, coronoid process; fb, frontal bone; hb, hyoid bone; in, incus; ip, interparietal bone; mc, Meckel's cartilage; ml, malleus; mn, mandible; MX, maxilla; nb, nasal bone; nc, nasal cartilage; ob, occipital bone; pb, parietal bone; PMX, premaxilla; pl, palatine; PPMX, palatal process of maxilla; Sq, squamous bone; st, stapes; Za, zygomatic arch. Scale bars= 500 μm (Adapted from Alam *et al.*, 2022)

3.4.5 *Snrpb*$^{ncc+/-}$ mutants have abnormal cranial and axial nerve development

In addition to the craniofacial skeletons, neural crest cells give rise to cranial nerves (CN) and axial nerves such as the dorsal root ganglia (DRG). To find if those derivatives of neural crest cells are abnormal in the *Snrpb*$^{ncc+/-}$ mutants, I stained the neurofilaments of the mutant embryos. Though only two group 2 E10.5 *Snrpb*$^{ncc+/-}$ embryos were analyzed and looking at more mutants would rule out natural variation of cranial nerves, both CN and DRG were abnormally formed in the mutants. The cranial ganglia were reduced in size, and all had abnormal projections into the pharyngeal arches (Figure 3.16 B). The ophthalmic branch of the trigeminal nerve (CN V) was reduced and did not extend over the lens, the maxillary projection appeared disorganized and missing. The mandibular projection was reduced and ectopic branching was found in CN V in the mutants. Furthermore, the proximal portions of the geniculate (CN VII) were thicker and formed unusual bundle-like structures in the *Snrpb*$^{ncc+/-}$ mutants. Similarly, the glossopharyngeal nerve (CN IX) was abnormally thicker in the proximal region before the pharyngeal arch, had ectopic projection into pharyngeal arch 2, and

reduced projection into pharyngeal arch 3. Finally, the proximal portion of the vagus nerve (CN X) was relatively normal but had an abnormal thickening at the distal end with reduced projections into the heart. Furthermore, the dorsal root ganglia, which are derived from trunk neural crest cells were reduced in size and bifurcated at the proximal ends (Figure 3.16 D).

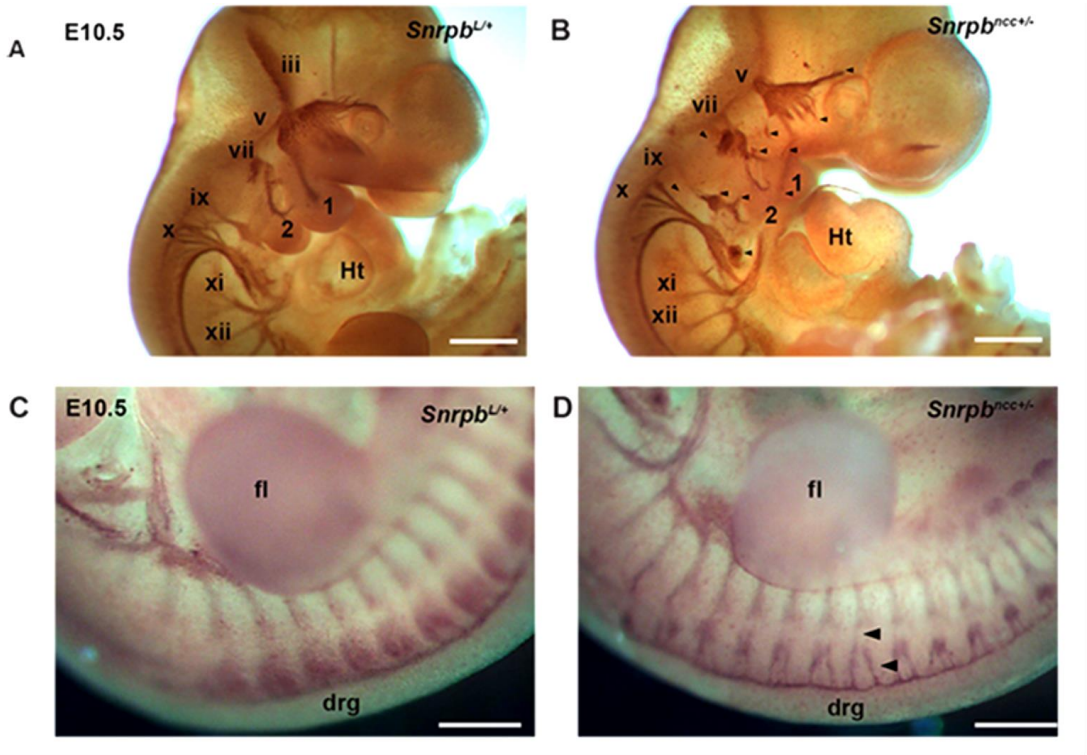

Figure 3.16: ***Abnormal cranial and dorsal root ganglia formation in Snrpb$^{ncc+/-}$ mutants.*** (A, B) Representative images of E10.5 somite-matched control (*Snrpb*$^{L/+}$) (A) and *Snrpb*$^{ncc+/-}$ (B) group 2 embryos stained with antibody against neurofilament (2H3). (B) *Snrpb*$^{ncc+/-}$ mutants (*n*=2) showed abnormal projections of nerves to the pharyngeal arches (cranial ganglion v and vii) and heart (cranial ganglion ix), and absence and abnormal bundling of cranial nerves (all are indicated by black arrowheads). (C, D) Compared to controls (*Snrpb*$^{L/+}$) (C), the dorsal root ganglia are bifurcated and reduced in mutants (black arrowheads). (D) fl, forelimb; hrt, heart; 1 and 2, pharyngeal arch 1 and 2; drg, dorsal root ganglia. Scale bar=500 µm (Adapted from Alam *et al.*, 2022)

3.4.6 MicroCT scan revealed abnormal brain and additional craniofacial anomalies along with abnormal cardiac neural crest cell derivatives in the *Snrpb*$^{ncc+/-}$ mutants

To look at the non-skeletal structures, I did microCT scans of *Snrpb*$^{ncc+/-}$ mutant embryos at different stages. At all stages, E12.5 (n=1), E14.5 (n=1) and E17.5 (n=1), the brain was abnormal with a thin cerebral cortex, and the lateral ventricles were enlarged (Figure 3.17). The scan also uncovered additional facial defects such as, the group 4 E14.5 embryo did not have nasal septum and nasopharyngeal cavity. However, the oropharynx, tongue and pituitary gland were present in that mutant (Figure 3.17 A). For the group 2 E17.5 mutant embryo, I found the aorticopulmonary septum, which is derived from cardiac neural crest cells and separates the blood from the pulmonary artery and aorta, did not differentiate while it was formed in the wild-type control embryo (Figure 3.17 B-E). Furthermore, the thymus gland, a derivative of the third pharyngeal pouch, also failed to form in this mutant embryo (Figure 3.17 F).

The morphological analysis indicates that *Snrpb* is required for the formation of structures that are derived from or induced by neural crests along the anterior-posterior axis. I also assume that cardiac anomaly might contribute to the death of *Snrpb*$^{ncc+/-}$ embryos and pups, especially for the ones with milder skeletal defects as shown in a group 1 P0 mutant.

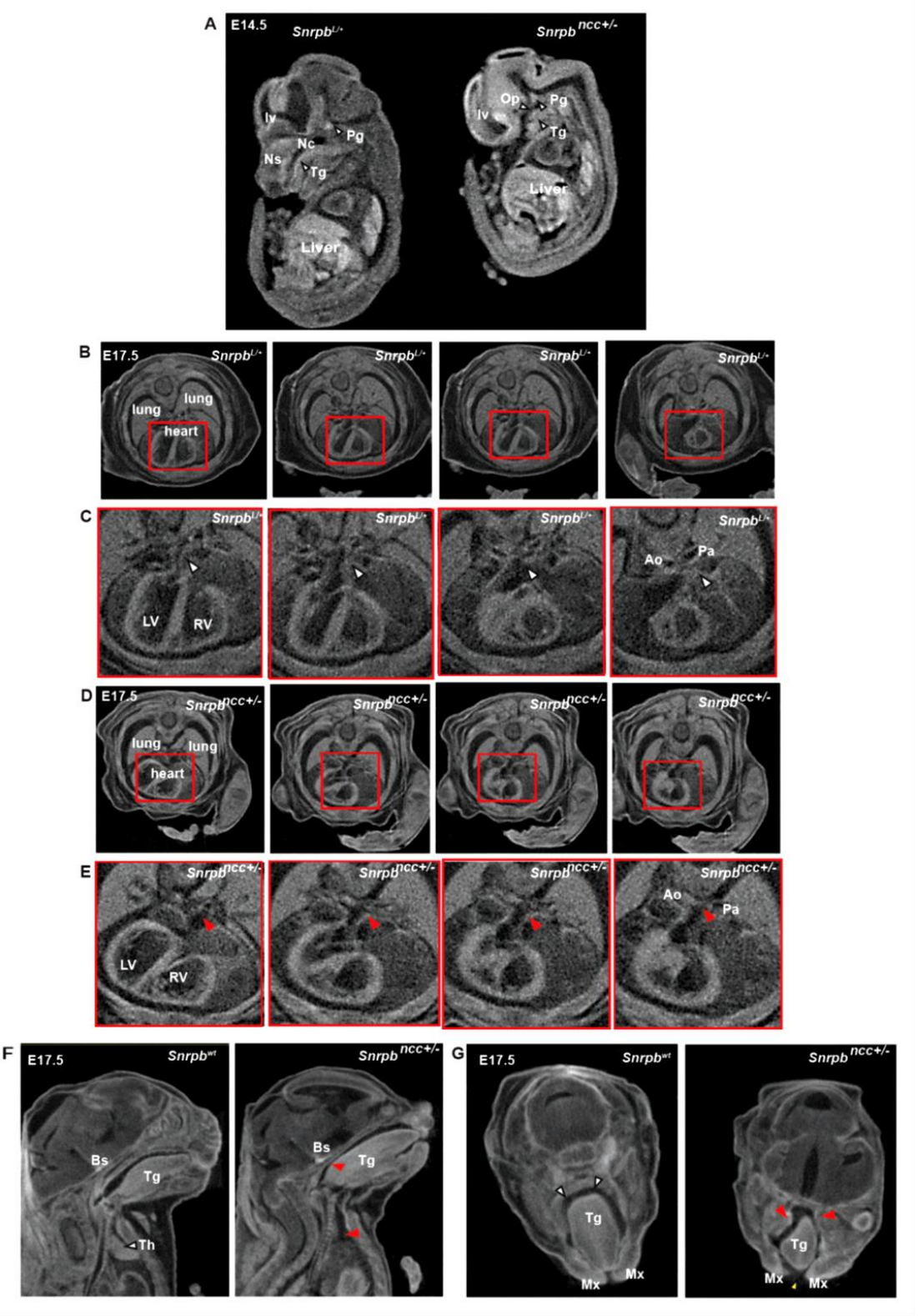

Figure 3.17: ***Micro CT scan of Snrpb$^{ncc+/-}$ mutants show abnormal heart, brain, palate and thymus developments.*** (A) Midsagittal MicroCT images of a control, (*Snprb$^{L/+}$*) embryo with normal morphological landmarks in the brain and face, and a *Snrpb$^{ncc+/-}$* group 4 mutant with

an enlarged lateral ventricle in the brain. The missing nasopharyngeal cavity and nasal septum can also be seen. (B) and (C) Transverse MicroCT images of the chest region of an E17.5 control embryo (*Snrpb*$^{L/+}$). Panel (C) show higher magnification of the heart (red box in panel B) from posterior to anterior (left to right of the panel), and the aorticopulmonary septum (white arrowhead) separating the aorta and pulmonary arteries in the control embryo (n=1). (D) and (E) Transverse MicroCT images of the chest and heart region of an E17.5 group 2 *Snrpb*$^{ncc+/-}$ mutant. (E). in the higher magnification of the heart (red box in panel D) the aorticopulmonary septum is missing (red arrowhead). (F) Mid-sagittal view of the same group 2 *Snrpb*$^{ncc+/-}$ mutant showing absence of the thymus (red arrowhead) which can be seen in the control embryo (white arrowhead). (G) Sagittal views of a control and a group 2 E17.5 embryo show the fused palatal shelves (white arrowheads) in the control, and clefts in the palate and the maxilla in the *Snrpb*$^{ncc+/-}$ mutant (red arrowheads). lv, lateral ventricle; Ns, nasal septum; Nc, nasopharyngeal cavity; Pg, pituitary gland; Tg, tongue; Op, oropharynx; LV, left ventricle; RV, right ventricle; Ao, aorta; Pa, pulmonary artery; Bs, basisphenoid bone; Th, thymus; Mx, maxilla. (Adapted from Alam *et al.*, 2022)

3.4.7 Neural crest cells were significantly reduced in the craniofacial region of the E10.5 *Snrpb* mutant embryos

In order track *Snrpb*$^{ncc+/-}$ heterozygous neural crest cells and their progenitors, I introduced the ROSA lacZ (Soriano P, 1999) and ROSA mT/mG (Mazumdar *et al.*, 2007) reporters into the *Snrpb* mutant line. In the double-fluorescent Cre ROSA mT/mG mice, cells express membrane-localized tdTomato (mT, in red) unless they are expressing Cre-recombinase. Recombination leads to *Wnt-1* expressing cells to express membrane green fluorescent protein (GFP, in green) meaning that the neural crest and their derivatives will fluoresce green. When we visualized GFP-positive Cre-expressing cells in control (n=3) and morphologically normal *Snrpb*$^{ncc+/-}$ mutants (n=3), no difference was found at E9.5 (Figure 3.18 A-F). The fluorescence expression of tdTomato was widespread in both controls and mutant embryos. At least 3 sections were analyzed per embryo. Similarly, using ROSA lacZ reporter revealed a comparable proportion of X-Gal positive cells in the head and pharyngeal arches (Figure 3.18 G-I) with no statistically significant differences between wild-type and *Snrpb*$^{ncc+/-}$ embryos at E9.5 morphologically normal (n=1) and abnormal (n=2) (3 sections analyzed per embryo of each genotype), suggesting the neural crest cells migrated to those regions. At the later stage of E10.5, quantification of X-gal positive cells in morphologically abnormal group 2 mutant embryos (n=4) showed a reduced proportion of X-gal positive cells in the head region (Figure 316 J-L), and this difference was statistically significant when compared to wild type (T-test, p=.003).

These data suggest that in *Snrpb*$^{ncc+/-}$ mutants neural crest cells are born, able to exit the neural plate border and migrate into the developing craniofacial region as at E9.5 there is no significant difference in the number of neural crest cells between the wild-type and mutant embryos. However, there are fewer neural crest cells in the craniofacial region of E10.5 mutants, suggesting increased cell death or reduced proliferation of the neural crest cells that might contribute to the phenotype I see at later embryonic stages.

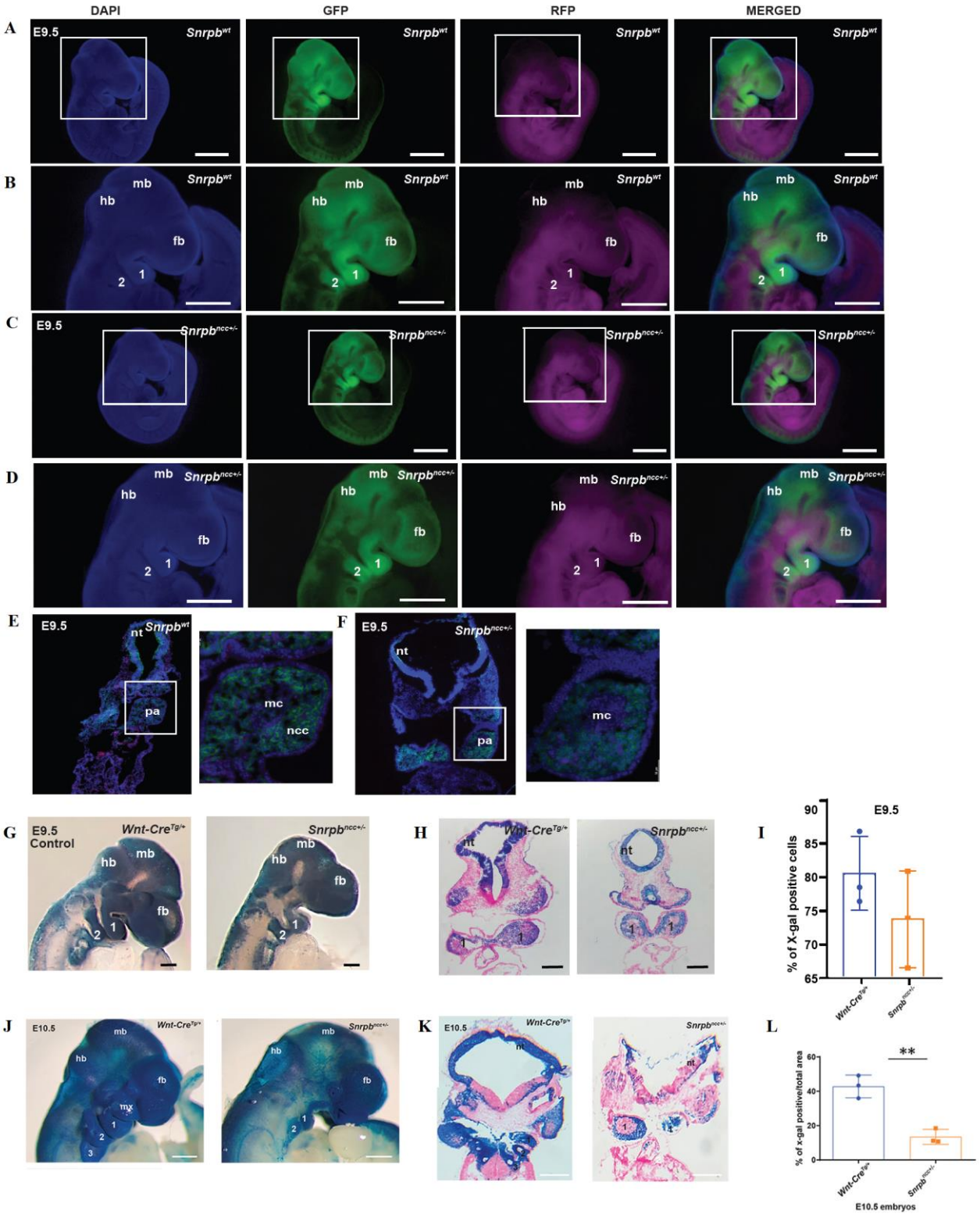

Figure 3.18: ***Neural crest cell number is not affected in E9.5 Snrpb$^{ncc+/-}$ mutants but becomes significantly lower at E10.5 in the craniofacial region.*** **(**A) Representative images of DAPI stained E9.5 control (*Snrpb*^{wt}) and (C) group 1 *Snrpb*$^{ncc+/-}$ embryos carrying the mT/mG

reporter, in lower magnification. Green-fluorescence marks Wnt1-cre-expressing cells. (B) and (D) Higher magnification of the craniofacial region (boxes in A and C) of control and mutant embryos, respectively, showing similar proportion of GFP+ cells in the mutant embryo. (E) and (F) A magnified view of the pharyngeal arch of cryosectioned embryos (n=4) of controls and mutants, respectively. There was no significant difference in the numbers of neural crest cells between the two genotypes. (G) Representative images of an X-gal stained E9.5 control and a group 2 *Snrpb*$^{ncc+/-}$ embryos. (H) Cryosection in a group 2 embryo and quantification of X-gal positive blue cells between control (n=3) and mutant (n=3) embryos. (J) and (K) Control (n=4) and *Snrpb*$^{ncc+/-}$ group 2 mutant (n=4) embryos at E10.5. (L) Quantification of the area stained with X-gal showed a significant reduction in mutants (*n*=3) compared to control littermates (*n*=3) (unpaired, two-tailed *t*-test, ***P*<0.005). Error bars indicate standard error of mean (SEM) hb, hindbrain; mb, midbrain; fb, forebrain; 1/2, pharyngeal arch 1 and 2 respectively; pa, pharyngeal arch; nt, neural tube; ncc, neural crest cells; mc, mesenchymal core. Scale bar= 500 µm (Adapted from Alam *et al.*, 2022)

3.4.8 *Snrpb* mutation in the neural crest cells causes increased cell death in the craniofacial region in the mutants

To determine if reduced proliferation and/or increased apoptosis contribute to the reduced number of X-Gal positive *Snrpb* heterozygous cells, E9.5 and E10.5 embryos were analyzed after Phosphohistone H3 immunostaining and TUNEL assay. A statistically significant increase in TUNEL positive cells in the developing head region of E9.5 *Snrpb*$^{ncc+/-}$ embryos (T-test, p=.029) (n=4; 3-group 1/normal and 1 group 2, at least four sections were analyzed per embryo) were found when compared to controls (Figure 3.19 A, B). However, no significant difference in proliferation was found between E9.5 control and *Snrpb*$^{ncc+/-}$ embryos (n=4; 3-

group 1/normal and 1 group 2) or at E10.5 (n=5; 1 group1/normal and 4 group 2) (Figure 3.19 C). This data indicates that *Snrpb* heterozygous cells migrate into the developing head region and the pharyngeal arches. However, a group of these cells undergoes apoptosis and are lost in mutant embryos by E10.5.

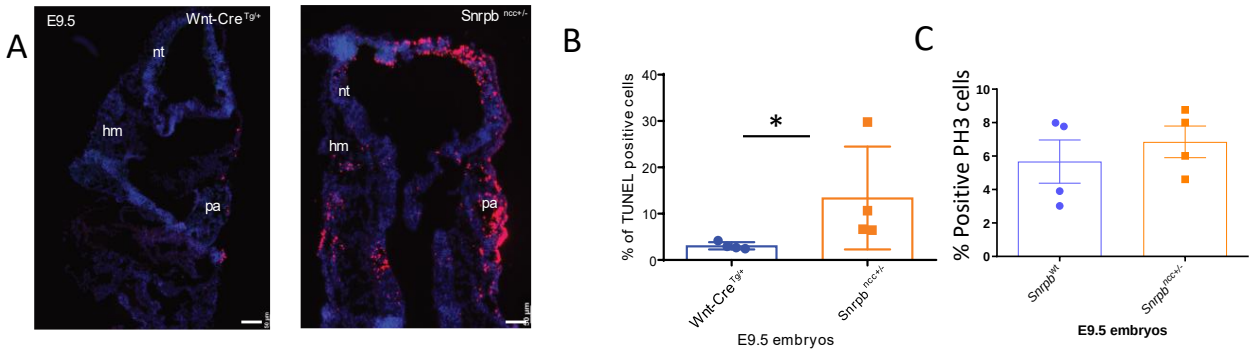

Figure 3.19: ***An increased cell death in the craniofacial region was seen in the Snrpb$^{ncc+/-}$ E9.5 mutants.*** (A) Representative images of sections of TUNEL-stained E9.5 control (*Snrpb^{wt}* or *Snrpb$^{L/+}$*) on the left and *Snrpb$^{ncc+/-}$* mutant on the right embryos. (B) Quantification showed an increase in the percentage of TUNEL-positive nuclei (red in A) in the craniofacial region of mutants (n=3) (unpaired, two-tailed t-test, *P<0.05). However, the *Snrpb$^{ncc+/-}$* mutant embryos did not show any significant decrease in proliferation in the same stage. (C) Graph shows the quantification of percentage of PH3 positive cells. Error bars indicate standard error of mean (SEM). nt, neural tube; pa, pharyngeal arch; hm, head mesenchyme. Scale bar=50 µm. (Adapted from Alam *et al*., 2022)

3.5 AIM 1 conclusion:

To understand the role of SNRPB in embryonic development, I set my first aim to generate a mouse model for CCMS by reducing *Snrpb* expression. I successfully introduced *Lox*P sequences in introns 1 and 3 of *Snrpb* to develop a conditional allele. This allele could be used to remove *Snrpb* from targeted tissues, resulting in a decrease of *Snrpb* expression. In addition, I generated a novel 61 base-pair deletion mutation in the intron 2, near the regulatory alternative exon 2 of *Snrpb*.

In the *Snrpb* Δ61-mutant model, I found phenotypes that resembles CCMS abnormalities such as craniofacial malformations and limb defects in a subset of mutants. Also, a subgroup of both heterozygous and homozygous mutants had skeletal defects in the craniofacial region, ribs and limbs. I found the deletion mutation reduces SNRPB protein levels in a subgroup of the mutants. Though it was non-significant, it is possible that mutants with the lower SNRPB levels show phenotypic abnormalities at later stages. However, around five percent of the $Snrpb^{\Delta 61/+}$ mutants (n=15/306) and six percent of the $Snrpb^{\Delta 61/\Delta 61}$ mutants (n=11/168) had phenotypic and skeletal abnormalities. Thus, though this model could phenocopy CCMS, due to low penetrance of the phenotypes, it has limited its use as a tool to study the syndrome and role of SNRPB in embryonic development.

In the next *Snrpb* mutant model, a global heterozygous deletion of *Snrpb* ($Snrpb^{+/-}$) was done using the conditional knockout mice. I found constitutive heterozygous elimination of *Snrpb* is embryonic lethal before organogenesis and thus these mutants cannot be used as model of CCMS. However, with further investigations it can be used to gain insight of SNRPB's role in early embryonic development.

By using *Mesp1-Cre* transgenic mice, I removed *Snrpb* from mesodermal cell lineage to model the rib anomalies of CCMS. $Snrpb^{mes+/-}$ mutant model recapitulated some of the craniofacial defects such as micrognathia and ear abnormalities along with rib and limb

malformations. With future studies, these mutants will be useful to understand SNRPB's role in mesodermal cells and their derivatives.

Finally, to model craniofacial abnormalities of CCMS in mice, I removed one allele of *Snrpb* from the neural crest cells (NCCs). The *Snrpb*$^{ncc+/-}$ mutants phenocopied most of the craniofacial structure abnormalities at a variable expressivity. The neural crest cell derived craniofacial cartilage and bone formation was interrupted in these mutants. Furthermore, a CCMS cardiac abnormality, cardiac septal defect were found in these mutants. From the results that I demonstrated for *Snrpb* NCC-specific mutant model, I conclude that this is an efficient mouse model to study the contribution of SNRPB in craniofacial development, that is perturbed in CCMS patients.

B. RESEARCH FINDINGS OF AIM 2

Based on the data generated in Aim1, I hypothesized that mutation of *Snrpb* in neural crest cells causes splicing aberrations in genes required for craniofacial development, thus resulting in the phenotypes in *Snrpb*$^{ncc+/-}$ mutants. As the mutants showed abnormal craniofacial development at E9.5, I sequence RNA from E9.0 embryos to capture what splicing changes cause the phenotypes later in the mutants. Doing RNA sequencing from the mutant heads before they become abnormal will provide us information on change in splicing or gene expressions that drive the abnormal craniofacial development.

3.6 RNA sequencing reveals mutation of *Snrpb* in the neural crest cells causes overall splicing aberrations

3.6.1 An increase in skipped exon and intron retention was predominantly captured in the transcriptome analysis of the *Snrpb*$^{ncc+/-}$ mutants

To identify the molecular etiology of the malformations seen in the *Snrpb*$^{ncc+/-}$ mutants, I collected heads of E9.0 *Snrpb*$^{ncc+/-}$ embryos (11-13 somite pairs), prior to morphological defects. RNA was isolated from those embryos and used for RNA sequencing analysis. Surprisingly, gene expression analysis did not reveal a major distinction between mutant (n=3 pools) and wild type (n=3 pools) embryos, and the samples did not cluster by genotype. This was further validated by differential gene expression (DEG) analysis, which identified only 76 DEGs: 50 upregulated and 26 downregulated, in the mutant embryos. This low number of DEGs is consistent with the lack of a phenotypic difference at this developmental stage. The DEGs identified were characterized into molecular pathways, where P53 signaling pathway was the most upregulated one followed by components of the spliceosome (Figure 3.20A).

Splicing analysis, however, revealed a large number of transcripts that were abnormally spliced. 722 significant (FDR = 0.1) differentially spliced events (DSE) between the *Snrpb*$^{ncc+/-}$ (Het) and wild-type (WT) samples were identified. The most abundant of these DSE have skipped exons (SE) and retained introns (RI) (Figure 3.20 B). A strong tendency towards increased exon skipping and intron inclusion in the mutant samples were observed; there were more SE (273 in Het versus 83 in WT) and RI (191 in Het versus 21 in WT) (Figure 3.20 B). However, though SEs were more likely to be alternative exons (non-constitutive) in heterozygous (p=0.0034) versus wild type (Figure 3.20 C-D), expression of transcripts with SE of constitutive exons was significantly reduced in mutants (p=0.0035) when compared to wild type (Figure 3.20 E-F). Consistent with the absence of significant gene expression changes, DSEs in *Snrpb*$^{ncc+/-}$ embryos did not lead to significant changes in inclusion of PTC-containing exons or introns (Figure 3.20 G-J). However, pathway analysis indicated that DSEs genes were significantly associated with mRNA processing (Figure 3.20 K).

Those global trends in splicing are consistent with those previously found in cell culture, suggesting that *SNRPB* deficiency results in increased skipping of alternatively spliced exons resulting from reduced recognition of splicing signals (Correa *et al.*, 2016).

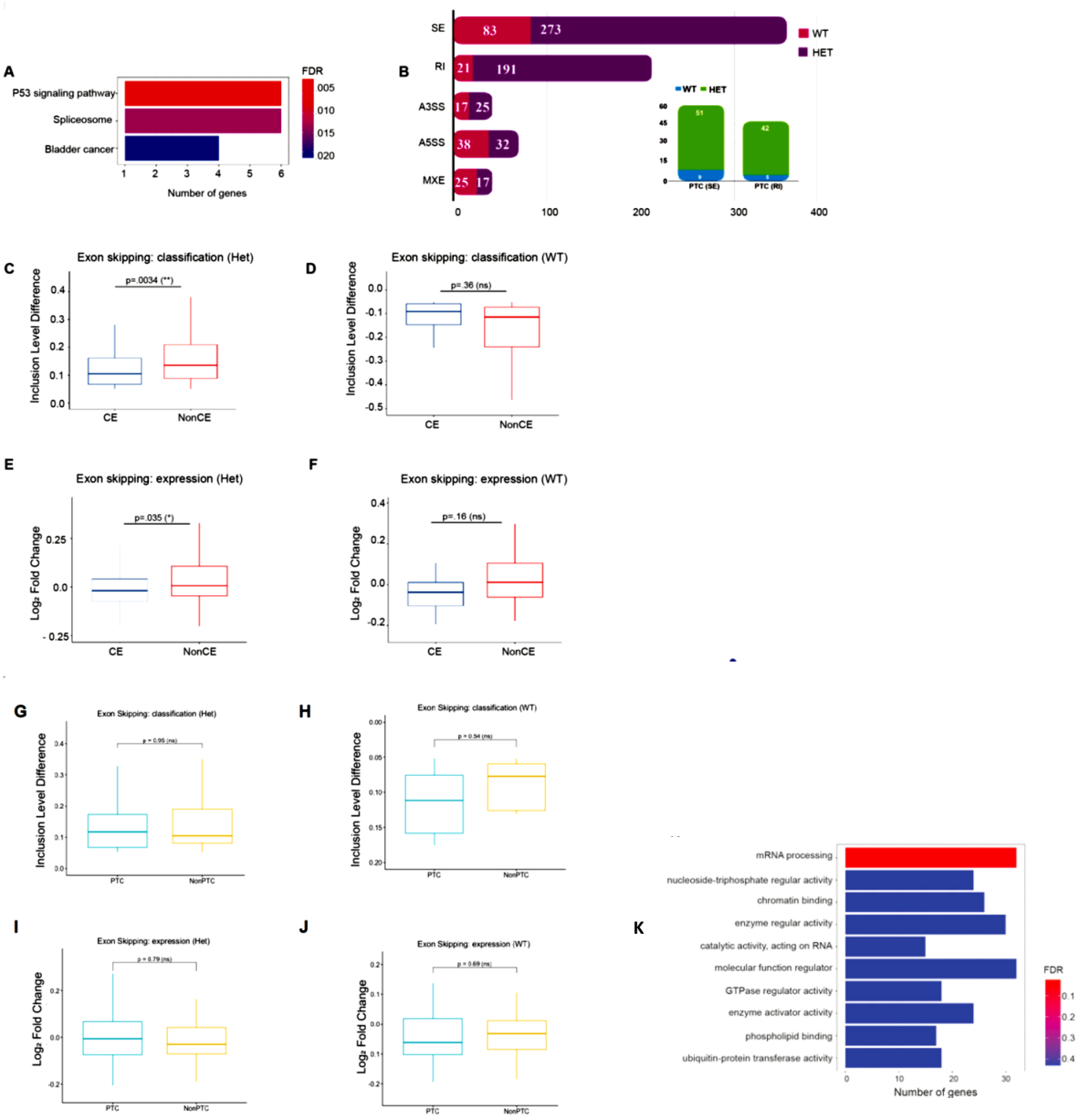

Figure 3.20*: Snrpb$^{ncc+/-}$ mutant heads show aberrant splicing, mostly increased exon skipping and intron retention.* (A) Differentially expressed genes (DEGs) identified in *Snrpb*$^{ncc+/-}$ (Het) mutants were grouped into molecular pathways. (B) Splicing events in *Snrpb*$^{ncc+/-}$ mutants compared to controls (*Snrpb*^{wt}). (C-F) In *Snrpb*$^{ncc+/-}$ mutants, exon skipping was significantly higher for non-constitutive exons (NonCE) when constitutive (CE) versus (NonCE) was examined (unpaired, two-tailed *t*-test). (G) and (H) Presence of a premature termination codons (PTCs) in exons that are more skipped in mutant (G) and wild-type embryos (H) do not impact exon inclusion level. (I-J) No effect of PTCs in exons that are

more skipped in mutant (I) and wild-type embryos (J) on the expression of genes carrying those exons. (K) Pathway analysis of genes with DSEs. ns, not significant; *P<0.05, **P<0.01. (Adapted from Alam *et al.*, 2022)

3.6.2 Distinguishable sequence features were not found to be associated with the events of increased skipped exon and intron retention in the *Snrpb*$^{ncc+/-}$ mutants

We next investigated if specific sequence features contributed to the aberrant splicing in the mutant embryos. We compared alternative events preferentially found in the mutants to two control groups: 1) events preferentially found in the wild-type embryos, and 2) a set of 1000 randomly chosen alternative events. Specifically, we aimed to test whether aberrant events in the mutants were associated with weaker splice signals. We saw 5'SS strength was significantly higher in *Snrpb*$^{ncc+/-}$heterozygous when compared to *Snrpb* wild type embryos (Figure 3.21 A), while the 3'SS was comparable between mutants and *Snrpb* wild types (Figure 3.21 B). While there was a very slight trend towards weaker splice site scores (MaxEntScan, Yeo *et al.*, 2004) of RI in mutant as compared to *Snrpb* wild type embryos, the differences were small and not statistically significant (Figure 3.21 C, D). We also analyzed the strength and position of predicted branch point (BP) signals (LaBranchoR, Paggi and Bejerano, 2018), but again did not find notable differences (Figure 3.21 E-H), except for a slight preference for a more distal branch point location of mutant-specific SE events (27 bp in mutant versus 25 bp in the random set, p= 0.026). Though the GC content in retained introns was slightly increased (Figure 3.21 I-J), no statistically significant difference was observed when we looked at general base composition in SE and RIs (Figure 3.21 K-N). No statistical differences in the length of SEs and RIs were found, although RIs were generally shorter in mutants when compared to wild-type. Finally, we scanned for the frequency of RNA-binding protein motifs around the mutant-

specific events (rMAPS2, Jae Y Hwang *et al.* 2020), but did not identify significant enrichment of recognition signals of known splicing factors.

Overall, we did not find a compelling indication that the splicing aberrations present in mutants are linked to identifiable sequence features. The slight preference for stronger 5' SS, branch point site location (BPS) and intronic nucleotide composition are notable but will need further scrutiny using more sensitive experimental designs.

Thus, the relatively large number of splicing aberrations, as compared to differentially expressed genes, detected at this developmental stage supports the hypothesis that these general splicing defects precede aberrations in gene expression and initiate the molecular cascade that leads to phenotypic changes.

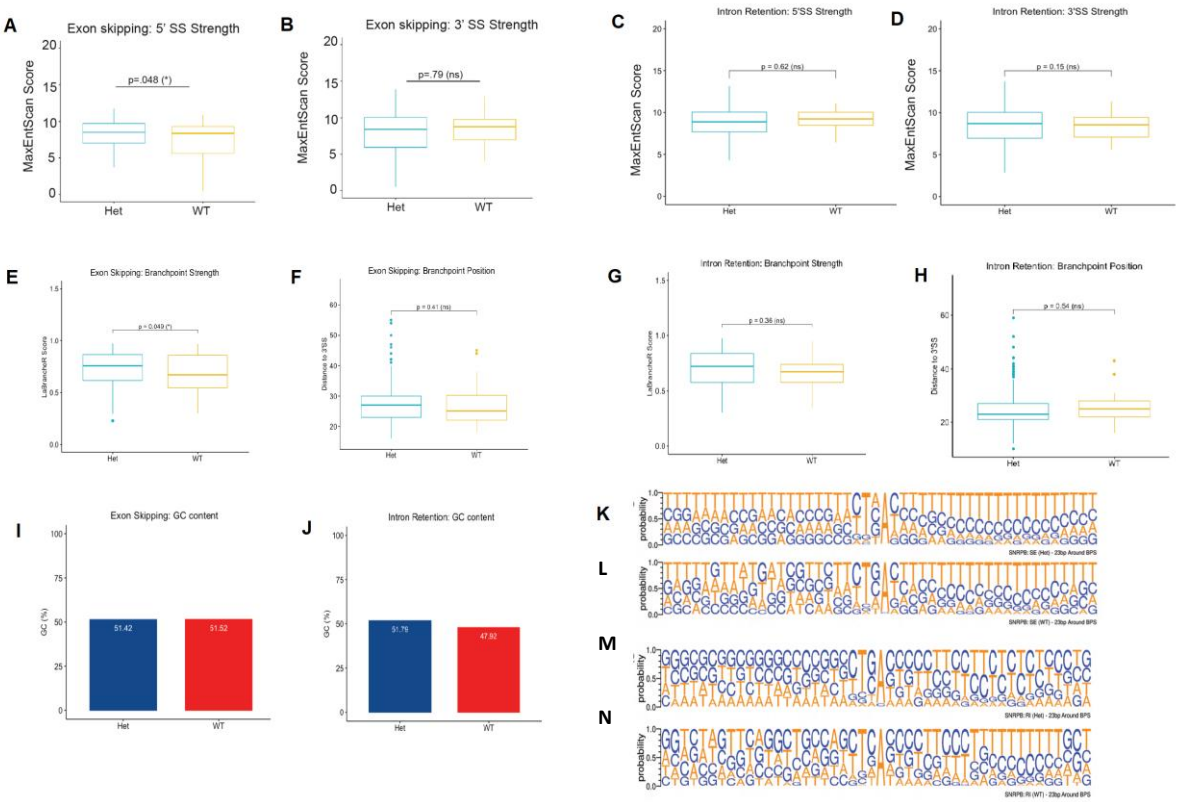

Figure 3.21: ***Increased branch point and 5' splice site strength might contribute to aberrant splicing in Snrpb$^{ncc+/-}$ mutants.*** (A-D) Splice site weakness assessment (MaxEntScan scores): comparative analysis of the 5 'splice site strength (A, C) and 3' splice site strength (B, D) of exons that are more skipped (A, B) and introns that are more retained (C, D) in mutant embryos and wild-type embryos, respectively. (E) Highlights a significant difference in the strength of the BP sites (t-test). (F) A mean comparison test (t-test) of the BP Distance from the 3'SS of the exons that are more skipped in mutant compared to the wild-type embryos. (G) Highlights a mean comparison test (t-test) of the LaBranchoR predicted BP Score from the introns that are more retained in mutant embryos in comparison to those more retained in the wild-type embryos, with no significant difference. (H) A mean comparison test (t-test) of the BP Distance from the 3'SS of the introns that are more retained in the mutant compared to the wild-type embryos. -Significance cutoffs used: p-value > 0.05 [ns] and p-value <= 0.05[*]. (I) and (J) show a GC content analysis of the 23bp sequences, upstream the LaBranchoR predicted BP of

exons that are more skipped (I) and more retained (J) in mutant and wild-type embryos. (K-L) A (consensus) motif analysis of the branchpoint site (23bp around the LaBranchoR predicted branchpoint [BP]) from exons that are more skipped in mutant embryos (K) and wild-type embryos (L). (M–N) A (consensus) motif analysis of the branchpoint sites (23bp around the LaBranchoR predicted BPS) from introns that are more retained in mutant (M) and wild-type embryos (N). (Adapted from Alam *et al.*, 2022)

3.7 P53 was found to be overexpressed due to splicing aberrations in *Snrpb*$^{ncc+/-}$ embryos but it is not solely responsible for the craniofacial anomalies

3.7.1 An increase in nuclear P53 was found in the *Snrpb*$^{ncc+/-}$ embryo heads, which is linked with the increased exon skipping of two P53 key negative regulators: *Mdm2* and *Mdm4*

As I aimed to find the key transcripts that, due to splicing errors, give rise to the craniofacial abnormalities seen in *Snrpb*$^{ncc+/-}$ mutants, first I looked at genes that could be associated with the upregulated pathways. In our RNA sequencing analysis, I found a significantly increased skipping of two major regulators of P53 pathway: exon 3 of *Mdm2* and exon 7 of *Mdm4.* These events were confirmed RT-PCR (Figure 3.22 A-B). We also found levels of the P53-regulated genes *Trp53inp1*, *Ccng1*, and *Phlda3* were increased, and that this increase was statistically significant when levels of *Ccng1*, and *Phlda3* were compared between E9.0 *Snrpb* wild type and mutant embryos, but not at E9.5 (Figure 3.22 C-D).

Based on the previous reports of increased levels of nuclear P53 because of same exon skipping in *Mdm2* and *Mdm4*, in cells and mice for spliceosomal mutations (Beauchamp *et al.*, 2021, Alstyne *et al.*, 2018, Correa *et al.*, 2016), as well as the increased cell death I saw in our mutants (Figure 3.22) along with the P53 regulated gene upregulation, I looked at nuclear P53 by

immunohistochemistry. This revealed a significant enrichment of nuclear P53 in E9.5 mutant heads (Figure 3.22 E-F).

Thus, I conclude that the increased exon skipping in *Mdm2* and *Mdm4* results in increased nuclear P53, and levels of P53 target genes in *Snrpb*$^{ncc+/-}$ embryos, before morphological abnormalities. Since P53 activation can lead to increased apoptosis, I postulate that increased P53 activity contributes to the apoptosis of *Snrpb*$^{ncc+/-}$ mutant cells.

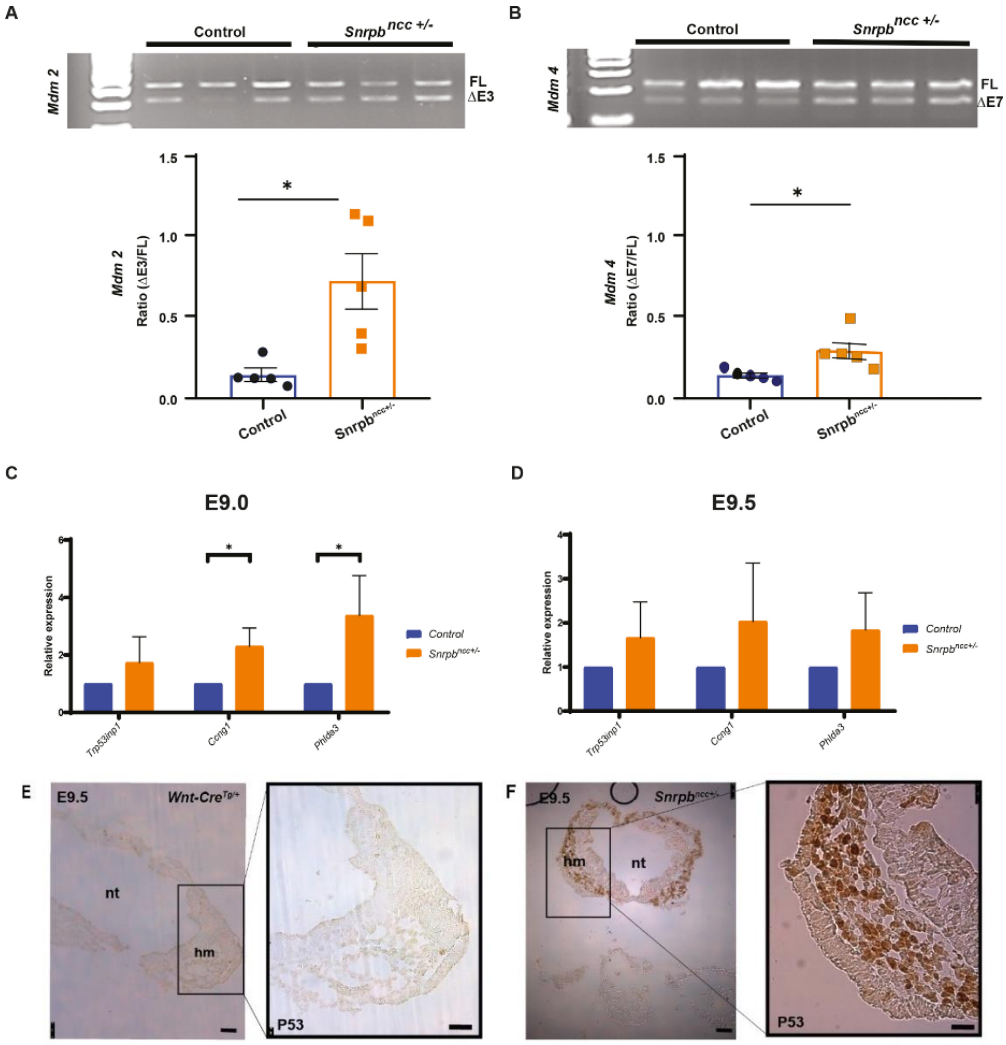

Figure 3.22: ***Increased exon skipping in two regulators of Mdm2* and *Mdm4*, and increased P53 expression was found in Snrpb$^{ncc+/-}$ mutant heads.*** (A, B) RT-PCR showing long (FL) and short transcripts (ΔE) produced in *Mdm2* (A) and *Mdm4* (B) in E9.0 control and *Snrpb*$^{ncc+/-}$ embryos. Lower panels show quantification of the ratio of *Mdm2* and *Mdm4* exon-skipped transcripts over the FL transcript (unpaired, two-tailed *t*-test, **P*<0.05). Error bars indicate standard deviation (SD). (C) Levels of P53 target gene expression in group1 E9.0 *Snrpb*$^{ncc+/-}$ and control embryos (unpaired, two-tailed *t*-test, **P*<0.05). (D) Levels of P53 target genes in control and *Snrpb*$^{ncc+/-}$ embryos. (E) and (F) Representative images of sections of heads of E9.5 control (n=3) and *Snrpb*$^{ncc+/-}$(n=3) embryos to detect P53 (brown). Error bars indicate standard error of mean (SEM). FL, full length transcript; ΔE3, transcript with exon 3 skipped; ΔE7, transcript with exon 7 skipped. (Adapted from Alam *et al.*, 2022)

3.7.2 Reducing levels of P53 in neural crest cells does not restore normal craniofacial development in *Snrpb*$^{ncc/+}$ embryos

As I hypothesized, P53 could drive the craniofacial malformations in *Snrpb*$^{ncc+/-}$ embryos by causing cell death, I reduced P53 levels in the mutants to test if it rescues abnormal development. I crossed *Trp53*$^{loxP/+}$; *Wnt1-cre2*^{tg} mice and *Snrpb*$^{loxP/+}$ mice and collected E10.5 and E17.5 *Snrpb*$^{ncc+/-}$; *P53*$^{ncc+/-}$ double heterozygous embryos for analysis. I found no significant difference in the proportion of *Snrpb*$^{ncc+/}$; *P53*$^{ncc+/-}$ embryos with mild to severe craniofacial defects (n=4/4), when compared to *Snrpb*$^{ncc+/-}$ mutants (n=3/3) (Figure 3.23 A, B). I then generated *Snrpb*$^{ncc+/-}$ with two mutant *Trp53* alleles in their neural crest cells (*Snrpb*$^{ncc+/-}$; *P53*$^{ncc-/-}$) for cartilage and skeletal analysis. E14.5 *Snrpb*$^{ncc+/-}$; *Trp53*$^{ncc-/-}$ mutant embryos (n=2) resembled *Snrpb*$^{ncc+/-}$ mutants found in group 2 (Figure 3.23 C). Similarly, E18.5 *Snrpb*$^{ncc+/-}$; *Trp53*$^{ncc-/-}$ mutant embryos (n=4) were morphologically like group 2 *Snrpb*$^{ncc+/-}$ mutants; they had microcephaly, a shorter snout and micrognathia (Figure 3.23 E). Cartilage and skeletal preps revealed reduced ossification of the frontal bone, cleft palate, and asymmetric and abnormal development of the lower jaw.

To determine whether homozygous deletion of Trp53 improves or rescues the survival of *Snrpb*$^{ncc/+}$ embryos, I allowed these mice to go to term and followed survival from P0 to P21, when the surviving pups were weaned. Of the 35 pups born, ten died within the first 2 days of life. Carcasses were recovered for five of these dead pups, and genotyping revealed that they were all *Snrpb*$^{ncc+/–}$; Trp53$^{ncc–/–}$. None of the surviving pups (n=25) were *Snrpb*$^{ncc+/–}$; *Trp53*$^{ncc–/–}$; chi-square analysis at P21 revealed this to be a significant deviation from expected Mendelian segregation (P=0.032). When I assumed that the dead pups were *Snrpb*$^{ncc+/–}$; *Trp53*$^{ncc–/–}$ embryos and performed a similar analysis, the significant difference was no longer found. Thus, the data suggest that the other six pups that died between P1 and P2 were likely

Snrpb$^{ncc+/-}$; *Trp53*$^{ncc-/-}$mutants. In fact, *Snrpb*$^{ncc+/-}$; *Trp53*$^{ncc-/-}$pups have not been found at P21 (n=0/36, four litters).

My data suggest that homozygous loss of Trp53 alleviates the most severe defects associated with reduced levels of *Snrpb* and allows these mutant pups to survive to birth.

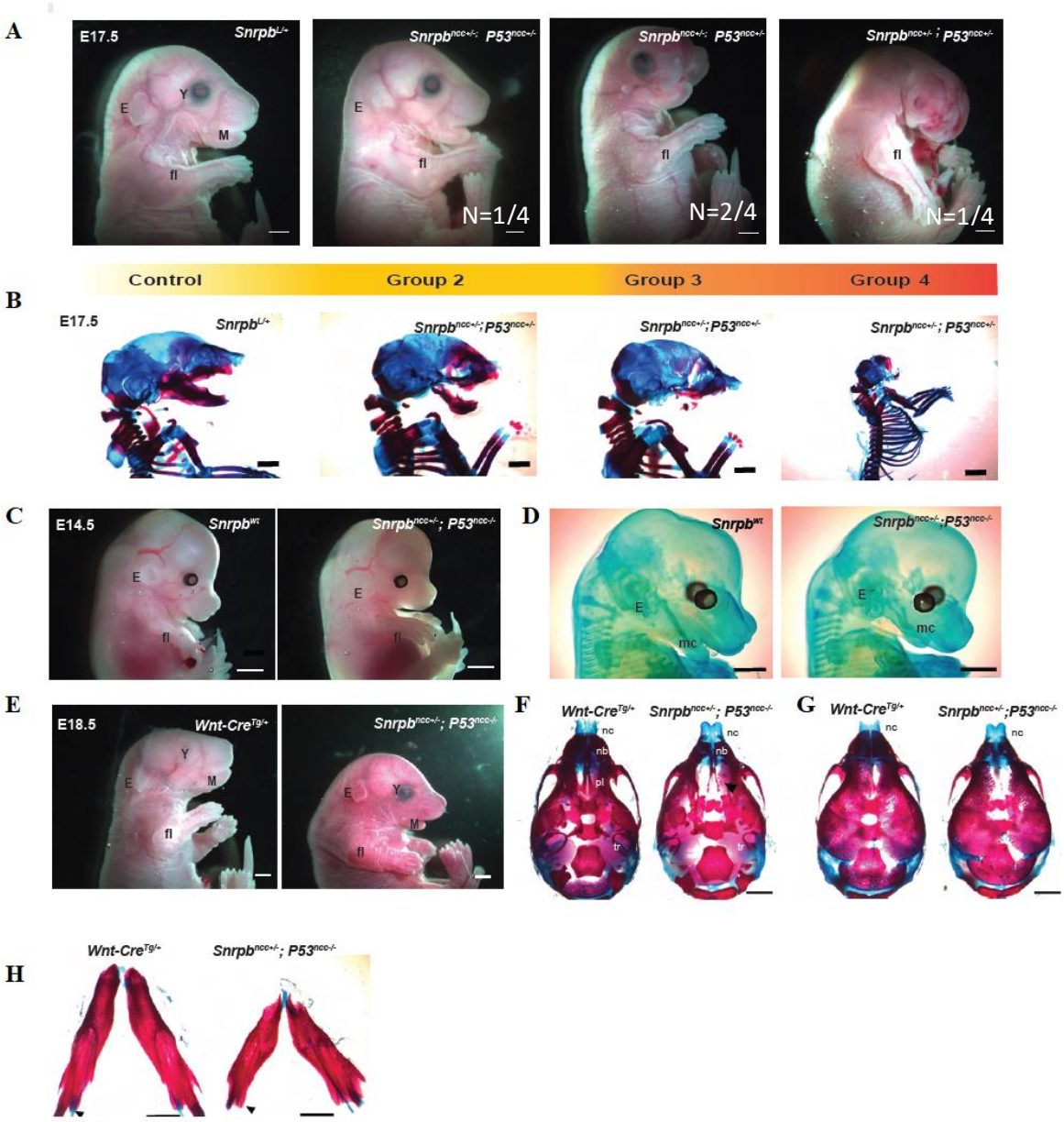

Figure 3.23: ***Knockdown of P53 in the neural crest cells does not rescue craniofacial abnormalities in Snrpb$^{ncc+/-}$ mutants.*** (A) Phenotypic abnormalities in E17.5 *Snrpb*$^{ncc+/-}$

embryos heterozygous for Trp53. (B) Representative images of skeletal staining of E17.5 control and *Snrpb*$^{ncc+/-}$; *P53*$^{ncc+/-}$ embryos. (C) Representative images of E14.5 control and *Snrpb*$^{ncc+/-}$*; P53*$^{ncc-/-}$ embryos showing micrognathia and hypoplasia of the head and outer ear in the mutant. (D) Representative images of E14.5 control and *Snrpb*$^{ncc+/-}$*; P53*$^{ncc-/-}$ embryos after Alcian blue staining of cartilages. (E) Representative images of E18.5 control and *Snrpb*$^{ncc+/-}$*; Trp53*$^{ncc-/-}$ embryos (n=4). (F) and (G) Representative images of Alcian blue and Alizarin red stained skulls of E18.5 control and E18.5 *Snrpb*$^{ncc+/-}$*; Trp53*$^{ncc-/-}$ embryos. (F) Cranial base view shows hypoplasia of the nasal bone, cleft palate (arrowhead) and hypoplasia of the tympanic ring in the Snrpb$^{ncc+/-}$; Trp53$^{ncc-/-}$ mutant. (G) Top view of the calvaria shows reduced ossification of the frontal bone, reduced ossification, and reduced ossification of the nasal bone in the mutant. (H) Representative images of the lower jaws of a control and a *Snrpb*$^{ncc+/-}$*; Trp53*$^{ncc-/-}$ mutants showing asymmetrical and abnormal development of the mutant mandible. Arrowhead in control indicates the angular process which is not discernable in the mutant (arrowhead). nt, neural tube; hm, head mesenchyme; E, ear; Y, eye; M, mandible; fl, forelimb; mc, Meckel's cartilage; nc, nasal cartilage; nb, nasal bone; tr, tympanic ring; pl, palate. Scale bar= 500 µm (Adapted from Alam *et al.*, 2022)

3.8 Genes required for craniofacial development are abnormally spliced in *Snrpb*$^{ncc+/-}$ mutants

To identify additional abnormal splicing events which could explain craniofacial malformations in *Snrpb*$^{ncc+/-}$ embryos, I queried the MGI database to determine if any transcripts with statistically significant DSEs were required for craniofacial development (Bogue *et al.*, 2017). I identified 13 transcripts required for craniofacial development or stem cell development with significant increases in exon skipping (Table 3.4). Increased exon skipping in 5 of these genes: *Pdpk1, Rere (Atr2), Mcph1, Nf1,* and *Dyrk2*, is predicted to introduce a pretermination codon. The remaining exon skipping events are not predicted to result in PTC but may alter gene expression and/or function. In fact, all except one of these DSEs were in constitutive exons. I then queried our RNAseq dataset to determine if the expression level of these genes was altered in *Snrpb* mutants. I found no significant changes in levels of transcripts with PTC or Non-PTC skipped exons. Then by RT-PCR, I validated the exon skipping events that were identified by the RNAseq analysis in 3 transcripts- *Smad2*, *Pou2f1* and *Rere* (Figure 3.24), although the percent spliced events for *Smad2* and *Pou2f1* were below 10% and not significant when the ratios of short/long transcript in control and mutant were compared. I postulated that abnormal increases in exon skipping in these 13-transcripts, which are required for normal craniofacial development, may contribute to craniofacial defects in *Snrpb*$^{ncc/+}$ mutants.

Table 3.4: ***Increased SE of craniofacial developmental genes in Snrpb$^{ncc+/-}$ mutants.*** Transcripts required for normal craniofacial development with a significant increase in skipped exons are not all predicted to result in PTC. (Adapted from Alam *et al.*, 2022)

Gene name	Skipped Exon	PTC	Phenotype	Constitutive exon
Smad2	Exon 3	No	Mandible hypoplasia (Nomura and Li, 1998)	No
Loxl3	Exon 2	No	Cleft palate, short and bent mandible (Zhang *et al.*, 2015)	No
Ror2	Exon 8	No	Midface hypoplasia, truncated Meckel's, middle ear defect (Schwabe, G.C. *et al.*, 2004)	Yes
Nisch	Exon 6	No	Short snout (Crompton, M. *et al.*, 2017)	Yes
Pou2f1	Exon 4	No	Abnormal nasal placode development when removed with *Sox2* (Donner, A.L. *et al.*, 2006)	Yes
Rgl1	Exon 3	No	Abnormal frontal bone, short snout, abnormal maxilla and mandibular morphology (Mouse Genome Informatics and the International Mouse Phenotyping Consortium, 2014)	Yes
Frem1	Exon 32	No	Midface hypoplasia, asymmetry, short snout (Vissers, L.E. *et al.*, 2011)	Yes
Smc3	Exon 5	No	Upturned snout (White, J.K. *et al.*, 2013)	Yes
Pdpk1	Exon 3	Yes	Abnormalities in the head, nasal cartilage (Lawlor, M.A. *et al.*, 2002)	Yes
Rere (*Atr2*)	Exon 4	Yes	Small pharyngeal arch (Zoltewicz, J.S. *et al.*, 2004)	Yes
Mcph1	Exon 13	Yes	Microcephaly (Gruber, R. *et al.*, 2011)	Yes
Nf1	Exon 56	Yes	Head hyperplasia, aorticopulmonary septal defect, heart defects (Brannan, C.I. *et al.*, 1994)	Yes
Dyrk2	Exon 2	Yes	Cleft palate (Yoshida, S. *et al.*, 2020)	No

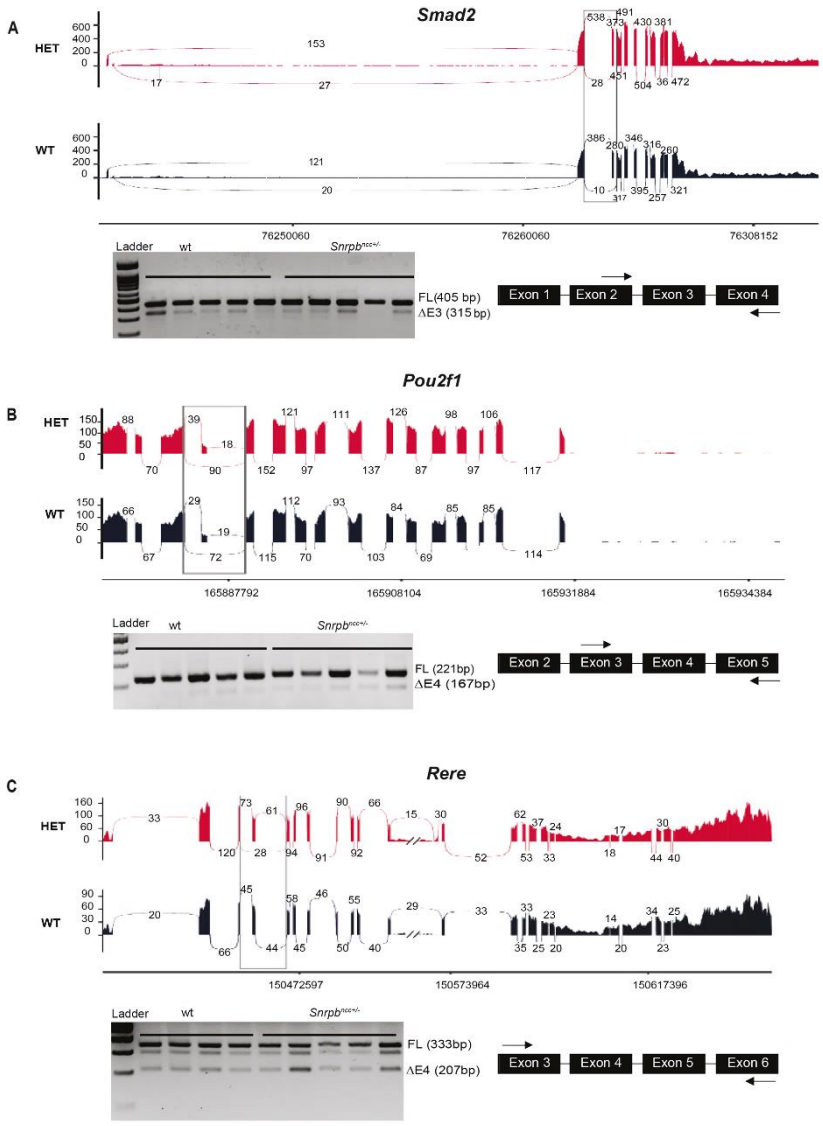

Figure 3.24*: Transcripts with exon skipping events are found in heads of E9.0 Snrpb control and mutant embryos.* (A-C) Sashimi plots for the exon skipping events found for *Smad2* (A), *Pou2f1* (B) and *Rere* (C). Under each sashimi plot, representative gel for RT-PCR showing the presence of transcripts with the predicted exon skipping event. The location of primers used to amplify transcripts is shown on the right. No significant difference was found in the ratio of short/long transcripts (unpaired, two-tailed *t*-test). Error bars in the graphs indicate standard error of mean (SEM). FL, full length; ΔE, skipped exon. (Adapted from Alam *et al.*, 2022)

3.9 Wild-type levels of *Snrpb* are required for normal expression of *Fgf8, Shh* and *Msx2*

The surface cephalic ectoderm, of which the facial ectoderm zone (FEZ) is a subregion, is essential for integrating proper growth of the craniofacial skeletons and brain and patterning the underlying neural crest (Griffin *et al.,* 2013). The severe malformations found in the face and brain of *Snrpb* mutants suggest that the FEZ might not have formed. Therefore, I used *in situ* hybridization to examine expression of *Shh* and *Fgf8,* which are expressed in surface cephalic ectoderm and together help to define the FEZ (Griffin *et al.,* 2013). At E9.5 before the FEZ forms, *Shh* was expressed in the ventral-most region of the neural tube, the floor plate, as well as the ventral prosencephalon of *Snrpb* wild type and *Snrpb*$^{ncc+/-}$ embryos (Figure 3.25 A, n=4; 3 group 1 and 1 group 2). At this stage, *Fgf8* was expressed in the mandibular epithelium, the frontonasal prominence, and the midbrain/hindbrain junction of control and *Snrpb*$^{ncc+/-}$ mutant embryos. However, the expression domain of *Fgf8* was abnormally expanded at these sites (n=4; 2 group 2 and 2 group 1) (Figure 3.25 B). Furthermore, expression of *Msx2,* a downstream target of *Fgf8* in the underlying neural crest cells (Griffin *et al.*,2013) was also abnormal in E9.5 *Snrpb*$^{ncc+/-}$ embryos. In *Snrpb*$^{ncc+/+}$ embryos (n=6), *Msx2* was expressed in the distal region of pharyngeal arches 1 and 2 (Figure 3.25 C). However, in *Snrpb*$^{ncc+/-}$ embryos, *Msx2* expression was abnormally extended proximally in these arches (n=4; 3 group 1 and 1 group 2) (Figure 3.25 C). *In situ* hybridization analysis revealed that normal levels of *Snrpb* are required in the neural crest cells to restrict expression of *Fgf8* and its downstream target *Msx2* in the developing head and face in both morphologically normal and abnormal embryos.

In E10.5 group 2 *Snrpb*$^{ncc+/-}$ mutant embryos missing the frontonasal prominence, expression of *Shh* was found in the diencephalon and the ventral forebrain (n=3; Figure 3.25 D). Furthermore, ectopic *Shh* expression was found in the dorsal and ventral optic lens (arrows in Figure 3.25 D). In group 1 mutant embryos, the lateral and medial nasal processes were further apart than in wild type embryos but, *Shh* expression was found in the developing mandibular

periderm, and bilaterally on the surface ectoderm of the medial nasal prominences (arrows in Fig 3.23 G, n=1). In E10.5 wild type embryos, *Fgf8* was expressed on the surface ectoderm of the mandible, the maxillary prominences, and frontonasal prominences. In group 2 *Snrpb*$^{ncc+/-}$ mutant embryos with a hypoplastic frontonasal and maxillary prominences, expression of *Fgf8* was found on the mandibular ectoderm and in the region where the maxillary prominence would normally form (n=2) (Figure 3.25 E). In group 1 E10.5 *Snrpb*$^{ncc+/-}$ embryos, *Fgf8* expression in the lateral nasal prominence was reduced, while ectopic expression of *Fgf8* was found on the surface ectoderm of the medial nasal process, towards the midline (n=3, Figure 3.25 H). Similarly, in E10.5 group 2 *Snrpb*$^{ncc+/-}$ mutants missing the frontonasal and maxillary prominences, *Msx2* expression was expressed in the maxillary and in the mandibular region of the hypoplastic first arch (n=3). In group 1 *Snrpb*$^{ncc+/-}$ mutants, *Msx2* was expressed in the lateral and medial nasal prominences, although expression appeared reduced but ventrally expanded in the medial frontal nasal region (n=2; Figure 3.25 F). Thus, in *Snrpb*$^{ncc+/-}$ embryos where the lateral and medial nasal prominences formed, reduced expression of *Fgf8* in the ectoderm results in abnormal expression of *Msx2* in the underlying neural crest.

I postulate that DSEs in genes important for midface development led to abnormal expression of *Shh, Fgf8* and *Msx2* expression and mis-patterning of the developing craniofacial region.

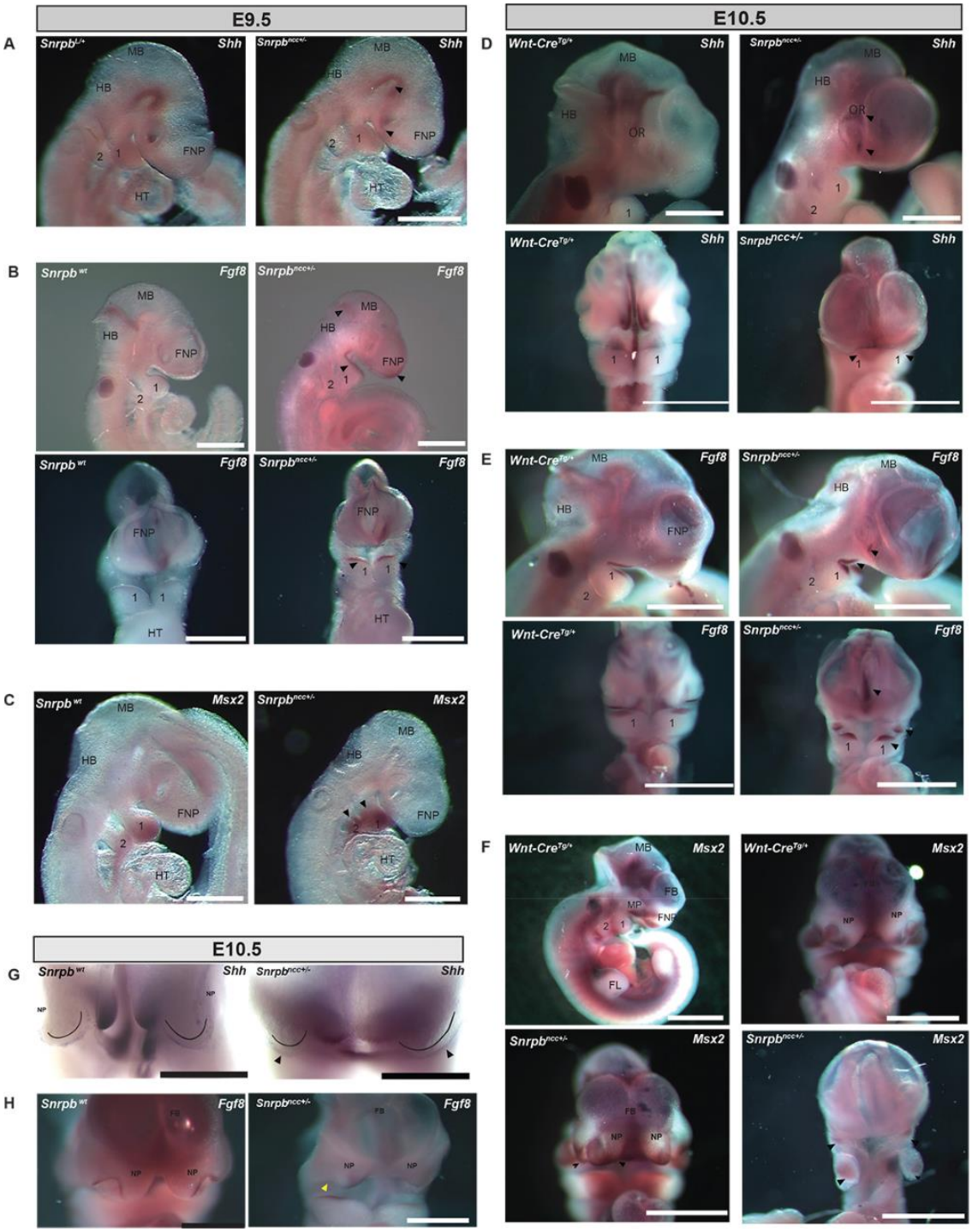

Figure 3.25: *Shh*, *Fgf8 and Msx2 are mis-expressed in Snrpb*$^{ncc+/-}$ *embryos.* (A) *Shh* at E9.5 was expression in the control and *Snrpb*$^{ncc+/-}$ embryos. (B) Lateral (top row) and ventral (bottom row) views of embryos showing that expanded expression (arrowheads) of *Fgf8* in the group 2 (*n*=4) mutant embryos. (C) Extended *Msx2* expression (arrowheads) to the proximal region of pharyngeal arches 1 and 2 in group 1 mutant (*n*=2). (D) At E10.5, top row: lateral

view of embryos showing *Shh* expression in a control and group 2 mutant embryo. Ectopic expression was found in the dorsal and ventral optic lens (arrowheads) of the mutant. Bottom row: ventral view showing expression of *Shh* on the oral ectoderm in a control and group 2 mutant (right) embryos. (E) Top row shows representative images of lateral views of a control embryo and mutant embryo. *Fgf8* expression was observed on the mandibular ectoderm and in the region where the maxillary prominence would normally form (*n*=3); ectopic expression was also detected in the lens. Bottom row shows frontal view of abnormal *Fgf8* expression in the mutants (black arrowheads). (F) Top row: lateral (left) and ventral (right) views of *Msx2* expression in E10.5 control embryos. Bottom row: E10.5 group 1 *Snrpb*$^{ncc+/-}$ mutant (left) with reduced and ventrally expanded *Msx2* expression in the medial frontal nasal region. On the right, in a group 2 *Snrpb*$^{ncc+/-}$ mutant *Msx2* was expressed in the region where the maxillary prominences would form and in the mandibular region of the hypoplastic first arch. (G, H) E10.5 embryos showing *Shh* expression in the developing mandibular periderm, and bilaterally on the surface ectoderm of the medial nasal prominences of control (left) and group 2 *Snrpb*$^{ncc+/-}$ (right) embryos (H) Abnormal *Fgf8* expression in group 2 mutants (yellow arrowhead) while compared to control E10.5 embryo. 1, 2, pharyngeal arches 1 and 2; FNP, frontonasal process; HB, hindbrain; HT, heart; MB, midbrain; MP, mandibular process; NP, nasal process; OR, optic region. Black arrowheads indicate abnormal expression in the mutants. Scale bar=500 μm (Adapted from Alam *et al.*, 2022)

3.10 AIM 2 Conclusion:

I aimed to find the genes and/or pathways that are associated with craniofacial abnormalities in the neural crest cell specific *Snrpb* mutant mouse model. I found, mutation of *Snrpb* in neural crest cells causes in a significant rise in exon skipping and intron retention. Similar splicing changes were found in glioblastoma cell line upon *SNRPB* knockdown (Correa *et al*., 2016).

In these mutants, there were many genes that had higher exon skipping. Of them, two P53 regulators: *Mdm2* and *Mdm4* had increased skipping of exons 3 and 7, respectively. These exon skippings cause increased stability of P53 resulting in an elevated cell death in the *Snrpb* mutant heads and lead to craniofacial abnormalities. However, normal craniofacial development cannot be restored by genetically reducing or removing P53 from the neural crest cells, suggesting involvement of other molecules to drive the craniofacial phenotypes.

Though I did not find many differentially expressed genes in the mutants that might contribute to the craniofacial malformations, I found exon skipping of 13 genes key for craniofacial development, including *Smad2, Rere* and *Pou2f1*. I also found misexpression of *Shh, Fgf8,* and *Msx2* in the $Snrpb^{ncc+/-}$ mutants, which are crucial for facial morphogenesis. I conclude, the misregulation of gene expression along with the P53-mediated cell death is responsible for the abnormal craniofacial development in the *Snrpb* mutant mice model.

CHAPTER IV

GENERAL DISCUSSION

Splicing is an essential and ubiquitous process that generates mature mRNAs and increases the number and diversity of proteins from the genome (Chen and Manley, 2009; Nilsen and Graveley, 2010). SNRPB is an indispensable protein that facilitates assembly of the snRNPs that carry out splicing. It is known that heterozygous point mutations in the PTC containing alternative exon 2 of *SNRPB* causes an increased inclusion of that alternative exon (Lynch *et al*., 2014). This increases levels of a non-functional *SNRPB* transcript result in CCMS, a craniofacial spliceosomopathy that is mostly associated with rib gap defects (Lynch *et al.*, 2014; Bacrot *et al.*, 2015; Beauchamp *et al.*, 2020). Though it is suggested, it is not known if a reduction in SNRPB protein level is causing the CCMS dysmorphologies. Moreover, why mutation in a common core splicing factor causes tissue-specific abnormalities in CCMS is not understood. *SNRPB* has been studied in several human cell lines (Correa *et al.*, 2016; Van Alystene *et al.*, 2018; Liu *et al.*, 2019; Zhan *et al.*, 2020) and its knockdown causes a general splicing anomaly (Correa *et al.*, 2016). However, contribution of SNRPB in embryonic development has never been shown.

In my PhD project, I hypothesized that *SNRPB* reduction causes tissue-specific gene-splicing differences that result in specific malformations of CCMS, such as craniofacial and rib defects. Thus, I tried to understand the role of *SNRPB* in embryonic development by using CCMS mouse model as a tool. While generating a conditional mutant mouse line, I retrieved the *Snrpb* intronic Δ61 mutant allele that mimicked CCMS features in mice. As the phenotypes seen in the Δ61 mutant line were poorly penetrant, I moved forward to removing *Snrpb* constitutively and tissue-specifically, using tissue-specific *Cre* lines.

4.1 The deleted 61 base-pair in intron 2 is a potential novel regulatory sequence of *Snrpb*

I have described a novel *Snrpb* mutant mouse line that had a 61 base-pair deletion in the intron 2. The deletion mutation is proximal to the regulatory alternative exon 2 and almost all CCMS patients are known to have mutations in the 5' and 3' ends of this highly conserved regulatory alternative exon 2 of the gene (Lynch *et al*., 2014, Bacrot *et al.*, 2015, Tooley *et al.*, 2016). Craniofacial malformation such as micrognathia is one of the most prevalent abnormalities in CCMS that is seen in around 90% of the patients. In the *Snrpb* Δ61 mutant model, I have shown Meckel's cartilage, that drives the formation of the mandible, was hypoplastic in E14.5 mutants and consistently, smaller lower jaws were observed in the mutant pups. Rib development is abnormal in CCMS and through skeletal staining it was found that a group of *Snrpb* Δ61 mutants had an extra pair of ribs. I conclude that, *Snrpb* Δ61 mutant mice recapitulate CCMS abnormalities at a low penetrance.

As mentioned before, reduction in *SNRPB* transcripts was seen in the CCMS patients suggesting that reduced SNRPB protein levels cause the developmental anomalies in CCMS. My hypothesis was that the deletion of the 61 base-pair from intron 2 was reducing SNRPB protein level by incorporating more of the nearby PTC containing alternative exon 2 in the transcript, that undergoes nonsense mediated decay. I showed that the 61 base-pair deletion resulted in increased inclusion of the deleterious alternative exon 2 in the mutants and a reduction in SNRPB protein level in a subset of the mutants (Figure 3.5). These findings support that this intronic region near alternative exon 2 is important for maintaining SNRPB levels in mice. This region in intron 2 of human *SNRPB* might also play a similar role and thus should be investigated to determine if there are mutations in this region in CCMS patients, who previously were reported to have no *SNRPB* mutations (Lynch *et al*., 2014, Bacrot *et al.*, 2015,

Tooley *et al*., 2016). In fact, there are at least two CCMS patients who were not found to have any mutation in *SNRPB,* through exome and Sanger sequencing (Lynch *et al*., 2014).

Intron sequences are known to play roles in regulating splicing and mutations in them are often found to cause diseases (Busslinger, 1981; Ichikawa *et al.,* 2014; Vaz-Drago *et al.,* 2017). There are several mechanisms by which such mutations can modulate splicing. Mostly, intronic mutations activate cryptic splice sites by creating a novel donor splice site or a novel acceptor splice site. Spliceosomes can recognize these new splice sites and promote the splicing process that will lead to improper intron removal or inclusion of pseudo-exons. For example, a well-known deep intronic change is a variant with a point mutation in the CFTR gene responsible for cystic fibrosis in Polish population. Located in intron 19, this mutation creates a novel donor site that results in the inclusion of an 84-bp pseudo-exon in the transcript (Anna and Monika, 2018). Like AE2 of *Snrpb,* that pseudo-exon contains a stop codon causing the transcript to encode a shorter and non-functional protein. The consequences of intronic mutation can also be exemplified by a patient with intronic point mutation in COG1, who have been shown to have donor splice site disruption mediated exon skipping that results in a CCMS like syndrome (Zeevaert R. *et al.,* 2009a.; Zeevaert R. *et al.,* 2009b). In addition to point mutations in the intronic sequence that cause pathogenic consequences, intronic deletions can potentially cause human diseases. Small deletions in the intronic sequence can cause aberrant splicing by 5′SS-branchpoint space constraint mechanism. Critical shortening of 5′SS-branchpoint minimal length was defined as a mechanistic basis and primary determinant for abnormal splicing in human genetic conditions (Bryen *et al.*, 2019). Though it was suggested that shortening of the spliceosome binding space due to intronic deletion can cause exon skipping, intron retentions were also shown to be possible due to small intronic deletions such as a 15 bp deletion in *DOK7* gene in congenital myasthenic syndrome (Bryen *et al.*, 2019). This space constraint mechanism could be one possibility of the mutants showing abnormalities with the bigger 61 base-pair

deletion whereas mutants with the smaller 46 base-pair deletion did not show abnormal embryonic development in the study.

in silico analysis using available tools will guide if deletion of the 61 base-pair intronic region is creating a new splice site or if the sequence has putative sites to bind specific proteins such as splicing factors, hnRNPs or SR proteins that regulate splicing. Chip-Seq (chromatin immunoprecipitation with sequencing) assay would be one powerful method for identifying binding sites for such proteins (Bieberstein *et al.,* 2014) with the 61 base-pair. Transfecting HeLa cells using SmB-minicassette that previously used by Saltzman *et al.* (2011) but with the 61 base-pair deletion will be useful to perform such molecular studies.

Compared to the other *Snrpb* mutant models (*Snrpb*$^{ncc+/-}$, *Snrpb*$^{mes+/-}$, *Snrpb*$^{+/-}$) in my study, where the penetrance of the phenotypes is complete, the Δ61 mutants have a very low penetrance. I hypothesize that the inclusion of alternative exon 2 of *Snrpb* causes reduction of the protein level below the threshold required for normal development in the abnormal mutant subgroup (Figure 4.1). It is speculated that below a certain threshold of splicing factors craniofacial malformations can occur (Beauchamp *et al.*, 2020). My hypothesis needs to be addressed by further investigation of the correlation between the phenotype and level of protein being made in specific mutants. One way to approach would be to take morphologically normal and abnormal embryos and looking at the protein level of individual embryo through western blot.

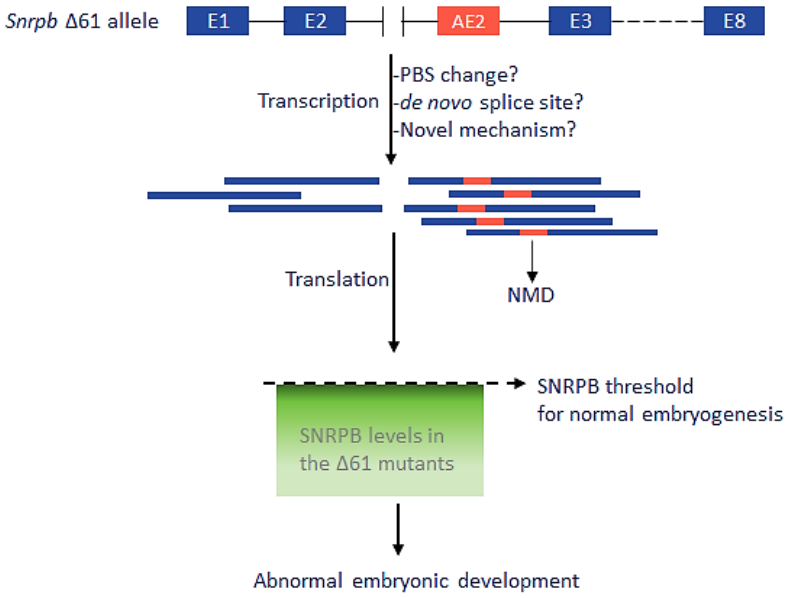

Figure 4.1: ***A schematic depiction of the hypothesis that the incomplete penetrance in the Snrpb Δ61 mutant model reflects protein level being made in each specific mutant.*** The 61-bp intron allele makes more of the transcripts with alternative exon 2 (AE2, red box) than the wild type of transcript without AE2 in a subset of mutants, through an unknown mechanism. This causes more of the transcripts to go through nonsense mediated decay (NMD) and decrease SNRPB levels in those embryos. When it is beneath the threshold level of SNRPB required for normal embryonic development, that subgroup of mutants' normal embryogenesis is compromised, resulting in the abnormal phenotypes. PBS-protein binding site.

4.2 Reduction of SNRPB in specific cell types during embryonic development determines the phenotypic outcome and severity

CCMS has been suggested to be an outcome of a reduced level of SNRPB (Lynch *et al.*, 2014). However, the level of reduction of SNRPB protein in the patients or in the specific affected tissue type is not known. Only a single CCMS patient carrying point mutation in the 5′ UTR of *SNRPB* that was predicted to result in a null allele had more severe anomalies and failed to survive gestation (Lynch *et al*., 2014). In my conditional mutant mouse line, deletion of exon 2, alternative exon 2 and exon 3 upon *Cre* recombination, generated a shorter *Snrpb* transcript of 527 bp that is speculated to encode for a non-functional protein. We found a 70% reduction in the *Snrpb* mRNA expression in the mutants. When *β-actin-Cre* was used to delete the *Lox*P-flanked exons, the resulting *Snrpb* heterozygous embryos died post-implantation. For the $Snrpb^{ncc+/-}$ and $Snrpb^{mes+/-}$ mutants, we predict a 70% reduction of *Snrpb* mRNA and protein in neural crest and mesoderm, respectively. In both mutants, fully penetrant tissue-specific phenotypes were seen. Although further studies are required to determine whether there is a general growth defect or other roles for *Snrpb* at the early stages of development, my study suggests that heterozygosity for a loss-of-function allele of *Snrpb* is lethal. Mutations in the alternative exon 2 in *SNRPB* is suggested to make it a hypomorphic allele in CCMS, except one very severe CCMS case where a 5'UTR point mutation is predicted to result in a null allele. My results support the hypothesis that *SNRPB* mutations commonly found in CCMS patients are not null mutations as null mutations would likely cause a more severe or lethal abnormalities in CCMS (Lynch *et al.*, 2014).

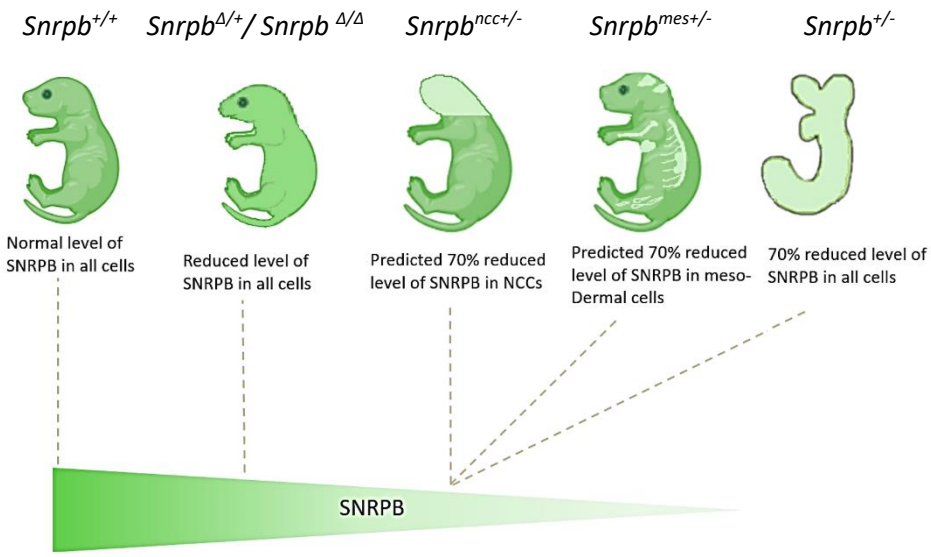

Figure 4.2: ***The Snrpb mutant mice models developed in the study suggest that the reduction level of*** **SNRPB** ***in specific cell types determines the phenotypic outcome and severity.*** Δ refers to the *Snrpb 61* base-pair intronic deletion.

4.3 Normal SNRPB level is essential for both prenatal and postnatal stages

Growth retardation and short stature is commonly seen in CCMS patients who survive infancy (Lynch *et al.*, 2014; Tooley *et al.*, 2016). CCMS patients have been reported to have birth weight below the 50th percentile. Growth parameters in childhood were also variable but tended to follow this trend (Tooley *et al.*, 2016). In addition, *SNRPB* has been shown to be postnatally important in human as somatic mutations in *SNRPB* are emerging as oncogenic factor in cervical, lung and hepatic cancers (Correa *et al.*, 2016; Yang *et al.*, 2018; Liu *et al.*, 2019; Zhan *et al.*, 2020).

In my study, I demonstrated that mutating *Snrpb* either constitutively (*Snrpb*$^{+/-}$) or in specific cell types such as in neural crest cells (*Snrpb*$^{ncc+/-}$) and mesoderm cells (*Snrpb*$^{mes+/-}$) cause abnormal embryonic development. Only in the *Snrpb*$^{ncc+/-}$ line, I found five mutant P0 pups

that were born, of which one had no abnormal phenotype except a slight curvature of bone in the palate (Figure 3.11). It is not known if the phenotypically normal P0 mutant would have survived to adulthood with that mild skeletal deformity if I had not sacrificed it. In the Δ61 mutant model, though *Snrpb*$^{\Delta 61/+}$ and *Snrpb*$^{\Delta 61/\Delta 61}$ animals were born at mendelian segregation, as I followed five litters of animals, I found a significant number of both heterozygous and homozygous mutants become sick and die within a year. A subgroup of mutants (~43%) was also significantly smaller from the wild-type littermates at birth and onward. In addition, while dissecting at least four of the freshly dead animals that became sick over time, I found lesions in the spleen and lung of those mice. Taken together, my findings suggest that normal level of SNRPB is required in both embryonic and postnatal stages.

4.4 *Snrpb* is required for proper cartilage formation and normal osteogenesis

In my study, *Snrpb* Δ61 mutants, *Snrpb*$^{ncc+/-}$ mutants and *Snrpb*$^{mes+/-}$ mutants showed abnormal development of cartilages, some of which go through endochondral ossification process. My data suggest that reduction in *Snrpb* hinders proper chondrogenesis, a finding supported by the evidence that *Snrpb* knocked down *Xenopus* model have reduced cartilage formation (Park *et al.,* 2022). Similar findings are shown *in vivo* (*Xenopus* and mice) for other splicing factor mutations associated with human syndromes similar to CCMS (Beauchamp *et al.*, 2021; Park *et al.*, 2022). Bones that are derived through both endochondral and intramembranous processes were abnormal in *Snrpb* mutants. As shown, bones developed through both intramembranous (such as frontal bone, sphenoid bones, mandible) and endochondral (anterior facial bones, middle ear bones, hyoid bone) processes were abnormally developed in *Snrpb*$^{ncc+/-}$ mutants.

In addition to reduced ossification, I showed neural crest cells with *Snrpb* mutation can give rise to ectopic cartilages and bones in some *Snrpb*$^{ncc+/-}$ mutants (Figures 3.14, 3.15). Similarly,

accessory ossicles in the hyoid bone were found after CT scan of two CCMS patients by Tooley *et al.* (2016). The wider expression patterns we saw for *Shh* and *Fgf8* in our mutants (Figure 3.25) might be associated with this phenotype. Overexpression of *Shh* in the non-oral ectoderm was shown to cause expansion of *Fgf8*, affecting the rostral–caudal axis of the developing first arch, and resulting in the formation of ectopic cartilages in chick (Haworth *et al.,* 2007). From my current data it is difficult to explain how reduced SNRPB levels in neural crest cells cause an expansion of *Shh* expression domain.

Though CCMS patients are suggested to have ossification defects in their intramembranous bone formation (Lynch *et al.*, 2014), my findings suggest that one allele of *Snrpb* is insufficient for normal cartilage formation and osteogenesis that occurs through both endochondral and intramembranous processes. Further investigation on how the skeletal malformations occur in the mutants could address the following questions: 1. does reduced cells in the head results in the hypoplasticity of the cartilages and later in bones; 2. differentiation of the neural crest cell progenitors to become chondrocytes and or osteocytes are disrupted. Moreover, degeneration of the chondrocytes might also be an underlying cause of the bone anomalies we saw later. Again, unsuccessful differentiation of cranial neural crest cell derived mesenchymal cells can be one possibility of the osteogenesis defect in the $Snrpb^{ncc+/-}$mutants. Runx2 is the first transcription factor required for determination of the osteoblast lineage and is a differentiation marker of immature osteoblasts. In the developing head, it is expressed in the neural crest-derived mesenchymal cells. In mice, neural crest cell specific deletion of Runx2 resulted in reduced ossification primarily of the anterior half of the craniofacial bones, including the frontal bone, jugal bone, squamous temporal bone, mandible, maxilla, and nasal bone (Shirai Y *et al*., 2019). Looking at *Runx2* expression in sectioned embryos could be one way to find if abnormal osteogenic differentiation happens in the mutants' developing head and face.

4.5 *Snrpb* is required in mesodermal cell lineages for proper craniofacial, cardiac and rib developments

Though haploinsufficiency of *SNRPB* is known to cause mostly craniofacial malformation and rib defects, other structures such as limbs and soft tissues such as heart, kidney or digestive tract anomalies were also reported in some CCMS patients (Table 1.1). To model CCMS rib abnormalities and understand the role of SNRPB in mesodermal cells, I removed *Snrpb* heterozygously from those cell populations by mating my conditional knockout mice with the *Mesp1-Cre* mice. No mutants were recovered at birth suggesting a requirement of normal levels of *Snrpb* in the mesoderm for embryonic survival. The developmental abnormalities of head, face and heart was visible from E9.5 in the $Snrpb^{mes+/-}$ embryos and the phenotypes were fully penetrant at E14.5.

The heart is mostly derived from embryonic mesodermal cells (Figure 1.12) that differentiate into mesothelium, endothelium and myocardium. Mesothelial pericardium forms the outer lining of the heart whereas the inner lining of the heart – the endocardium, lymphatic and blood vessels, develop from endothelium. Phenotypic observation of the embryos showed abnormal heart in $Snrpb^{mes+/-}$ mutants. The massive dorsal edema, which is an indication of cardiac malformation as seen in other mutants with heart anomalies (Schneider *et al.*, 2004), was observed at E14.5 mutants. This also suggests that the phenotypically normal embryos before E14.5 might have cardiac malformations that cause their death later. However, the other possible cardiac defects of CCMS such as cardiac septal defects or outflow tract abnormalities can only be confidently detected after E14.5 (Schneider *et al.*, 2004). To interpret the fine detail of any cardiac malformations in addition to pericardium formation or any other visceral organ defect in the *Snrpb Mesp1-Cre* mutants that might cause their death, it will need serial histological sectioning or computer tomography imaging of the embryos. However, my preliminary data suggest normal level of SNRPB is required for proper cardiac development.

The characteristic feature of CCMS that is unique from Pierre Robin sequence is the costovertebral anomalies, mostly rib gap defects. Ribs are derived from sclerotome cells of the somites, a derivative of paraxial mesoderm (Figure 1.12). I predicted removing *Snrpb* from mesoderm cells would affect rib formation in mice, that would mimic CCMS. In the E14.5 *Snrpb*$^{mes+/-}$ mutants, the ribs were abnormal with smaller size, irregular spacing and sternum base was absent (Figure 3.9). However, as I did not recover mutants after E14.5, I could not investigate if either ossification defect or skeletal degeneration in later stages would cause any rib gaps in the *Snrpb*$^{mes+/-}$ mutants. Though somites in the mutants looked normal during phenotypic analysis, it is possible that *Snrpb* mutation perturbs genes or pathways that are required for rib development at later stage of sclerotome specification and differentiation. Transcription factor *Pax1* is predominantly expressed in the region of the future vertebral bodies and intervertebral discs **(**Deutsch *et al.*, 1988), whereas the *Pax9* expression domain extends more laterally in the region of the future proximal part of the ribs **(**Neubüser *et al.*, 1995). Looking at such markers in the mutants at E10.5 through *in situ* hybridization can provide information if the sclerotomes are properly developed in the *Snrpb*$^{mes+/-}$ mutants.

4.6 Splicing anomalies are presumably occurring in the *Snrpb*$^{mes+/-}$ mutants that results in the phenotypes

Further investigations are needed to understand the molecular mechanism by which *Snrpb* heterozygous mutation in mesodermal cells causes developmental abnormalities. *SNRPB* knockdown in cell lines has been shown to cause aberrant splicing of transcripts (Correa *et al.*, 2016). In the *Snrpb*$^{ncc+/-}$ mutants, we found significant changes in exon skipping in many genes. For the phenotypes that we see in the *Snrpb*$^{mes+/-}$ mutants, I hypothesize splicing aberrations such as increased exon skipping occurs in genes that are important in the development of the structures that are abnormal in this mutant model. As we see craniofacial defects in the *Snrpb*$^{mes+/-}$ mutants with smaller mandible and head, it is also possible that the mutants undergo

increased apoptosis or proliferation defects. Increased cell death is suggested to be associated with craniofacial spliceosomapathies such as loss of neural crest progenitors through apoptosis was shown in *Xenopus* model for Nager syndrome (Jones *et al.*, 2008; Mao *et al*., 2016; Devotta *et al.*, 2016). Increased exon skipping in *Mdm2/ Mdm4* caused increased P53 activity that presumably leads to higher cell death in the *Snrpb*$^{ncc+/-}$ mutants. Increased exon skipping in *Mdm2* was shown in *Eftud2* neural crest cell specific mutant mice model for MFDM syndrome (Beauchamp *et al.,* 2021). Hence, in the *Snrpb*$^{mes+/-}$ mutants, *Snrpb* mutation might cause increased P53 function through similar *Mdm2/ Mdm4* splicing defect to cause malformations, especially the craniofacial defects.

4.7 *Snrpb* is presumably required in neural crest cells and their derivatives

To study the role of SNRPB in craniofacial development, I used the *Wnt1-Cre2* transgenic mouse line to generate embryos with heterozygous mutation of *Snrpb* in their neural tube and neural crest cells. In *Snrpb*$^{ncc+/-}$ mutant embryos, craniofacial development was abnormal with variable expressivity suggesting that normal SNRPB level is required in the neural crest cells for the proper head and face development.

Neural crest cells are specified to cranial, cardiac, vagal and trunk neural crest cells- each having own potential to give rise specific derivative structures. These cells give rise to craniofacial and dorsal root ganglia in addition to the skeletal components. By staining the cranial nerves with 2H3 antibody, that marks the cytoplasmic neurofilaments in the neurons, I saw irregular development of the cranial and axial nerves. The cardiac neural crest cells, on the other hand, considerably contribute to the formation of the aorticopulmonary septum and conotruncal cushions. CT scan of one *Snrpb*$^{ncc+/-}$ E17.5 mutant showed the aorticopulmonary septum of the embryo did not form. From these findings, I hypothesize that normal level of SNRPB is presumably required in all neural crest cells and their derivatives. I also propose that

aorticopulmonary septal defects and or palatal clefts such as the ones found in E17.5 mutants contribute to death of *Snrpb*$^{ncc+/-}$ embryos, as was found in *Eftud2*$^{ncc-/-}$ mutants (Beauchamp *et al.*, 2021).

4.8 Heterozygous removal of *Snrpb* from either neural crest cells or mesoderm cell lineage can diminish the intercellular crosstalk for craniofacial development

Craniofacial development requires highly precise interactions between the neural crest cell and the mesodermal cells (Noden 1978; Schneider, 1999; Jiang *et al.*, 2002; Noden and Trainor, 2005; Cibi *et al.*, 2019; M. C. McKinney *et al.*, 2020 and Galea *et al.*, 2021). In the previous sections, I discussed about my findings that normal level of SNRPB is required in each of these specific cell type. However, my data suggest that reduced expression of *Snrpb* in either of these cells disrupts the crosstalk among neural crest cells and mesodermal cell lineages. In all the *Snrpb*$^{mes+/-}$ E14.5 mutants, the Meckel's cartilage, which is entirely derived from the neural crest cells was abnormally formed. On the other hand, in the *Snrpb*$^{ncc+/-}$ mutants, I found mesodermal cell-derived skeletal structures such as parietal bone (Yoshida *et al.*, 2008) were abnormally developed from being hypoplastic to absent. The hypophyseal cartilage in the developing head is derived from neural crest cells, but the basisphenoid bone that replaces it has some mesodermal cell contributions in its caudal portion (Mc-Bratney Owen *et al.*, 2008). In the *Snrpb*$^{ncc+/-}$ mutants, we found the basisphenoid bone is reduced at E17.5. As *Snrpb* mutation in the neural crest cells results in abnormal development of both neural crest cell and mesodermal cell lineages, it suggests the interplay between these two cell types are lost in these mutants.

The ear is derived from the first and second pharyngeal arch and is a composite structure made from tissues of neural crest, mesoderm, endoderm and ectodermal origin. The lining of the ear canal is continuous with the skin and the outer surface of the tympanic membrane, both of which are derived from ectodermal cells. The mammalian middle ear epithelia are of dual

origin whereas the ossicles and the tympanic ring are primarily of neural crest origin. The middle ear muscles are of mesodermal origin (Thompson and Tucker, 2013). In the *Snrpb*$^{ncc+/-}$ mutants, the neural crest cell derived skeletal structures such as tympanic ring, stapes, mellus and incus were abnormally formed. Intriguingly, the ectoderm derived pinna was hypoplastic in the E17.5 and P0 group mutants, suggesting mutation of *Snrpb* in neural crest cells hinders the pinna development by interrupting the interplay between the ectoderm and the underlying NCC derives mesenchymes. It was previously shown that aberrant expression of genes such as *Hoxa2* in first pharyngeal arch neural crest cells causes a duplicated pinna formation by transcription factor Eya1 regulation (Minoux *et al.*, 2013). Again, *Tbx1* mutant mice fail to form pinna when the gene is deleted from the endoderm derived first pharyngeal pouch (Arnold *et al.*, 2006). In human, neurocristopathies like Treacher-Collins syndrome, caused by *TCOF1* mutations is also associated with pinna deformities (Jones *et al.*, 2008).

More investigations are needed to resolve exactly how *Snrpb* mutation in neural crest cells causes mesoderm derived structures to become abnormal or vice-versa or how it results in the ectoderm derived outer ear dysmorphology, but the findings suggest that the cell-cell communication to develop the craniofacial components are perturbed by *Snrpb* haploinsufficiency in either mesodermal or neural crest cells and their cell lineages.

4.9 P53 mediated increase in apoptosis does not drive CCMS abnormalities

P53 stability and activity are known to be upregulated in response to mutation or disruption in the level of splicing factors (Correa *et al*., 2016; Lei *et al.*, 2017; Van Alstyne *et al*., 2018; Zhu *et al*., 2020). In fact, I found increased skipping in two P53 regulators, *Mdm2* (exon 3) and *Mdm4* (exon 7), increased nuclear P53 and an upregulation of P53 target genes in the heads of E9.0 *Snrpb*$^{ncc+/-}$ mutants. In zebrafish and mouse, increased P53 activity contributes to craniofacial defects, and knocking down or removing P53 genetically reduced apoptosis and

improved development (Jones *et al.,* 2008; Lei *et al.*, 2017; Mao *et al.,* 2016). Additionally, administration of P53 inhibitor Pifithrin-α in the pregnant mice improved head and brain development in embryos with *Eftud2* mutation in the neural tube and neural crest (Beauchamp *et al.,* 2021). However, in my study reducing or removing P53 genetically in the neural crest cells did not prevent craniofacial defects in *Snrpb*$^{ncc+/-}$ mutant embryos. Although the variable expressivity found in *Snrpb*$^{ncc+/-}$ embryos makes it difficult to rule out a partial rescue, my findings indicate that P53 alone is probably not responsible for the craniofacial malformations.

4.10 Splicing anomalies in transcripts and misexpression of genes for craniofacial development along with P53 mediated cell death causes craniofacial dysmorphogenesis of CCMS

I found *Snrpb* is required for normal splicing of key regulators of P53, and transcripts required for normal craniofacial development, as well as expression of *Fgf8* and *Shh*. I show that morphological defects in *Snrpb* mutants were not associated with significant changes in gene expression but with disruptions in alternative splicing and patterning of the craniofacial region. I suggest, altered transcript ratios and expression of genes important for patterning the craniofacial region are responsible for malformations and embryonic death of mutant embryos.

RNAseq is a sensitive method for examining gene expression (Wang *et al.,* 2009), and my data indicate that reduced expression of *Snrpb* in mutant neural crest disrupts splicing and expression of genes important for craniofacial development. In fact, my RNAseq analysis using the head of morphologically normal E9.0 *Snrpb*$^{ncc+/-}$ embryos revealed many more DSEs than DEGs. I identified 13 transcripts important for craniofacial development that were abnormally spliced in *Snrpb*$^{ncc+/-}$ embryos. A DSE may perturb gene expression levels, for example with the introduction of pretermination codon, or alter the activity or localization of the resulting gene product. For example, the DSE associated with exon 3 of *Smad2* is predicted to increase

the proportion of transcript that encodes a much more potent effector of TGFβ/Nodal than the full-length SMAD2. This shorter protein heterodimerizes with SMAD3 to regulate many developmental processes, including growth of the mandible (Dunn *et al*., 2005). Similarly, increased skipping of exon 8 of *Ror2* may disrupt the ability of this receptor to interact with *Wnt5* during midface, ear and jaw development (Schwabe *et al.*, 2004). Furthermore, deletions of constitutive exons may change the open reading frame, insert a pretermination codon or generate an unstable transcript that is removed by nonsense-mediated decay. Hence, I predict that an increase in the proportion of transcripts with a missing constitutive exon will reduce levels of the associated proteins. Abnormal expression of *Fgf8*, which is regulated by SMAD2 (Liu *et al.*, 2004), and *Rere* (Kumar and Duester, 2014) may be one of the consequences of mis-splicing. Nonetheless, reduced migration of neural crest cells into the frontonasal region could also explain abnormal expression of *Fgf8* and *Shh.* Although I found no significant differences in the number of neural crest cells in heads of E9.0 control and *Snrpb* mutant embryos, reduced levels of *Nisch*, which binds to integrins to block cell migration (Ding *et al.*, 2008), may disrupt migration of a specific subset of neural crest cells that cannot be identified with my current techniques. In the future, investigation will be required to understand the contribution of DSEs to abnormal expression of *Fgf8* and *Shh* and to craniofacial defects in *Snrpb* mutants.

If, as I postulate, malformations in *Snrpb* mutants are due to a DSE that leads to increased cell death and disruption of multiple pathways important for patterning, the variable penetrance found in mutants may reflect the proportion of cells that undergo cell death and the level of disruption in patterning. Thus, embryos in which a large number of cells die would have absent craniofacial structure formations, and resemble group 3 or 4, whereas a lesser amount of cell death would lead to mutants classified as group 1/2. Furthermore, for those in group 1 and 2, the severity of craniofacial malformation would then depend on the level of DSEs in the genes

critical for patterning of the region. The absence of group 3 or 4 *Snrpb; Trp53* mutants supports this hypothesis. Loss of P53 may reduce cell death and allow for development of craniofacial structures in these mutants. However, DSEs in patterning genes are presumably independent of P53 and may lead to malformations and embryonic death. Future characterization of cell death and patterning in *Snrpb; Trp53* double mutant embryos, along with RNAseq experiments using morphologically normal and abnormal mutant heads, may allow us to tease out these different contributors to craniofacial malformation and aid in identifying DSEs and pathways regulated by *Snrpb.*

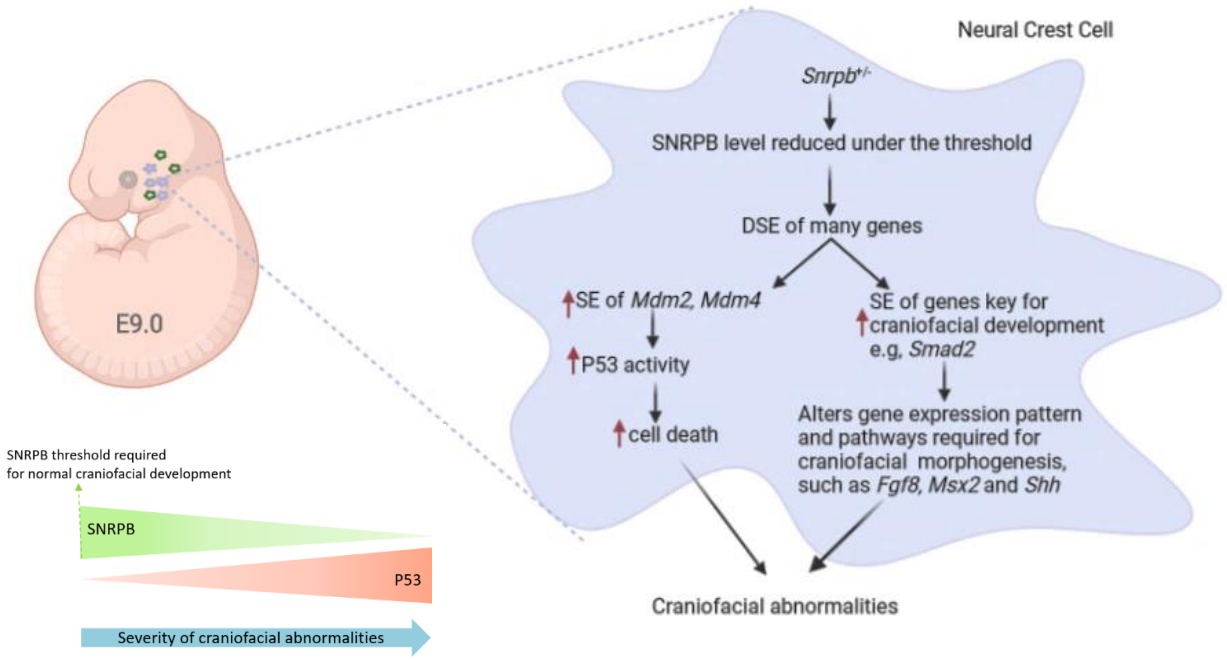

Figure 4.3*: Proposed mechanism of craniofacial abnormalities seen in CCMS mouse model.* *Snrpb* heterozygosity in neural crest cells causes increased exon skipping of P53 regulators *Mdm2* and *Mdm4* that results in increased P53 mediated cell death. Genes pivotal for craniofacial development with increases exon skippings result in aberrant expression of molecules crucial for craniofacial morphogenesis signaling pathways. The cell death along with mis-expressed genes causes abnormal craniofacial development. The severity of the phenotype depends on the extent of the reduction of SNRPB level and increase of P53 activity.

CHAPTER V

CONCLUSIONS & FUTURE DIRECTIONS

5.1 Conclusion summary

SNRPB is an essential core component of the small nuclear ribronucleoproteins (SnRNPs) that is involved in both major and minor spliceosomal processes. The role of SNRPB in embryonic development is not known except mutation of *SNRPB* causes a developmental syndrome, CCMS. During my PhD study, I focused on understanding the role of SNRPB in embryonic development, by generating mouse models for CCMS. I believe that my work using the first CCMS animal model shows evidence for both ubiquitous and development-specific roles of *Snrpb* during morphogenesis and provides much needed insights into the role of this splicing factor during embryogenesis. Moreover, with further investigations, the mouse models that I have established in my project by using tissue specific knockouts for *Snrpb* can provide molecular etiology of CCMS, with a hope of finding therapeutic targets in future.

My working model is that dysregulation in the level of SNRPB, even if modest – as is likely the case with inclusion of the PTC-containing alternative exon 2, perturbs the efficiency of splicing at the level of spliceosome assembly. This is evident with my mutant line with 61 base pair intronic region of *Snrpb,* that also provides clue for a possible novel regulation mechanism of the gene. Furthermore, although cells with reduced levels of *Snrpb* have an increased propensity to undergo apoptosis as seen in neural crest cell specific *Snrpb* heterozygous mutants, increased DSEs are found before they die. Therefore, I conclude that splicing changes in important developmental genes, the proportion of cells that undergo apoptosis, and the timing of apoptosis may all contribute to the abnormal embryonic development with variable expressivity found in *Snrpb* heterozygous mice and in CCMS patients.

5.2 Future Directions

The aim of this thesis was to understand the role of SNRPB in embryonic development, through modeling CCMS in mice. The substantial work performed to reach the aim provided new insights for SNRPB's role in development and can help future investigations to gain a more in-depth understanding of how mutation in *SNRPB* results in specific developmental anomalies and variable expressivity of CCMS.

A consistent theme throughout the thesis was the emphasis on the level of SNRPB protein that is required for normal embryonic development. I have suggested that the SNRPB level is potentially a critical determinant of the severity of the craniofacial phenotypes in *Snrpb* mutants (Figure 4.3). To address the question of how much reduction of SNRPB results in abnormal craniofacial development, *Snrpb* expression specifically in the mutant cells, in both phenotypically normal and abnormal $Snrpb^{ncc+/-}$embryos could be investigated. Reduction of SNRPB level in $Snrpb^{ncc+/-}$ mutant heads would be difficult to determine by western blot because of a higher population of other cell types with wild-type *Snrpb*. As mentioned in the previous chapter, the correlation of the protein level with the phenotype could also be drawn in *Snrpb* Δ61 mutants, where the embryos with global *Snrpb* mutation survive after organogenesis.

Stability of *Snrpb* mRNA produced by a single functional allele can also be associated with the variable expressivity in CCMS and in *Snrpb* mutant mice models. mRNA stability and decay can dramatically modulate protein expression. Though no study has been performed that detects the half-life of SNRPB protein, it was investigated for half-life of *SNRPB* mRNA in HeLa cells, where the transcript was found to be long-lived (Tani *et al.*, 2012). Intriguingly, a later study suggested that a higher RNA stability score (RS-score) for *SNRPB* is associated with a cis-acting single nucleotide polymorphism in two Asian populations (Nguyen, 2013).

Even though additional studies should be commenced to understand if CCMS patients have specific polymorphisms that correlate with the *Snrpb* mRNA stability, increased half-life of *Snrpb* transcript or perdurance of the protein in specific cell types during development might be associated with the range of phenotypic variability in *Snrpb* mutant mice and CCMS.

To directly test the hypothesis that reduced levels of *Snrpb* is incompatible with embryonic development, we made mouse embryos with heterozygous deletion of *Snrpb*. Our findings confirm that reduced level of SNRPB is responsible for CCMS malformations. However, for identifying the etiology of the full range of clinical manifestations of CCMS, a high phenotypic penetrant mouse model with a constitutive reduction of SNRPB level that survives late gestation will be essential. This can be approached by reducing SNRPB levels to varying extents using the tamoxifen (TAM)- inducible ER-*Cre* mice that gives an advantage of studying genes whose early ablation or overexpression can cause developmental defects or embryonic lethality (Hayashi and McMahon, 2002; Donocoff *et al.*, 2020). In ER-*Cre*, Cre is fused with a mutated ligand-binding domain of ER (Estrogen receptor), which does not bind to estrogen but binds to tamoxifen with high affinity (Metzger *et al.*, 1995; Feil *et al.*, 1997). ER-Cre proteins are sequestered in the cytoplasm and upon addition of tamoxifen, tamoxifen-bound ER-Cre translocate to the nucleus, where it carries out site-specific recombination between flanking *Lox*P sites. As the constitutive heterozygous mutants in the study die post implantation, *Snrpb* can be deleted later at gestation utilizing the TAM inducible Cre system, with a potential of generating a complete CCMS model and a better understanding of SNRPB's role in embryonic development.

CHAPTER VI

REFERENCES

Abdalla, W., A. Panigrahy and S. C. Bartoletti (2011). "Cerebro-costo-mandibular syndrome: Report of two cases." Radiol Case Rep 6(3): 495.

Abramyan, J. (2019). "Hedgehog Signaling and Embryonic Craniofacial Disorders." J Dev Biol 7(2).

Abramyan, J. (2019). "Hedgehog Signaling and Embryonic Craniofacial Disorders." J Dev Biol 7(2).

Abu-Issa, R., G. Smyth, I. Smoak, K.-i. Yamamura and E. N. Meyers (2002). "Fgf8 is required for pharyngeal arch and cardiovascular development in the mouse." Development 129(19): 4613-4625.

Abzhanov, A. and C. J. Tabin (2004). "Shh and Fgf8 act synergistically to drive cartilage outgrowth during cranial development." Dev Biol 273(1): 134-148.

Achilleos, A. and P. A. Trainor (2012). "Neural crest stem cells: discovery, properties and potential for therapy." Cell Res 22(2): 288-304.

Ahlgren, S. C. and M. Bronner-Fraser (1999). "Inhibition of sonic hedgehog signaling in vivo results in craniofacial neural crest cell death." Curr Biol 9(22): 1304-1314.

Ahlgren, S. C., V. Thakur and M. Bronner-Fraser (2002). "Sonic hedgehog rescues cranial neural crest from cell death induced by ethanol exposure." Proc Natl Acad Sci U S A 99(16): 10476-10481.

Anders, S., P. T. Pyl and W. Huber (2014). "HTSeq—a Python framework to work with high-throughput sequencing data." Bioinformatics 31(2): 166-169.

Anderson, J., H. D. Burns, P. Enriquez-Harris, A. O. Wilkie and J. K. Heath (1998). "Apert syndrome mutations in fibroblast growth factor receptor 2 exhibit increased affinity for FGF ligand." Hum Mol Genet 7(9): 1475-1483.

Anna, A. and G. Monika (2018). "Splicing mutations in human genetic disorders: examples, detection, and confirmation." J Appl Genet 59(3): 253-268.

Arnold, J. S., E. M. Braunstein, T. Ohyama, A. K. Groves, J. C. Adams, M. C. Brown and B. E. Morrow (2006). "Tissue-specific roles of Tbx1 in the development of the outer, middle and inner ear, defective in 22q11DS patients." Hum Mol Genet 15(10): 1629-1639.

Bacrot, S., M. Doyard, C. Huber, O. Alibeu, N. Feldhahn, D. Lehalle, D. Lacombe, S. Marlin, P. Nitschke, F. Petit, M. P. Vazquez, A. Munnich and V. Cormier-Daire (2015). "Mutations in SNRPB, encoding components of the core splicing machinery, cause cerebro-costo-mandibular syndrome." Hum Mutat 36(2): 187-190.

Baltzinger, M., M. Ori, M. Pasqualetti, I. Nardi and F. M. Rijli (2005). "Hoxa2 knockdown in Xenopus results in hyoid to mandibular homeosis." Developmental Dynamics 234(4): 858-867.

Bamshad, M. J. (2016). 1149TP63 and the Ectodermal Dysplasia, Ectrodactyly, and Cleft Lip and/or Palate (EEC), Limb-Mammary (LMS), Ankyloblepharon, Ectrodactyly, and Cleft Lip/Palate (AEC, Hay-Wells), Acro-Dermato-Ungual-Lacrimal-Digit (ADULT), and Rapp-Hodgkin Syndromes and Ectrodactyly (Split Hand/Foot Malformation). Epstein's Inborn Errors of Development: The Molecular Basis of Clinical Disorders of Morphogenesis. R. P. Erickson and A. J. Wynshaw-Boris, Oxford University Press: 0.

Baxter, D. and A. L. Shanks (2022). Pierre Robin Syndrome. StatPearls. Treasure Island (FL), StatPearls Publishing

Beauchamp, M. C., S. S. Alam, S. Kumar and L. A. Jerome-Majewska (2020). "Spliceosomopathies and neurocristopathies: Two sides of the same coin?" Dev Dyn 249(8): 924-945.

Benouaiche, L., Y. Gitton, C. Vincent, G. Couly and G. Levi (2008). "Sonic hedgehog signalling from foregut endoderm patterns the avian nasal capsule." Development 135(13): 2221-2225.

Berglund, J. A., N. Abovich and M. Rosbash (1998). "A cooperative interaction between U2AF65 and mBBP/SF1 facilitates branchpoint region recognition." Genes Dev 12(6): 858-867.

Bernier, F. P., O. Caluseriu, S. Ng, J. Schwartzentruber, K. J. Buckingham, A. M. Innes, E. W. Jabs, J. W. Innis, J. L. Schuette, J. L. Gorski, P. H. Byers, G. Andelfinger, V. Siu, J. Lauzon, B. A. Fernandez, M. McMillin, R. H. Scott, H. Racher, J. Majewski, D. A. Nickerson, J. Shendure, M. J. Bamshad and J. S. Parboosingh (2012). "Haploinsufficiency of SF3B4, a component of the pre-mRNA spliceosomal complex, causes Nager syndrome." Am J Hum Genet 90(5): 925-933.

Bhatt, S., R. Diaz and P. A. Trainor (2013). "Signals and switches in Mammalian neural crest cell differentiation." Cold Spring Harb Perspect Biol 5(2).

Bieberstein, N. I., K. Straube and K. M. Neugebauer (2014). "Chromatin immunoprecipitation approaches to determine co-transcriptional nature of splicing." Methods Mol Biol 1126: 315-323.

Blentic, A., P. Tandon, S. Payton, J. Walshe, T. Carney, R. N. Kelsh, I. Mason and A. Graham (2008). "The emergence of ectomesenchyme." Dev Dyn 237(3): 592-601.

Bouveret, E., G. Rigaut, A. Shevchenko, M. Wilm and B. Séraphin (2000). "A Sm-like protein complex that participates in mRNA degradation." Embo j 19(7): 1661-1671.

Bradley, T., M. E. Cook and M. Blanchette (2015). "SR proteins control a complex network of RNA-processing events." Rna 21(1): 75-92.

Braunschweig, U., N. L. Barbosa-Morais, Q. Pan, E. N. Nachman, B. Alipanahi, T. Gonatopoulos-Pournatzis, B. Frey, M. Irimia and B. J. Blencowe (2014). "Widespread intron retention in mammals functionally tunes transcriptomes." Genome Res 24(11): 1774-1786.

Brito, J. M., M.-A. Teillet and N. M. Le Douarin (2006). "An early role for Sonic hedgehog from foregut endoderm in jaw development: Ensuring neural crest cell survival." Proceedings of the National Academy of Sciences 103(31): 11607-11612.

Brito, J. M., M.-A. Teillet and N. M. Le Douarin (2006). "An early role for Sonic hedgehog from foregut endoderm in jaw development: Ensuring neural crest cell survival." Proceedings of the National Academy of Sciences 103(31): 11607-11612.

Britsch, S., D. E. Goerich, D. Riethmacher, R. I. Peirano, M. Rossner, K. A. Nave, C. Birchmeier and M. Wegner (2001). "The transcription factor Sox10 is a key regulator of peripheral glial development." Genes Dev 15(1): 66-78.

Bryen, S. J., H. Joshi, F. J. Evesson, C. Girard, R. Ghaoui, L. B. Waddell, A. C. Testa, B. Cummings, S. Arbuckle, N. Graf, R. Webster, D. G. MacArthur, N. G. Laing, M. R. Davis, R. Lührmann and S. T. Cooper (2019). "Pathogenic Abnormal Splicing Due to Intronic Deletions that Induce Biophysical Space Constraint for Spliceosome Assembly." Am J Hum Genet 105(3): 573-587.

Busslinger, M., N. Moschonas and R. A. Flavell (1981). "Beta + thalassemia: aberrant splicing results from a single point mutation in an intron." Cell 27(2 Pt 1): 289-298.

Carey, J. C., R. M. Fineman and F. A. Ziter (1982). "The Robin sequence as a consequence of malformation, dysplasia, and neuromuscular syndromes." J Pediatr 101(5): 858-864.

Cartegni, L., S. L. Chew and A. R. Krainer (2002). "Listening to silence and understanding nonsense: exonic mutations that affect splicing." Nat Rev Genet 3(4): 285-298.

Chan, C. T. and P. Thorogood (1999). "Pleiotropic features of syndromic craniosynostoses correlate with differential expression of fibroblast growth factor receptors 1 and 2 during human craniofacial development." Pediatr Res 45(1): 46-53.

Chow, L. T., R. E. Gelinas, T. R. Broker and R. J. Roberts (1977). "An amazing sequence arrangement at the 5' ends of adenovirus 2 messenger RNA." Cell 12(1): 1-8.

Chu, G. C., N. R. Dunn, D. C. Anderson, L. Oxburgh and E. J. Robertson (2004). "Differential requirements for Smad4 in TGFbeta-dependent patterning of the early mouse embryo." Development 131(15): 3501-3512.

Chu, J. L. and K. B. Elkon (1991). "The small nuclear ribonucleoproteins, SmB and B', are products of a single gene." Gene 97(2): 311-312.

Cibi, D. M., M. M. Mia, S. Guna Shekeran, L. S. Yun, R. Sandireddy, P. Gupta, M. Hota, L. Sun, S. Ghosh and M. K. Singh (2019). "Neural crest-specific deletion of Rbfox2 in mice leads to craniofacial abnormalities including cleft palate." Elife 8.

Clay, M. R. and M. C. Halloran (2011). "Regulation of cell adhesions and motility during initiation of neural crest migration." Curr Opin Neurobiol 21(1): 17-22.

Cordero, D. R., S. Brugmann, Y. Chu, R. Bajpai, M. Jame and J. A. Helms (2011). "Cranial neural crest cells on the move: their roles in craniofacial development." Am J Med Genet A 155a(2): 270-279.

Correa, B. R., P. R. de Araujo, M. Qiao, S. C. Burns, C. Chen, R. Schlegel, S. Agarwal, P. A. Galante and L. O. Penalva (2016). "Functional genomics analyses of RNA-binding proteins reveal the splicing regulator SNRPB as an oncogenic candidate in glioblastoma." Genome Biol 17(1): 125.

Couly, G., S. Creuzet, S. Bennaceur, C. Vincent and N. M. Le Douarin (2002). "Interactions between Hox-negative cephalic neural crest cells and the foregut endoderm in patterning the facial skeleton in the vertebrate head." Development 129(4): 1061-1073.

Couly, G., S. Creuzet, S. Bennaceur, C. Vincent and N. M. Le Douarin (2002). "Interactions between Hox-negative cephalic neural crest cells and the foregut endoderm in patterning the facial skeleton in the vertebrate head." Development 129(4): 1061-1073.

Couly, G., A. Grapin-Botton, P. Coltey, B. Ruhin and N. M. Le Douarin (1998). "Determination of the identity of the derivatives of the cephalic neural crest: incompatibility between Hox gene expression and lower jaw development." Development 125(17): 3445-3459.

Creuzet, S., G. Couly, C. Vincent and N. M. Le Douarin (2002). "Negative effect of Hox gene expression on the development of the neural crest-derived facial skeleton." Development 129(18): 4301-4313.

Crump, J. G., L. Maves, N. D. Lawson, B. M. Weinstein and C. B. Kimmel (2004). "An essential role for Fgfs in endodermal pouch formation influences later craniofacial skeletal patterning." Development 131(22): 5703-5716.

da Costa, M. C., A. G. Trentin and G. W. Calloni (2018). "FGF8 and Shh promote the survival and maintenance of multipotent neural crest progenitors." Mech Dev 154: 251-258.

Dale, J. K., C. Vesque, T. J. Lints, T. K. Sampath, A. Furley, J. Dodd and M. Placzek (1997). "Cooperation of BMP7 and SHH in the induction of forebrain ventral midline cells by prechordal mesoderm." Cell 90(2): 257-269.

David, C. J. and J. Massagué (2018). "Contextual determinants of TGFβ action in development, immunity and cancer." Nat Rev Mol Cell Biol 19(7): 419-435.

Depew, M. J., T. Lufkin and J. L. Rubenstein (2002). "Specification of jaw subdivisions by Dlx genes." Science 298(5592): 381-385.

Derynck, R. and X. H. Feng (1997). "TGF-beta receptor signaling." Biochim Biophys Acta 1333(2): F105-150.

DeSesso, J. M. and A. R. Scialli (2018). "Bone development in laboratory mammals used in developmental toxicity studies." Birth Defects Res 110(15): 1157-1187.

Deutsch, U., G. R. Dressler and P. Gruss (1988). "Pax 1, a member of a paired box homologous murine gene family, is expressed in segmented structures during development." Cell 53(4): 617-625.

Diewert, V. M. (1985). "Development of human craniofacial morphology during the late embryonic and early fetal periods." Am J Orthod 88(1): 64-76.

Dobin, A., C. A. Davis, F. Schlesinger, J. Drenkow, C. Zaleski, S. Jha, P. Batut, M. Chaisson and T. R. Gingeras (2012). "STAR: ultrafast universal RNA-seq aligner." Bioinformatics 29(1): 15-21.

Donocoff, R. S., N. Teteloshvili, H. Chung, R. Shoulson and R. J. Creusot (2020). "Optimization of tamoxifen-induced Cre activity and its effect on immune cell populations." Sci Rep 10(1): 15244.

Doss, M. X., J. A. Gaspar, J. Winkler, J. Hescheler, H. Schulz and A. Sachinidis (2012). "Specific gene signatures and pathways in mesodermal cells and their derivatives derived from embryonic stem cells." Stem Cell Rev Rep 8(1): 43-54.

Dupin, E. S., L. (2012). "Neural crest progenitors and stem cells: from early development to adulthood." Developmental Biology.

Dworkin, S., Y. Boglev, H. Owens and S. J. Goldie (2016). "The Role of Sonic Hedgehog in Craniofacial Patterning, Morphogenesis and Cranial Neural Crest Survival." J Dev Biol 4(3).

Echelard, Y., D. J. Epstein, B. St-Jacques, L. Shen, J. Mohler, J. A. McMahon and A. P. McMahon (1993). "Sonic hedgehog, a member of a family of putative signaling molecules, is implicated in the regulation of CNS polarity." Cell 75(7): 1417-1430.

Erkelenz, S., W. F. Mueller, M. S. Evans, A. Busch, K. Schöneweis, K. J. Hertel and H. Schaal (2013). "Position-dependent splicing activation and repression by SR and hnRNP proteins rely on common mechanisms." Rna 19(1): 96-102.

Farach, L. S., M. E. Little, A. L. Duker, C. V. Logan, A. Jackson, J. T. Hecht and M. Bober (2018). "The expanding phenotype of RNU4ATAC pathogenic variants to Lowry Wood syndrome." Am J Med Genet A 176(2): 465-469.

Faustino, N. A. and T. A. Cooper (2003). "Pre-mRNA splicing and human disease." Genes Dev 17(4): 419-437.

Favaro, F. P., L. Alvizi, R. M. Zechi-Ceide, D. Bertola, T. M. Felix, J. de Souza, S. Raskin, S. R. Twigg, A. M. Weiner, P. Armas, E. Margarit, N. B. Calcaterra, G. R. Andersen, S. J. McGowan, A. O. Wilkie, A. Richieri-Costa, M. L. de Almeida and M. R. Passos-Bueno (2014). "A noncoding expansion in EIF4A3 causes Richieri-Costa-Pereira syndrome, a craniofacial disorder associated with limb defects." Am J Hum Genet 94(1): 120-128.

Feil, R., J. Wagner, D. Metzger and P. Chambon (1997). "Regulation of Cre recombinase activity by mutated estrogen receptor ligand-binding domains." Biochem Biophys Res Commun 237(3): 752-757.

Fitriasari, S. and P. A. Trainor (2021). "Diabetes, Oxidative Stress, and DNA Damage Modulate Cranial Neural Crest Cell Development and the Phenotype Variability of Craniofacial Disorders." Front Cell Dev Biol 9: 644410.

Fredericks, A. M., K. J. Cygan, B. A. Brown and W. G. Fairbrother (2015). "RNA-Binding Proteins: Splicing Factors and Disease." Biomolecules 5(2): 893-909.

Galea, G. L., M. R. Zein, S. Allen and P. Francis-West (2021). "Making and shaping endochondral and intramembranous bones." Developmental Dynamics 250(3): 414-449.

Gangopadhyay, N., D. A. Mendonca and A. S. Woo (2012). "Pierre robin sequence." Semin Plast Surg 26(2): 76-82.

García-Castro, M. I., C. Marcelle and M. Bronner-Fraser (2002). "Ectodermal Wnt function as a neural crest inducer." Science 297(5582): 848-851.

Geuens, T., D. Bouhy and V. Timmerman (2016). "The hnRNP family: insights into their role in health and disease." Hum Genet 135(8): 851-867.

Giudice, A., S. Barone, K. Belhous, A. Morice, V. Soupre, F. Bennardo, N. Boddaert, M. P. Vazquez, V. Abadie and A. Picard (2018). "Pierre Robin sequence: A comprehensive narrative review of the literature over time." J Stomatol Oral Maxillofac Surg 119(5): 419-428.

Gordon, C. T., I. M. Brinas, F. A. Rodda, A. J. Bendall and P. G. Farlie (2010). "Role of Dlx genes in craniofacial morphogenesis: Dlx2 influences skeletal patterning by inducing ectomesenchymal aggregation in ovo." Evol Dev 12(5): 459-473.

Graham, A. (2003). "Development of the pharyngeal arches." Am J Med Genet A 119A(3): 251-256.

Grammatopoulos, G. A., E. Bell, L. Toole, A. Lumsden and A. S. Tucker (2000). "Homeotic transformation of branchial arch identity after Hoxa2 overexpression." Development 127(24): 5355-5365.

Gray, T. A., M. J. Smithwick, M. A. Schaldach, D. L. Martone, J. A. Graves, J. R. McCarrey and R. D. Nicholls (1999). "Concerted regulation and molecular evolution of the duplicated SNRPB'/B and SNRPN loci." Nucleic Acids Res 27(23): 4577-4584.

Grevellec, A. and A. S. Tucker (2010). "The pharyngeal pouches and clefts: Development, evolution, structure and derivatives." Semin Cell Dev Biol 21(3): 325-332.

Griffin, C. and J. P. Saint-Jeannet (2020). "Spliceosomopathies: Diseases and mechanisms." Dev Dyn 249(9): 1038-1046.

Guglielmi, L., C. Heliot, S. Kumar, Y. Alexandrov, I. Gori, F. Papaleonidopoulou, C. Barrington, P. East, A. D. Economou, P. M. W. French, J. McGinty and C. S. Hill (2021). "Smad4 controls signaling robustness and morphogenesis by differentially contributing to the Nodal and BMP pathways." Nat Commun 12(1): 6374.

Gushchina, L. V., E. C. Frair, N. Rohan, A. J. Bradley, T. R. Simmons, H. D. Chavan, H. J. Chou, M. Eggers, M. A. Waldrop, N. Wein and K. M. Flanigan (2021). "Lack of Toxicity in Nonhuman Primates Receiving Clinically Relevant Doses of an AAV9.U7snRNA Vector Designed to Induce DMD Exon 2 Skipping." Hum Gene Ther 32(17-18): 882-894.

Hall, B. K. (2000). "The neural crest as a fourth germ layer and vertebrates as quadroblastic not triploblastic." Evol Dev 2(1): 3-5.

Hameed, Z., S. Taylor and D. Lindfield (2018). "Ocular Features of Cerebro-Costo-Mandibular Syndrome." J Glaucoma 27(1): e21-e23.

Han, J., M. Ishii, P. Bringas, Jr., R. L. Maas, R. E. Maxson, Jr. and Y. Chai (2007). "Concerted action of Msx1 and Msx2 in regulating cranial neural crest cell differentiation during frontal bone development." Mech Dev 124(9-10): 729-745.

Harrow, J., F. Denoeud, A. Frankish, A. Reymond, C. K. Chen, J. Chrast, J. Lagarde, J. G. Gilbert, R. Storey, D. Swarbreck, C. Rossier, C. Ucla, T. Hubbard, S. E. Antonarakis and R. Guigo (2006). "GENCODE: producing a reference annotation for ENCODE." Genome Biol 7 Suppl 1(Suppl 1): S4 1-9.

Hatje, K., R. U. Rahman, R. O. Vidal, D. Simm, B. Hammesfahr, V. Bansal, A. Rajput, M. E. Mickael, T. Sun, S. Bonn and M. Kollmar (2017). "The landscape of human mutually exclusive splicing." Mol Syst Biol 13(12): 959.

Haworth, K. E., J. M. Wilson, A. Grevellec, M. T. Cobourne, C. Healy, J. A. Helms, P. T. Sharpe and A. S. Tucker (2007). "Sonic hedgehog in the pharyngeal endoderm controls arch pattern via regulation of Fgf8 in head ectoderm." Dev Biol 303(1): 244-258.

Hayashi, S. and A. P. McMahon (2002). "Efficient recombination in diverse tissues by a tamoxifen-inducible form of Cre: a tool for temporally regulated gene activation/inactivation in the mouse." Dev Biol 244(2): 305-318.

He, W. and R. Parker (2000). "Functions of Lsm proteins in mRNA degradation and splicing." Curr Opin Cell Biol 12(3): 346-350.

Helms, J. A., D. Cordero and M. D. Tapadia (2005). "New insights into craniofacial morphogenesis." Development 132(5): 851-861.

Hermann, H., P. Fabrizio, V. A. Raker, K. Foulaki, H. Hornig, H. Brahms and R. Lührmann (1995). "snRNP Sm proteins share two evolutionarily conserved sequence motifs which are involved in Sm protein-protein interactions." Embo j 14(9): 2076-2088.

Hou, W., S. Gupta, M. C. Beauchamp, L. Yuan and L. A. Jerome-Majewska (2017). "Non-alcoholic fatty liver disease in mice with heterozygous mutation in TMED2." PLoS One 12(8): e0182995.

Hu, D. and R. S. Marcucio (2009). "Unique organization of the frontonasal ectodermal zone in birds and mammals." Dev Biol 325(1): 200-210.

Hu, D., R. S. Marcucio and J. A. Helms (2003). "A zone of frontonasal ectoderm regulates patterning and growth in the face." Development 130(9): 1749-1758.

Hu, D. H., J. A. (1999). "The role of Sonic hedgehog in normal and abnormal morphogenesis." Development 126: 4873-4884.

Hunter, M. P. and V. E. Prince (2002). "Zebrafish hox paralogue group 2 genes function redundantly as selector genes to pattern the second pharyngeal arch." Dev Biol 247(2): 367-389.

Huntriss, J. D., D. S. Latchman and D. G. Williams (1993). "The snRNP core protein SmB and tissue-specific SmN protein are differentially distributed between snRNP particles." Nucleic Acids Res 21(17): 4047-4053.

Ibba, R. M., A. Corda, M. A. Zoppi, M. Floris, P. Todde and G. Monni (1997). "Cerebro-costo-mandibular syndrome: early sonographic prenatal diagnosis." Ultrasound Obstet Gynecol 10(2): 142-144.

Ichikawa, S., S. Tuchman, L. R. Padgett, A. K. Gray, H. J. Baluarte and M. J. Econs (2014). "Intronic deletions in the SLC34A3 gene: a cautionary tale for mutation analysis of hereditary hypophosphatemic rickets with hypercalciuria." Bone 59: 53-56.

Ishii, M., A. E. Merrill, Y. S. Chan, I. Gitelman, D. P. Rice, H. M. Sucov and R. E. Maxson, Jr. (2003). "Msx2 and Twist cooperatively control the development of the neural crest-derived skeletogenic mesenchyme of the murine skull vault." Development 130(24): 6131-6142.

Jabs, E. W., X. Li, A. F. Scott, G. Meyers, W. Chen, M. Eccles, J. I. Mao, L. R. Charnas, C. E. Jackson and M. Jaye (1994). "Jackson-Weiss and Crouzon syndromes are allelic with mutations in fibroblast growth factor receptor 2." Nat Genet 8(3): 275-279.

James, P. A. and S. Aftimos (2003). "Familial cerebro-costo-mandibular syndrome: a case with unusual prenatal findings and review." Clin Dysmorphol 12(1): 63-68.

Jeong, J., X. Li, R. J. McEvilly, M. G. Rosenfeld, T. Lufkin and J. L. Rubenstein (2008). "Dlx genes pattern mammalian jaw primordium by regulating both lower jaw-specific and upper jaw-specific genetic programs." Development 135(17): 2905-2916.

Jeong, J., J. Mao, T. Tenzen, A. H. Kottmann and A. P. McMahon (2004). "Hedgehog signaling in the neural crest cells regulates the patterning and growth of facial primordia." Genes Dev 18(8): 937-951.

Jiang, X., S. Iseki, R. E. Maxson, H. M. Sucov and G. M. Morriss-Kay (2002). "Tissue origins and interactions in the mammalian skull vault." Dev Biol 241(1): 106-116.

Jin, Y., O. H. Tam, E. Paniagua and M. Hammell (2015). "TEtranscripts: a package for including transposable elements in differential expression analysis of RNA-seq datasets." Bioinformatics 31(22): 3593-3599.

John, N., P. Cinelli, M. Wegner and L. Sommer (2011). "Transforming Growth Factor β-Mediated Sox10 Suppression Controls Mesenchymal Progenitor Generation in Neural Crest Stem Cells." Stem Cells 29(4): 689-699.

Jones, N. C., M. L. Lynn, K. Gaudenz, D. Sakai, K. Aoto, J. P. Rey, E. F. Glynn, L. Ellington, C. Du, J. Dixon, M. J. Dixon and P. A. Trainor (2008). "Prevention of the neurocristopathy Treacher Collins syndrome through inhibition of p53 function." Nat Med 14(2): 125-133.

Jurica, M. S., L. J. Licklider, S. R. Gygi, N. Grigorieff and M. J. Moore (2002). "Purification and characterization of native spliceosomes suitable for three-dimensional structural analysis." RNA 8(4): 426-439.

Kambach, C., S. Walke, R. Young, J. M. Avis, E. de la Fortelle, V. A. Raker, R. Luhrmann, J. Li and K. Nagai (1999). "Crystal structures of two Sm protein complexes and their implications for the assembly of the spliceosomal snRNPs." Cell 96(3): 375-387.

Kanzler, B., S. J. Kuschert, Y.-H. Liu and M. Mallo (1998). "Hoxa-2 restricts the chondrogenic domain and inhibits bone formation during development of the branchial area." Development 125(14): 2587-2597.

Kobrynski, L. J. and K. E. Sullivan (2007). "Velocardiofacial syndrome, DiGeorge syndrome: the chromosome 22q11.2 deletion syndromes." Lancet 370(9596): 1443-1452.

Koren, E., G. Lev-Maor and G. Ast (2007). "The emergence of alternative 3' and 5' splice site exons from constitutive exons." PLoS Comput Biol 3(5): e95.

Kubota, Y. and K. Ito (2000). "Chemotactic migration of mesencephalic neural crest cells in the mouse." Developmental Dynamics 217(2): 170-179.

Le Douarin, N., & Kalcheim, C. (1999). The Neural Crest (2nd ed., Developmental and Cell Biology Series). Cambridge: Cambridge University Press. doi:10.1017/CBO9780511897948

Le Douarin, N. M., S. Creuzet, G. Couly and E. Dupin (2004). "Neural crest cell plasticity and its limits." Development 131(19): 4637-4650.

Lee, J. W., E. J. Lee, S. H. Hong, W. H. Chung, H. T. Lee, T. W. Lee, J. R. Lee, H. T. Kim, J. G. Suh, T. Y. Kim and Z. Y. Ryoo (2001). "Circling mouse: possible animal model for deafness." Comp Med 51(6): 550-554.

Lee, M. H., Y. J. Kim, H. J. Kim, H. D. Park, A. R. Kang, H. M. Kyung, J. H. Sung, J. M. Wozney, H. J. Kim and H. M. Ryoo (2003). "BMP-2-induced Runx2 expression is mediated by Dlx5, and TGF-beta 1 opposes the BMP-2-induced osteoblast differentiation by suppression of Dlx5 expression." J Biol Chem 278(36): 34387-34394.

Lehalle, D., D. Wieczorek, R. M. Zechi-Ceide, M. R. Passos-Bueno, S. Lyonnet, J. Amiel and C. T. Gordon (2015). "A review of craniofacial disorders caused by spliceosomal defects." Clinical Genetics 88(5): 405-415.

Lesciotto, K. M., S. M. Motch Perrine, M. Kawasaki, T. Stecko, T. M. Ryan, K. Kawasaki and J. T. Richtsmeier (2020). "Phosphotungstic acid-enhanced microCT: Optimized protocols for embryonic and early postnatal mice." Developmental Dynamics 249(4): 573-585.

Lewandoski, M., E. N. Meyers and G. R. Martin (1997). "Analysis of Fgf8 gene function in vertebrate development." Cold Spring Harb Symp Quant Biol 62: 159-168.

Lewis, A. E., H. N. Vasudevan, A. K. O'Neill, P. Soriano and J. O. Bush (2013). "The widely used Wnt1-Cre transgene causes developmental phenotypes by ectopic activation of Wnt signaling." Dev Biol 379(2): 229-234.

Li, Y. R., D. Guo, D. F. Chen, G. F. Lu, M. D. Ren and S. X. He (2022). "[Regulatory effect of small nuclear ribonucleoprotein-associated protein B on proliferation and metastasis of liver cancer cells]." Zhonghua Gan Zang Bing Za Zhi 30(1): 63-68.

Liang, J., J. Von den Hoff, J. Lange, Y. Ren, Z. Bian and C. E. Carels (2016). "MSX1 mutations and associated disease phenotypes: genotype-phenotype relations." Eur J Hum Genet 24(12): 1663-1670.

Liang, W. W. and S. C. Cheng (2015). "A novel mechanism for Prp5 function in prespliceosome formation and proofreading the branch site sequence." Genes Dev 29(1): 81-93.

Lines, M. A., L. Huang, J. Schwartzentruber, S. L. Douglas, D. C. Lynch, C. Beaulieu, M. L. Guion-Almeida, R. M. Zechi-Ceide, B. Gener, G. Gillessen-Kaesbach, C. Nava, G. Baujat, D. Horn, U. Kini, A. Caliebe, Y. Alanay, G. E. Utine, D. Lev, J. Kohlhase, A. W. Grix, D. R. Lohmann, U. Hehr, D. Böhm, J. Majewski, D. E. Bulman, D. Wieczorek and K. M. Boycott (2012). "Haploinsufficiency of a spliceosomal GTPase encoded by EFTUD2 causes mandibulofacial dysostosis with microcephaly." Am J Hum Genet 90(2): 369-377.

Liu, N., Z. Wu, A. Chen, Y. Wang, D. Cai, J. Zheng, Y. Liu and L. Zhang (2019). "SNRPB promotes the tumorigenic potential of NSCLC in part by regulating RAB26." Cell Death Dis 10(9): 667.

Logjes, R. J. H., C. C. Breugem, G. Van Haaften, E. C. Paes, G. H. Sperber, M. H. van den Boogaard and P. G. Farlie (2018). "The ontogeny of Robin sequence." Am J Med Genet A 176(6): 1349-1368.

Love, M. I., W. Huber and S. Anders (2014). "Moderated estimation of fold change and dispersion for RNA-seq data with DESeq2." Genome Biol 15(12): 550.

Lumsden, A., N. Sprawson and A. Graham (1991). "Segmental origin and migration of neural crest cells in the hindbrain region of the chick embryo." Development 113(4): 1281-1291.

Lynch, D. C., T. Revil, J. Schwartzentruber, E. J. Bhoj, A. M. Innes, R. E. Lamont, E. G. Lemire, B. N. Chodirker, J. P. Taylor, E. H. Zackai, D. R. McLeod, E. P. Kirk, J. Hoover-Fong, L. Fleming, R. Savarirayan, C. Care4Rare, J. Majewski, L. A. Jerome-Majewska, J. S. Parboosingh and F. P. Bernier (2014). "Disrupted auto-regulation of the spliceosomal gene SNRPB causes cerebro-costo-mandibular syndrome." Nat Commun 5: 4483.

Marasco, L. E. and A. R. Kornblihtt (2022). "The physiology of alternative splicing." Nat Rev Mol Cell Biol.

Marchini, M., D. Hu, L. Lo Vercio, N. M. Young, N. D. Forkert, B. Hallgrímsson and R. Marcucio (2021). "Wnt Signaling Drives Correlated Changes in Facial Morphology and Brain Shape." Front Cell Dev Biol 9: 644099.

Marcucio, R. S., D. R. Cordero, D. Hu and J. A. Helms (2005). "Molecular interactions coordinating the development of the forebrain and face." Dev Biol 284(1): 48-61.

Marino, S., M. Vooijs, H. van Der Gulden, J. Jonkers and A. Berns (2000). "Induction of medulloblastomas in p53-null mutant mice by somatic inactivation of Rb in the external granular layer cells of the cerebellum." Genes Dev 14(8): 994-1004.

Martinez-Contreras, R., P. Cloutier, L. Shkreta, J. F. Fisette, T. Revil and B. Chabot (2007). "hnRNP proteins and splicing control." Adv Exp Med Biol 623: 123-147.

Masuyama, N., H. Hanafusa, M. Kusakabe, H. Shibuya and E. Nishida (1999). "Identification of two Smad4 proteins in Xenopus. Their common and distinct properties." J Biol Chem 274(17): 12163-12170.

Matlin, A. J., F. Clark and C. W. Smith (2005). "Understanding alternative splicing: towards a cellular code." Nat Rev Mol Cell Biol 6(5): 386-398.

McBratney-Owen, B., S. Iseki, S. D. Bamforth, B. R. Olsen and G. M. Morriss-Kay (2008). "Development and tissue origins of the mammalian cranial base." Dev Biol 322(1): 121-132.

McFarlane, L., V. Truong, J. S. Palmer and D. Wilhelm (2013). "Novel PCR assay for determining the genetic sex of mice." Sex Dev 7(4): 207-211.

McKinney, M. C., R. McLennan, R. Giniunaite, R. E. Baker, P. K. Maini, H. G. Othmer and P. M. Kulesa (2020). "Visualizing mesoderm and neural crest cell dynamics during chick head morphogenesis." Dev Biol 461(2): 184-196.

Merkin, J., C. Russell, P. Chen and C. B. Burge (2012). "Evolutionary dynamics of gene and isoform regulation in Mammalian tissues." Science 338(6114): 1593-1599.

Metzger, D., J. Clifford, H. Chiba and P. Chambon (1995). "Conditional site-specific recombination in mammalian cells using a ligand-dependent chimeric Cre recombinase." Proc Natl Acad Sci U S A 92(15): 6991-6995.

Meyers, G. A., D. Day, R. Goldberg, D. L. Daentl, K. A. Przylepa, L. J. Abrams, J. M. Graham, Jr., M. Feingold, J. B. Moeschler, E. Rawnsley, A. F. Scott and E. W. Jabs (1996). "FGFR2 exon IIIa and IIIc mutations in Crouzon, Jackson-Weiss, and Pfeiffer syndromes: evidence for missense changes, insertions, and a deletion due to alternative RNA splicing." Am J Hum Genet 58(3): 491-498.

Minoux, M., C. F. Kratochwil, S. Ducret, S. Amin, T. Kitazawa, H. Kurihara, N. Bobola, N. Vilain and F. M. Rijli (2013). "Mouse Hoxa2 mutations provide a model for microtia and auricle duplication." Development 140(21): 4386-4397.

Monsoro-Burq, A. H., R. B. Fletcher and R. M. Harland (2003). "Neural crest induction by paraxial mesoderm in Xenopus embryos requires FGF signals." Development 130(14): 3111-3124.

Monteuuis, G., J. J. L. Wong, C. G. Bailey, U. Schmitz and J. E. J. Rasko (2019). "The changing paradigm of intron retention: regulation, ramifications and recipes." Nucleic Acids Research 47(22): 11497-11513.

Moosa, S. and B. Wollnik (2016). "Altered FGF signalling in congenital craniofacial and skeletal disorders." Semin Cell Dev Biol 53: 115-125.

Mori-Akiyama, Y., H. Akiyama, D. H. Rowitch and B. de Crombrugghe (2003). "Sox9 is required for determination of the chondrogenic cell lineage in the cranial neural crest." Proceedings of the National Academy of Sciences 100(16): 9360-9365.

Moury, J. D. and A. G. Jacobson (1990). "The origins of neural crest cells in the axolotl." Dev Biol 141(2): 243-253.

Muenke, M. and U. Schell (1995). "Fibroblast-growth-factor receptor mutations in human skeletal disorders." Trends Genet 11(8): 308-313.

Muenke, M., U. Schell, A. Hehr, N. H. Robin, H. W. Losken, A. Schinzel, L. J. Pulleyn, P. Rutland, W. Reardon, S. Malcolm and et al. (1994). "A common mutation in the fibroblast growth factor receptor 1 gene in Pfeiffer syndrome." Nat Genet 8(3): 269-274.

Muzumdar, M. D., B. Tasic, K. Miyamichi, L. Li and L. Luo (2007). "A global double-fluorescent Cre reporter mouse." genesis 45(9): 593-605.

Nagasawa, H., Y. Yamamoto and Y. Kohno (2010). "Cerebro-costo-mandibular syndrome: prognosis and proposal for classification." Congenit Anom (Kyoto) 50(3): 171-174.

Neubuser, A., H. Koseki and R. Balling (1995). "Characterization and developmental expression of Pax9, a paired-box-containing gene related to Pax1." Dev Biol 170(2): 701-716.

Nguyen, T. T. and C. Seoighe (2013). "Integrative analysis of mRNA expression and half-life data reveals trans-acting genetic variants associated with increased expression of stable transcripts." PLoS One 8(11): e79627.

Nie, X., C. X. Deng, Q. Wang and K. Jiao (2008). "Disruption of Smad4 in neural crest cells leads to mid-gestation death with pharyngeal arch, craniofacial and cardiac defects." Dev Biol 316(2): 417-430.

Nilsen, T. W. and B. R. Graveley (2010). "Expansion of the eukaryotic proteome by alternative splicing." Nature 463(7280): 457-463.

Noden, D. M. (1983). "The role of the neural crest in patterning of avian cranial skeletal, connective, and muscle tissues." Dev Biol 96(1): 144-165.

Noden, D. M. (1988). "Interactions and fates of avian craniofacial mesenchyme." Development 103 Suppl: 121-140.

Noden, D. M. and P. A. Trainor (2005). "Relations and interactions between cranial mesoderm and neural crest populations." J Anat 207(5): 575-601.

Ogasawara, K., Y. Honda and M. Hosoya (2014). "Ex utero intrapartum treatment for an infant with cerebro-costo-mandibular syndrome." Pediatr Int 56(4): 613-615.

Paggi, J. M. and G. Bejerano (2018). "A sequence-based, deep learning model accurately predicts RNA splicing branchpoints." Rna 24(12): 1647-1658.

Pan, Q., O. Shai, L. J. Lee, B. J. Frey and B. J. Blencowe (2008). "Deep surveying of alternative splicing complexity in the human transcriptome by high-throughput sequencing." Nat Genet 40(12): 1413-1415.

Park, B. Y., M. Tachi-Duprat, C. Ihewulezi, A. Devotta and J. P. Saint-Jeannet (2022). "The Core Splicing Factors EFTUD2, SNRPB and TXNL4A Are Essential for Neural Crest and Craniofacial Development." J Dev Biol 10(3).

Pasqualetti, M., M. Ori, I. Nardi and F. M. Rijli (2000). "Ectopic Hoxa2 induction after neural crest migration results in homeosis of jaw elements in Xenopus." Development 127(24): 5367-5378.

Patro, R., G. Duggal, M. I. Love, R. A. Irizarry and C. Kingsford (2017). "Salmon provides fast and bias-aware quantification of transcript expression." Nat Methods 14(4): 417-419.

Peyrard-Janvid, M., E. J. Leslie, Y. A. Kousa, T. L. Smith, M. Dunnwald, M. Magnusson, B. A. Lentz, P. Unneberg, I. Fransson, H. K. Koillinen, J. Rautio, M. Pegelow, A. Karsten, L. Basel-Vanagaite, W. Gordon, B. Andersen, T. Svensson, J. C. Murray, R. A. Cornell, J. Kere and B. C. Schutte (2014). "Dominant mutations in GRHL3 cause Van der Woude Syndrome and disrupt oral periderm development." Am J Hum Genet 94(1): 23-32.

Pillai, R. S., C. L. Will, R. Lührmann, D. Schümperli and B. Müller (2001). "Purified U7 snRNPs lack the Sm proteins D1 and D2 but contain Lsm10, a new 14 kDa Sm D1-like protein." Embo j 20(19): 5470-5479.

Pohl, M., R. H. Bortfeldt, K. Grutzmann and S. Schuster (2013). "Alternative splicing of mutually exclusive exons--a review." Biosystems 114(1): 31-38.

Pomeranz Krummel, D. A., C. Oubridge, A. K. Leung, J. Li and K. Nagai (2009). "Crystal structure of human spliceosomal U1 snRNP at 5.5 A resolution." Nature 458(7237): 475-480.

Prochazkova, M., J. Prochazka, P. Marangoni and O. D. Klein (2018). "Bones, Glands, Ears and More: The Multiple Roles of FGF10 in Craniofacial Development." Front Genet 9: 542.

Pusch, C., E. Hustert, D. Pfeifer, P. Südbeck, R. Kist, B. Roe, Z. Wang, R. Balling, N. Blin and G. Scherer (1998). "The SOX10/Sox10 gene from human and mouse: sequence, expression, and transactivation by the encoded HMG domain transcription factor." Hum Genet 103(2): 115-123.

Qiu, M., A. Bulfone, I. Ghattas, J. J. Meneses, L. Christensen, P. T. Sharpe, R. Presley, R. A. Pedersen and J. L. Rubenstein (1997). "Role of the Dlx homeobox genes in proximodistal patterning of the branchial arches: mutations of Dlx-1, Dlx-2, and Dlx-1 and -2 alter morphogenesis of proximal skeletal and soft tissue structures derived from the first and second arches." Dev Biol 185(2): 165-184.

Qiu, M., A. Bulfone, S. Martinez, J. J. Meneses, K. Shimamura, R. A. Pedersen and J. L. Rubenstein (1995). "Null mutation of Dlx-2 results in abnormal morphogenesis of proximal first and second branchial arch derivatives and abnormal differentiation in the forebrain." Genes Dev 9(20): 2523-2538.

Raatikka, M., J. Rapola, L. Tuuteri, I. Louhimo and E. Savilahti (1981). "Familial third and fourth pharyngeal pouch syndrome with truncus arteriosus: DiGeorge syndrome." Pediatrics 67(2): 173-175.

Raker, V. A., G. Plessel and R. Lührmann (1996). "The snRNP core assembly pathway: identification of stable core protein heteromeric complexes and an snRNP subcore particle in vitro." Embo j 15(9): 2256-2269.

Ramaswamy, P., S. Negus, T. Homfray and L. De Rooy (2016). "Severe micrognathia with rib dysplasia: cerebro-costo-mandibular syndrome." Arch Dis Child Fetal Neonatal Ed 101(1): F85.

Raudvere, U., L. Kolberg, I. Kuzmin, T. Arak, P. Adler, H. Peterson and J. Vilo (2019). "g:Profiler: a web server for functional enrichment analysis and conversions of gene lists (2019 update)." Nucleic Acids Research 47(W1): W191-W198.

Ray, A. T., P. Mazot, J. R. Brewer, C. Catela, C. J. Dinsmore and P. Soriano (2020). "FGF signaling regulates development by processes beyond canonical pathways." Genes Dev 34(23-24): 1735-1752.

Reardon, W. and R. M. Winter (1995). "The molecular pathology of syndromic craniosynostosis." Mol Med Today 1(9): 432-437.

Reardon, W., R. M. Winter, P. Rutland, L. J. Pulleyn, B. M. Jones and S. Malcolm (1994). "Mutations in the fibroblast growth factor receptor 2 gene cause Crouzon syndrome." Nat Genet 8(1): 98-103.

Reid, B. S., H. Yang, V. S. Melvin, M. M. Taketo and T. Williams (2011). "Ectodermal Wnt/beta-catenin signaling shapes the mouse face." Dev Biol 349(2): 261-269.

Revil, T. and L. A. Jerome-Majewska (2013). "During Embryogenesis, Esrp1 Expression Is Restricted to a Subset of Epithelial Cells and Is Associated With Splicing of a Number of Developmentally Important Genes." Developmental Dynamics 242(3): 281-290.

Reynolds, K., P. Kumari, L. Sepulveda Rincon, R. Gu, Y. Ji, S. Kumar and C. J. Zhou (2019). "Wnt signaling in orofacial clefts: crosstalk, pathogenesis and models." Dis Model Mech 12(2).

Rigueur, D. and K. M. Lyons (2014). "Whole-mount skeletal staining." Methods Mol Biol 1130: 113-121.

Rijli, F. M., M. Mark, S. Lakkaraju, A. Dierich, P. Dolle and P. Chambon (1993). "A homeotic transformation is generated in the rostral branchial region of the head by disruption of Hoxa-2, which acts as a selector gene." Cell 75(7): 1333-1349.

Robinson, H. B., Jr. (1975). "DiGeorge's or the III-IV pharyngeal pouch syndrome: pathology and a theory of pathogenesis." Perspect Pediatr Pathol 2: 173-206.

Robledo, R. F., L. Rajan, X. Li and T. Lufkin (2002). "The Dlx5 and Dlx6 homeobox genes are essential for craniofacial, axial, and appendicular skeletal development." Genes Dev 16(9): 1089-1101.

Roessler, E., E. Belloni, K. Gaudenz, P. Jay, P. Berta, S. W. Scherer, L. C. Tsui and M. Muenke (1996). "Mutations in the human Sonic Hedgehog gene cause holoprosencephaly." Nat Genet 14(3): 357-360.

Roessler, E., D. E. Ward, K. Gaudenz, E. Belloni, S. W. Scherer, D. Donnai, J. Siegel-Bartelt, L. C. Tsui and M. Muenke (1997). "Cytogenetic rearrangements involving the loss of the Sonic Hedgehog gene at 7q36 cause holoprosencephaly." Hum Genet 100(2): 172-181.

Ruhin, B., S. Creuzet, C. Vincent, L. Benouaiche, N. M. Le Douarin and G. Couly (2003). "Patterning of the hyoid cartilage depends upon signals arising from the ventral foregut endoderm." Developmental Dynamics 228(2): 239-246.

Saga, Y., N. Hata, S. Kobayashi, T. Magnuson, M. F. Seldin and M. M. Taketo (1996). "MesP1: a novel basic helix-loop-helix protein expressed in the nascent mesodermal cells during mouse gastrulation." Development 122(9): 2769-2778.

Sakurai, T., S. Watanabe, A. Kamiyoshi, M. Sato and T. Shindo (2014). "A single blastocyst assay optimized for detecting CRISPR/Cas9 system-induced indel mutations in mice." BMC Biotechnol 14: 69.

Saltzman, A. L., Y. K. Kim, Q. Pan, M. M. Fagnani, L. E. Maquat and B. J. Blencowe (2008). "Regulation of multiple core spliceosomal proteins by alternative splicing-coupled nonsense-mediated mRNA decay." Mol Cell Biol 28(13): 4320-4330.

Saltzman, A. L., Q. Pan and B. J. Blencowe (2011). "Regulation of alternative splicing by the core spliceosomal machinery." Genes Dev 25(4): 373-384.

Santagati, F. and F. M. Rijli (2003). "Cranial neural crest and the building of the vertebrate head." Nat Rev Neurosci 4(10): 806-818.

Sarkar, S., A. Petiot, A. Copp, P. Ferretti and P. Thorogood (2001). "FGF2 promotes skeletogenic differentiation of cranial neural crest cells." Development 128(11): 2143-2152.

Sato, T., N. Sasai and Y. Sasai (2005). "Neural crest determination by co-activation of Pax3 and Zic1 genes in Xenopus ectoderm." Development 132(10): 2355-2363.

Satokata, I., L. Ma, H. Ohshima, M. Bei, I. Woo, K. Nishizawa, T. Maeda, Y. Takano, M. Uchiyama, S. Heaney, H. Peters, Z. Tang, R. Maxson and R. Maas (2000). "Msx2 deficiency in mice causes pleiotropic defects in bone growth and ectodermal organ formation." Nat Genet 24(4): 391-395.

Satokata, I. and R. Maas (1994). "Msx1 deficient mice exhibit cleft palate and abnormalities of craniofacial and tooth development." Nat Genet 6(4): 348-356.

Schneider, J. E., J. Böse, S. D. Bamforth, A. D. Gruber, C. Broadbent, K. Clarke, S. Neubauer, A. Lengeling and S. Bhattacharya (2004). "Identification of cardiac malformations in mice lacking Ptdsr using a novel high-throughput magnetic resonance imaging technique." BMC Dev Biol 4: 16.

Schneider, R. A. (1999). "Neural crest can form cartilages normally derived from mesoderm during development of the avian head skeleton." Dev Biol 208(2): 441-455.

Schneider, R. A. and J. A. Helms (2003). "The cellular and molecular origins of beak morphology." Science 299(5606): 565-568.

Selleck, M. A. and M. Bronner-Fraser (1995). "Origins of the avian neural crest: the role of neural plate-epidermal interactions." Development 121(2): 525-538.

Shirai, Y., K. Kawabe, I. Tosa, S. Tsukamoto, D. Yamada and T. Takarada (2019). "Runx2 function in cells of neural crest origin during intramembranous ossification." Biochem Biophys Res Commun 509(4): 1028-1033.

Smith, D. W., K. Theiler and G. Schachenmann (1966). "Rib-gap defect with micrognathia, malformed tracheal cartilages, and redundant skin: a new pattern of defective development." J Pediatr 69(5): 799-803.

Soriano, P. (1999). "Generalized lacZ expression with the ROSA26 Cre reporter strain." Nat Genet 21(1): 70-71.

Su, N., M. Jin and L. Chen (2014). "Role of FGF/FGFR signaling in skeletal development and homeostasis: learning from mouse models." Bone Res 2: 14003.

Talhouarne, G. J. S. and J. G. Gall (2018). "Lariat intronic RNAs in the cytoplasm of vertebrate cells." Proceedings of the National Academy of Sciences 115(34): E7970-E7977.

Tan, S. S. and G. Morriss-Kay (1985). "The development and distribution of the cranial neural crest in the rat embryo." Cell Tissue Res 240(2): 403-416.

Tani, H., R. Mizutani, K. A. Salam, K. Tano, K. Ijiri, A. Wakamatsu, T. Isogai, Y. Suzuki and N. Akimitsu (2012). "Genome-wide determination of RNA stability reveals hundreds of short-lived noncoding transcripts in mammals." Genome Res 22(5): 947-956.

Tani, S., U. I. Chung, S. Ohba and H. Hojo (2020). "Understanding paraxial mesoderm development and sclerotome specification for skeletal repair." Exp Mol Med 52(8): 1166-1177.

Tazi, J., N. Bakkour and S. Stamm (2009). "Alternative splicing and disease." Biochim Biophys Acta 1792(1): 14-26.

Theveneau, E. and R. Mayor (2012). "Neural crest delamination and migration: from epithelium-to-mesenchyme transition to collective cell migration." Dev Biol 366(1): 34-54.

Thomas, A. J. and C. A. Erickson (2009). "FOXD3 regulates the lineage switch between neural crest-derived glial cells and pigment cells by repressing MITF through a non-canonical mechanism." Development 136(11): 1849-1858.

Thompson, H. and A. S. Tucker (2013). "Dual origin of the epithelium of the mammalian middle ear." Science 339(6126): 1453-1456.

Tooley, M., D. Lynch, F. Bernier, J. Parboosingh, E. Bhoj, E. Zackai, A. Calder, N. Itasaki, E. Wakeling, R. Scott, M. Lees, J. Clayton-Smith, M. Blyth, J. Morton, D. Shears, U. Kini, T. Homfray, A. Clarke, A. Barnicoat, C. Wallis, R. Hewitson, A. Offiah, M. Saunders, S. Langton-Hewer, T. Hilliard, P. Davis and S. Smithson (2016). "Cerebro-costo-mandibular syndrome: Clinical, radiological, and genetic findings." Am J Med Genet A 170A(5): 1115-1126.

Trainor, P. A. and B. T. Andrews (2013). "Facial dysostoses: Etiology, pathogenesis and management." American Journal of Medical Genetics Part C: Seminars in Medical Genetics 163(4): 283-294.

Trainor, P. A. and P. P. Tam (1995). "Cranial paraxial mesoderm and neural crest cells of the mouse embryo: co-distribution in the craniofacial mesenchyme but distinct segregation in branchial arches." Development 121(8): 2569-2582.

Tsuchiya, Y., Y. Mii, K. Okada, M. Furuse, T. Okubo and S. Takada (2018). "Ripply3 is required for the maintenance of epithelial sheets in the morphogenesis of pharyngeal pouches." Development, Growth & Differentiation 60(2): 87-96.

Tuttle, A. H., V. M. Philip, E. J. Chesler and J. S. Mogil (2018). "Comparing phenotypic variation between inbred and outbred mice." Nat Methods 15(12): 994-996.

Urlaub, H., V. A. Raker, S. Kostka and R. Lührmann (2001). "Sm protein-Sm site RNA interactions within the inner ring of the spliceosomal snRNP core structure." Embo j 20(1-2): 187-196.

Vaglia, J. L. and B. K. Hall (1999). "Regulation of neural crest cell populations: occurrence, distribution and underlying mechanisms." Int J Dev Biol 43(2): 95-110.

Van Alstyne, M., C. M. Simon, S. P. Sardi, L. S. Shihabuddin, G. Z. Mentis and L. Pellizzoni (2018). "Dysregulation of Mdm2 and Mdm4 alternative splicing underlies motor neuron death in spinal muscular atrophy." Genes Dev 32(15-16): 1045-1059.

van Dam, A., I. Winkel, J. Zijlstra-Baalbergen, R. Smeenk and H. T. Cuypers (1989). "Cloned human snRNP proteins B and B' differ only in their carboxy-terminal part." Embo j 8(12): 3853-3860.

van den Ende, J. J., C. Schrander-Stumpel, E. Rupprecht, P. Meinecke, P. Maroteaux, C. de Die-Smulders and B. C. Hamel (1998). "The cerebro-costo-mandibular syndrome: seven patients and review of the literature." Clin Dysmorphol 7(2): 87-95.

Van Otterloo, E., I. Milanda, H. Pike, J. A. Thompson, H. Li, K. L. Jones and T. Williams (2022). "AP-2alpha and AP-2beta cooperatively function in the craniofacial surface ectoderm to regulate chromatin and gene expression dynamics during facial development." Elife 11.

Vandesompele, J., K. De Preter, F. Pattyn, B. Poppe, N. Van Roy, A. De Paepe and F. Speleman (2002). "Accurate normalization of real-time quantitative RT-PCR data by geometric averaging of multiple internal control genes." Genome Biol 3(7): RESEARCH0034.

Vaz-Drago, R., N. Custódio and M. Carmo-Fonseca (2017). "Deep intronic mutations and human disease." Hum Genet 136(9): 1093-1111.

Veistinen, L., M. Takatalo, Y. Tanimoto, D. A. Kesper, A. Vortkamp and D. P. Rice (2012). "Loss-of-Function of Gli3 in Mice Causes Abnormal Frontal Bone Morphology and Premature Synostosis of the Interfrontal Suture." Front Physiol 3: 121.

Verheij, J. B., S. A. de Munnik, T. Dijkhuizen, N. de Leeuw, D. Olde Weghuis, G. J. van den Hoek, R. S. Rijlaarsdam, Y. E. Thomasse, F. G. Dikkers, C. L. Marcelis and C. M. van Ravenswaaij-Arts (2009). "An 8.35 Mb overlapping interstitial deletion of 8q24 in two patients with coloboma, congenital heart defect, limb abnormalities, psychomotor retardation and convulsions." Eur J Med Genet 52(5): 353-357.

Vortkamp, A., M. Gessler and K. H. Grzeschik (1991). "GLI3 zinc-finger gene interrupted by translocations in Greig syndrome families." Nature 352(6335): 539-540.

Wada, N., Y. Javidan, S. Nelson, T. J. Carney, R. N. Kelsh and T. F. Schilling (2005). "Hedgehog signaling is required for cranial neural crest morphogenesis and chondrogenesis at the midline in the zebrafish skull." Development 132(17): 3977-3988.

Wallin, J., J. Wilting, H. Koseki, R. Fritsch, B. Christ and R. Balling (1994). "The role of Pax-1 in axial skeleton development." Development 120(5): 1109-1121.

Watanabe, M., N. Masuyama, M. Fukuda and E. Nishida (2000). "Regulation of intracellular dynamics of Smad4 by its leucine-rich nuclear export signal." EMBO Rep 1(2): 176-182.

Watson, T. A., O. J. Arthurs, N. Muthialu and A. D. Calder (2014). "Multi-detector thoracic CT findings in cerebro-costo-mandibular syndrome: rib gaps and failure of costo-vertebral separation." Skeletal Radiol 43(2): 263-266.

Wieczorek, D., W. G. Newman, T. Wieland, T. Berulava, M. Kaffe, D. Falkenstein, C. Beetz, E. Graf, T. Schwarzmayr, S. Douzgou, J. Clayton-Smith, S. B. Daly, S. G. Williams, S. S. Bhaskar, J. E. Urquhart, B. Anderson, J. O'Sullivan, O. Boute, J. Gundlach, J. C. Czeschik, A. J. van Essen, F. Hazan, S. Park, A. Hing, A. Kuechler, D. R. Lohmann, K. U. Ludwig, E. Mangold, L. Steenpass, M. Zeschnigk, J. R. Lemke, C. M. Lourenco, U. Hehr, E. C. Prott, M. Waldenberger, A. C. Bohmer, B. Horsthemke, R. T. O'Keefe, T. Meitinger, J. Burn, H. J. Ludecke and T. M. Strom (2014). "Compound heterozygosity of low-frequency promoter deletions and rare loss-of-function mutations in TXNL4A causes Burn-McKeown syndrome." Am J Hum Genet 95(6): 698-707.

Wild, A., M. Kalff-Suske, A. Vortkamp, D. Bornholdt, R. König and K. H. Grzeschik (1997). "Point mutations in human GLI3 cause Greig syndrome." Hum Mol Genet 6(11): 1979-1984.

Wilkie, A. O., S. F. Slaney, M. Oldridge, M. D. Poole, G. J. Ashworth, A. D. Hockley, R. D. Hayward, D. J. David, L. J. Pulleyn, P. Rutland and et al. (1995). "Apert syndrome results from localized mutations of FGFR2 and is allelic with Crouzon syndrome." Nat Genet 9(2): 165-172.

Will, C. L., C. Schneider, M. Hossbach, H. Urlaub, R. Rauhut, S. Elbashir, T. Tuschl and R. Lührmann (2004). "The human 18S U11/U12 snRNP contains a set of novel proteins not found in the U2-dependent spliceosome." Rna 10(6): 929-941.

Wilusz, C. J. and J. Wilusz (2005). "Eukaryotic Lsm proteins: lessons from bacteria." Nat Struct Mol Biol 12(12): 1031-1036.

Wu, M. Y. and C. S. Hill (2009). "Tgf-beta superfamily signaling in embryonic development and homeostasis." Dev Cell 16(3): 329-343.

Wurdak, H., L. M. Ittner, K. S. Lang, P. Leveen, U. Suter, J. A. Fischer, S. Karlsson, W. Born and L. Sommer (2005). "Inactivation of TGFbeta signaling in neural crest stem cells leads to multiple defects reminiscent of DiGeorge syndrome." Genes Dev 19(5): 530-535.

Xu, H., T. Xiao, C. H. Chen, W. Li, C. A. Meyer, Q. Wu, D. Wu, L. Cong, F. Zhang, J. S. Liu, M. Brown and X. S. Liu (2015). "Sequence determinants of improved CRISPR sgRNA design." Genome Res 25(8): 1147-1157.

Xu, M., Y. A. Xie, H. Abouzeid, C. T. Gordon, A. Fiorentino, Z. Sun, A. Lehman, I. S. Osman, R. Dharmat, R. Riveiro-Alvarez, L. Bapst-Wicht, D. Babino, G. Arno, V. Busetto, L. Zhao, H. Li, M. A. Lopez-Martinez, L. F. Azevedo, L. Hubert, N. Pontikos, A. Eblimit, I. Lorda-Sanchez, V. Kheir, V. Plagnol, M. Oufadem, Z. T. Soens, L. Yang, C. Bole-Feysot, R. Pfundt, N. Allaman-Pillet, P. Nitschke, M. E. Cheetham, S. Lyonnet, S. A. Agrawal, H. Li, G. Pinton, M. Michaelides, C. Besmond, Y. Li, Z. Yuan, J. von Lintig, A. R. Webster, H. Le Hir, P. Stoilov, U. K. I. R. D. Consortium, J. Amiel, A. J. Hardcastle, C. Ayuso, R. Sui, R. Chen, R. Allikmets and D. F. Schorderet (2017). "Mutations in the Spliceosome Component CWC27 Cause Retinal Degeneration with or without Additional Developmental Anomalies." Am J Hum Genet 100(4): 592-604.

Yamagishi, C., H. Yamagishi, J. Maeda, T. Tsuchihashi, K. Ivey, T. Hu and D. Srivastava (2006). "Sonic hedgehog is essential for first pharyngeal arch development." Pediatr Res 59(3): 349-354.

Yoshida, T., P. Vivatbutsiri, G. Morriss-Kay, Y. Saga and S. Iseki (2008). "Cell lineage in mammalian craniofacial mesenchyme." Mech Dev 125(9-10): 797-808.

Zakariyah, A., W. Hou, R. Slim and L. Jerome-Majewska (2012). "TMED2/p24β1 is expressed in all gestational stages of human placentas and in choriocarcinoma cell lines." Placenta 33(3): 214-219.

Zeevaert, R., F. Foulquier, D. Cheillan, I. Cloix, N. Guffon, L. Sturiale, D. Garozzo, G. Matthijs and J. Jaeken (2009). "A new mutation in COG7 extends the spectrum of COG subunit deficiencies." Eur J Med Genet 52(5): 303-305.

Zeevaert, R., F. Foulquier, B. Dimitrov, E. Reynders, R. Van Damme-Lombaerts, E. Simeonov, W. Annaert, G. Matthijs and J. Jaeken (2009). "Cerebrocostomandibular-like syndrome and a mutation in the conserved oligomeric Golgi complex, subunit 1." Hum Mol Genet 18(3): 517-524.

Zhan, Y. T., L. Li, T. T. Zeng, N. N. Zhou, X. Y. Guan and Y. Li (2020). "SNRPB-mediated RNA splicing drives tumor cell proliferation and stemness in hepatocellular carcinoma." Aging (Albany NY) 13(1): 537-554.

COPYRIGHT PERMISSIONS

Through Copyright Clearance Centre, copyright permissions have been obtained for all figures and tables adapted from previous publications.

Figure 1.2: Tooley *et al.* Cerebro-costo-mandibular syndrome: Clinical, radiological, and genetic findings. Am J Med Genet A 2016; 170A (5): 1115-1126.

Permission has been obtained from John Wiley and Sons under the license number 547262149023.

Figure 1.3: Lynch *et al.* Disrupted auto-regulation of the spliceosomal gene SNRPB causes cerebro-costo-mandibular syndrome. Nat Commun 2014; 5: 4483.

Figure 1.4: Cartegni. Listening to silence and understanding nonsense: exonic mutations that affect splicing. Nat Rev Genet 2002: 3(4): 285-298.

Permission has been obtained from Springer Nature under the license number 5472631138095.

Figure 1.6 and Table 1.1: Beauchamp *et al.* Spliceosomopathies and neurocristopathies: Two sides of the same coin? Dev Dyn 2020; 249(8): 924-945.

Permission has been obtained from John Wiley and Sons under the license number 5472630375534.

Figure 1.8: Dworkin *et al.* The Role of Sonic Hedgehog in Craniofacial Patterning, Morphogenesis and Cranial Neural Crest Survival. J Dev Biol 2016; 4(3)

Figure 1.9: Cibi *et al.* Neural crest-specific deletion of Rbfox2 in mice leads to craniofacial abnormalities including cleft palate. Elife 2019; 8

Figure 1.10: Fitriasari and Trainor. Diabetes, Oxidative Stress, and DNA Damage Modulate Cranial Neural Crest Cell Development and the Phenotype Variability of Craniofacial Disorders. Front Cell Dev Biol 2021; 9: 644410.

Figure 1.11: Bhatt *et al.* Signals and switches in Mammalian neural crest cell differentiation. Cold Spring Harb Perspect Biol 2013; 5(2).

Permission granted from Cold Spring Harbor Laboratory Press. Confirmed by: Carol C. Brown, Books Development, Marketing and Sales, Cold Spring Harbor Laboratory Press, 500 Sunnyside Blvd. Woodbury, NY. 11797. brown@cshl.edu